Hot mix asphalt mixtures with high levels of reclaimed asphalt pavement

Evaluation of material properties using multi-scale characterization

Master thesis

Jorn van Akker

TU Delft

EVALUATION OF MATERIAL PROPERTIES OF HOT MIX ASPHALT MIXTURES WITH HIGH LEVELS OF RECLAIMED ASPHALT PAVEMENT USING MULTI-SCALE CHARACTERIZATION

By

Jorn van Akker

in partial fulfillment of the requirements for the degree of

Master of Science
in Structural Engineering

at the Delft University of Technology
to be defended publicly on 24th November 2022

Student number:	4695623	
Thesis committee:	- Dr. K. Anupam (chair)	Delft University of Technology
	- Prof. dr. ir. S.M.J.G. Erkens	Delft University of Technology
	- Dr. ir. M. Luković	Delft University of Technology
	- Ir. R. Naus	Dura Vermeer

Preface

This thesis report is the final product of the study about evaluation of material properties of hot mix asphalt mixtures with high levels of reclaimed asphalt pavement using multi-scale characterization. The research is about the influence of reclaimed asphalt material on the functional properties of asphalt concrete mixtures. This thesis was written as part of the completion of the Master's program in Civil Engineering at Delft University of Technology in cooperation with Dura Vermeer. The thesis is the final in-depth assignment of this two-year program in which all the knowledge acquired serves as the basis for writing this thesis.

Both literature research and material tests have been done to be able to achieve the research objective. Those material tests were done in the lab of Dura Vermeer in Eemnes and I am very grateful to them for allowing me to conduct these tests there.

I would like to thank ir. Robbert Naus and Niels Heins from Dura Vermeer for the opportunity to graduate with Dura Vermeer and the expert advice they have given. Also, the whole Dura Vermeer laboratory team I am very grateful for all the help with the test executions. Furthermore, I would like to thank dr. Kumar Anupam for the guidance from TU Delft. In addition, I would like to thank prof.dr.ir. Sandra Erkens for helping me set up the thesis and delineating the topic.

Lastly, I would like to thank my boyfriend and parents for all the support and encouragement during my master's studies.

The last thing that remains for me is to wish you, the reader, lots of reading pleasure!

Jorn van Akker
Den Haag, November 2022

Abstract

Because of the sustainability transition in the asphalt industry, it is increasingly popular to apply reclaimed asphalt pavement (RAP) instead of new asphalt. Then, less new material is needed and the amount of waste products is reduced. However, there are questions regarding the performance of asphalt mixtures with high RAP percentages, particularly in terms of potentially excessive high stiffness and a decrease in workability. Further, there are doubts about how well the aged and the virgin binder blend together. In the Netherlands, a RAP content of 60% in combination with a softer binder is common practice, but an increase in RAP content means that rejuvenators are often required.

The research objective was to study the multi-scale material properties of hot mix asphalt mixtures with high reclaimed asphalt pavement percentages using micromechanics. At binder level, the DSR test was done and it was also used to select and reject the rejuvenators which are applied at mixture level. The chosen rejuvenators, Neomex HR and Cecabase RWI, were applied to the mixtures with 80% RAP. Besides that, a reference mixture was tested with 65% RAP and a reference mixture of 80% RAP. Further, the results were used to fit a modified micromechanical Hirsch model for RAP mixtures with rejuvenators.

Based on the material tests and comparing it with the reference (65% RAP mixture), it turned out that there is potential to implement 80% RAP mixtures. Both moisture sensitivity and the rutting resistance are improved when a higher RAP content is applied, while the total fracture toughness has remained the same. The stiffness of the 80% RAP mixture is substantially higher, but it is still applicable. The biggest concern is the fatigue resistance, because the fatigue resistance of the 80% RAP mixture without rejuvenator is worse for higher strains.
The application of the rejuvenating additives led to the properties of the 80% mixtures being more similar to the 65% RAP mixture and the workability is improved. However, it did appear that the dosage of the additives is on the high side. The stiffness is lower than the reference mixture, especially the mixture with Neomex HR. Also, the rutting resistance is lower than the reference mixture, especially the mixture with Cecabase RWI. Future research may optimize the dosage to improve results.

The micromechanical Hirsch model provided stiffness results with a reasonably accuracy, although this model used general model coefficients. The simplified Hirsch model with inclusion of the factor P_a could not be simply adopted when it is fit for other types of mixtures. The predicted stiffness for all three mixtures was much higher than it actually is. The adjustment of the fitting parameters, according to the laboratory results of the 80% RAP, led to accurate results making the simplified Hirsch model with inclusion of the factor P_a applicable to the mixtures with 80% RAP and a rejuvenating additive.

Table of contents

List of figures

List of tables

1.Introduction

1.1 General introduction

In the more recent years, a sustainability transition has taken place in almost all the industries and they look how to make their processes more sustainable so that greenhouse gas emissions are reduced, including the asphalt industry (Zimek & Baumgartner, 2017),(Van Dam et al., 2015). In the previous century, this industry was known to cause polluting damage to the environment (Lundy, 1972). The production of asphalt pavements leads to greenhouse gas emissions that impact the environment (Thives & Ghisi, 2017). Because of the concerns about the harmful impacts on the environment, processes are viewed from a circularity perspective (Mantalovas & Di Mino, 2020).

A circular economy can namely contribute significantly to the reduction of greenhouse gas emissions (European Environment Agency, 2020). The European Commission has set a goal with the European Green Deal to become fully circular by 2050, which means that waste products will not exist and raw materials will be used again (European Comission, 2019). This is also applicable to the pavement industry. The goal of the Department of Waterways and Public Works in the Netherlands is to achieve 50% reduction in raw materials by 2030 and a circular economy by 2050 (Ministerie van Infrastructuur en Waterstaat & Rijkswaterstaat Water Verkeer en Leefomgeving (RWS WVL), 2020). This means that there is a major focus on reuse, whereby waste becomes a fully new raw material again. Eventually, this leads to a closed material flow, with zero waste (Rijksoverheid, 2016).

To achieve the circular economy in the pavement industry, the recycling of asphalt material offers great potential (Mantalovas & Di Mino, 2020). Old asphalt concrete is namely considered an ideal material that can be reprocessed in the asphalt mix production cycle (Im et al., 2016). Such reprocessed asphalt material is called reclaimed asphalt pavement (RAP) (European Asphalt Pavement Association, 2020).

According to Dinis-Almeida et al. (2016), the advantage of applying RAP is twofold. At first, less new material is needed because old material is used, so less raw resources are utilized. At second, the total landfill use is reduced, because there are no waste products. When the asphalt mixture exists of 100% RAP material, no new material is needed at all. A closed material flow and circular process is achieved.

To meet the goals of the European Green Deal and achieve a shift to a circular economy, 100% RAP will eventually thus have to be applied. Nowadays, asphalt mixtures containing 50% to 70% RAP material are common in the Netherlands (Cirkel et al., 2015). The highest levels of RAP material are applied in the binder and base layer of the asphalt pavement, because there are no limits for this layer regarding RAP content (CROW, 2020).

The implementation of the abovementioned RAP content is mostly done by applying softer bitumen, aiming to get the same properties as a virgin mixture. Further increasing the RAP content reduces the proportion of new bitumen, which makes it difficult to soften the binder enough. In such cases, rejuvenators are often used (van de Wall et al., 2018).

1.2 Problem description

As explained in the previous section, asphalt mixtures containing high percentages of RAP are an important aspect for pavement engineering nowadays. There are many questions regarding the feasibility of the production of those mixtures with high percentages of RAP (Zaumanis et al., 2014). Also, the exact influence of using RAP materials on the performance on the longer term is questioned (Tran et al., 2012). This has multiple reasons. First of all, there is a great variability in the RAP materials, which makes it difficult to universally characterize the properties of the RAP materials (Tarsi et al., 2020). Furthermore, it is unclear how the RAP materials blend with the virgin materials and what the consequences are for the material properties of the whole mixture (Shirodkar et al., 2011). In addition, RAP materials can have negative influence on some of the material properties (Tarsi et al., 2020). For example, the mixture stiffness may increase too much and the workability may decrease, both of which are undesirable effects (Farooq et al., 2018).

The abovementioned reasons show the challenge of implementing asphalt mixtures with very high percentages of RAP in practice. However, as explained in paragraph 1.1, sustainable solutions are needed to meet the specified goal in terms of circularity. Therefore, more information about the performance of asphalt mixtures with RAP is required so that it can be applied in practice and makes it easier to predict the functional properties of the asphalt mixture.

1.3 Research goal and research questions

The goal of this project is to look into the effect of higher levels of RAP in asphalt concrete mixtures on material properties, so that it becomes possible to implement very high levels of RAP towards almost 100% RAP usage in practice. As discussed in section 1.2, mixtures with 65% RAP in combination with softer bitumen are widely used in the Netherlands. For higher levels of RAP, a softer bitumen may not be sufficient, but studies have shown that additives in the form of rejuvenators can be applied to mitigate the negative effects of the application of RAP such as undesirable increasing stiffness (Nazzal et al., 2015) and (Tran et al., 2012). Therefore, two different RAP percentages are studied: 65% RAP and 80% RAP. The 65% RAP content is chosen as reference. The 80% RAP content is chosen to apply the rejuvenating additives to look if those additives make it possible to set a further step towards 100% recycling.

For the mixture composition, the focus is on the base/binder layer of an asphalt pavement. As mentioned in section 1.1, this layer is the most suitable for applying high levels of RAP.

To be able to characterize the material properties of the asphalt mixtures with high RAP percentages, a multi-scale approach is used. This multi-scale approach means that the testing will be done at different levels of scale to get more insight in the behaviour of the mixture.

The test results will be used to link to a specific micromechanical model, the Hirsch model. This model will be used as a support of the above-mentioned characterization. A modification of the Hirsch model is evaluated as well whether it can accurately predict the stiffness of the mixtures.

The research objective is as follows:
To study the multi-scale material properties of hot mix asphalt (HMA) mixtures with high reclaimed asphalt pavement (RAP) percentages using micromechanics.

The following sub-questions are formulated:
1. What characterizes a HMA with RAP?
2. Which additives can be used in HMA with high RAP percentages?
3. What is the influence of high RAP content on the functional properties of the asphalt binder and asphalt mixture?
4. What is the influence of the rejuvenators on the functional properties of the asphalt binder and asphalt mixture?
5. Can micromechanical models (Hirsch model) be used to predict the functional properties of the asphalt mixtures containing a high percentage of RAP?

1.4 Global research methodology

Firstly, to answer the first two sub-questions, literature research is needed. The literature review starts with an overview of HMA mixtures, the current state of the use of RAP and suitable additives/rejuvenators. Moreover, the mix design and the performance of HMA-RAP are discussed. Furthermore, micromechanical models regarding the prediction of the mixture stiffness will be discussed.

To be able to achieve the objective and answer the questions, functional tests are needed to get more insight in the influence of using high percentages RAP in the asphalt mixture and the influence of different rejuvenating additives in combination with RAP on the functional properties. Binder tests and mixture tests will be done on specimens with different variations. There are two parameters (percentage of RAP and rejuvenating additive) that will be varied in this research, linked to sub-question 3 and 4. Eventually, the stiffness results will be compared with the predicted stiffness values according to the Hirsch model, so that it becomes clear whether those predictions are accurate.

1.5 Thesis outline

The thesis is organized in six chapters. A brief description is presented below:

1. Introduction

In this chapter, a general introduction into the topic is given. The problem statement follows from this general introduction and the research objective will be formulated. Out of this, the sub-questions are formulated. Furthermore, the structure of the research will be made clear.

2. Theoretical background

In this chapter, a theoretical background will be provided. This background is based on past research studies. Basic information about HMA mixtures, RAP materials and rejuvenators is provided. Furthermore, relevant literature reviews pertaining to the performance of mixtures containing different RAP percentages will be presented

3. Materials and methodology

This chapter gives the description of the used materials, the mixture components and the rejuvenators. In addition, the methodology for the research is explained. After that, the testing plan is presented and the used functional tests are described.

4. Results

In this chapter, the results of the research tests are presented. The outcomes of the measurements are reported and the results are discussed.

5. Micromechanical prediction of the stiffness of mixtures with high RAP percentages

In this chapter, a specific micromechanical model, the Hirsch model, is used to predict the stiffness modulus of the asphalt mixtures. Also, a simplification of the Hirsch model is applied.

6. Conclusions and recommendations

In this chapter, conclusions of research findings will be presented. In addition, recommendations are done for follow-up research.

2 Theoretical background

In this chapter, a theoretical background will be provided. Papers and scientific studies are used to outline what has been researched in the field of asphalt mixtures in combination with RAP. Also, micromechanical models for predicting the mixture stiffness are discussed.

2.1 Introduction to hot mix asphalt with RAP

The theoretical background starts with basic information about the asphalt mixtures that will be used in this study. The characteristic components in this research, RAP material and possible rejuvenating additives, are explored. In addition, HMA in general is briefly discussed.

2.1.1 Hot mix asphalt mixtures

In essence, an asphalt mixture is a combination of bitumen and aggregates. The bitumen acts as a binder which holds the aggregates together. Bitumen is a dark material from the petroleum industry and it is obtained especially by the process of crude oils (Partal & Martínez-Boza, 2011). It can also occur in nature (CROW, 2010). However, in the application of asphalt mixtures, it is desired that the bitumen is of good quality (Roberts et al., 1996). Because this can be monitored better in an industrial environment, petroleum bitumen is preferable to natural bitumen.

The largest share in the mixture exists of minerals. Those aggregates exist mainly of sand and (crushed) rock. Those aggregates are sieved so that these can be divided over different aggregate sizes. This is used to achieve a correct blending and grading of the aggregate sizes so that a proper mix is obtained. For example, in order to obtain a dense asphalt mix, it is important that all aggregate sizes are represented (Yuan et al., 2021).

The bitumen is heated so that it is liquid and capable to mix it with the aggregates. The result is a hot mix asphalt mixture. It is called hot mix asphalt because it is mixed at a temperature roughly between 120 °C and 190 °C, although until 150 °C it can be considered as well as warm mix asphalt (EAPA, 2014). After mixing, it is transported to the construction site, where it is spread with a paver and compacted with a roller (Mazumder et al., 2016). Thereafter, once the asphalt is cooled, the asphalt pavement can be used.

Because bitumen is a viscoelastic material, it can be expected that the asphalt mixture behaves in a viscoelastic way as well. The behaviour of the mixture is dependent on temperature and loading time (frequency). For example, asphalt mixtures behave in an elastic way at lower temperatures while at higher temperatures, a more viscous behaviour is dominant (Mackiewicz & Szydło, 2019).

As indicated in the introduction, there is an increasing focus on a circularity transition in the asphalt industry. Asphalt production has namely a relatively high environmental impact, partly because of the high mixing temperature of HMA (Almeida-Costa & Benta, 2016). This is because during the asphalt production, the bitumen has to be liquid, which requires a lot of energy

(Blankendaal et al., 2014). The mineral aggregates must be warm too, else bitumen will cool down immediately.

The production of bitumen is also a energy intensive process, because it exists of the residue during the distillation process of crude oil, for which a high temperature is required (Blankendaal et al., 2014).

To better understand the broader environmental impact of a product or process, the life cycle assessment (LCA) was developed (International Standard, 2006). This tool makes use of multiple impact categories to determine the environmental impact for different areas. (McManus & Taylor, 2018). The LCA tool is applied on HMA mixtures in the study of Mazumder et al. (2016). In this study, the biggest environmental effects due to the production of HMA are identified. It states that the production of bitumen leads to negative effects on human and eco toxicity, the production of aggregate leads to depletion of minerals and fossil fuels and the HMA production leads to depletion of fossil fuels and global warming. Those negative effects demonstrate the need to improve HMA production regarding environmental impact with for example the application of RAP material.

2.1.2 Reclaimed Asphalt Pavement (RAP)

2.1.2.1 Application

The application of RAP material started already in 1915 (Kennedy et al., 1998). However, it became economically attractive during the oil crisis in the 1970s (Milad et al., 2020). Due to the oil crisis, the price for bitumen increased strongly, leading to an exploration of recycle opportunities. This led to many developments regarding the application of RAP material (Milad et al., 2020).

Nowadays, the application of RAP material is popular in the transition to a more circular process (Im et al., 2016). At this moment, almost all available RAP is reused in the pavement industry. Taking numbers of 2019 in Europe, 76% of the total amount reclaimed asphalt is reused in new mixtures and another 20% is reused as granular material for lower layers in the pavement. This means that only 4% is unused and processed as waste (EAPA, 2021).

So, asphalt concrete has a high recycling rate. However, an almost completely circular process has not yet been achieved. In 2019, in Europe, only 51.4% of the total asphalt mixtures exist of RAP materials (Tarsi et al., 2020). This means that almost half of the new asphalt pavement exists still from new asphalt instead of recycled asphalt concrete. This is due to the fact that more new asphalt is needed than is made available annually for recycling. From the abovementioned data, it can be determined that almost double the amount of asphalt is needed than becomes available in old asphalt. Across the industry as a whole, only an application of 50% RAP material is then possible on average. This provides an additional challenge to make the entire process fully circular.

The Netherlands has a long experience with the use of RAP (van de Wall et al., 2018). Already in the 1950s, the first experiments are done regarding the recycling of asphalt. From the 1970s onwards, the oil crisis prompted the reuse of asphalt to save on raw materials. From then on, the proportion of old asphalt was increased in steps. Until the mid 1980s, the RAP content was limited to 30%. The used technique prevented a higher proportion of RAP material. In the production, a batch mixer was used with cold addition of the RAP material. (Voskuilen, 2017).

Later on, technical research, such as the introduction of the parallel drum, made reuse of higher RAP content possible with a comparable quality as asphalt with only new raw material. Nowadays, the usage of the parallel drum enables a RAP content of 70% (CROW, 2010). However, the regulations only allowed the use of up to 50% RAP until 2007. After 2007, this limit was lifted for the base layer and the binder layer and from then on it was permitted to apply as high a content as one wished for those layers (Voskuilen, 2017).

Theoretically, it is possible to apply mixtures with 100% RAP material (Zaumanis et al., 2014). Although the bitumen in the old asphalt ages over time, it is possible to fully regenerate the properties of the asphalt. To counter the consequences due to the aging of the bitumen, rejuvenating additives can be added to the asphalt mixture (Tran et al., 2012). However, in the Netherlands, it is common to mix in a softer binder to compensate for hardening due to the aging process (CROW, 2010). Rejuvenators are only used when a softer binder is not sufficient (van de Wall et al., 2018). This is the case with very high RAP content, as the proportion of virgin bitumen is so small that sufficient compensation for hardening becomes difficult. This will be discussed in more detail in paragraph 2.2. The rejuvenating additives are addressed in more detail in paragraph 2.4.

2.1.2.2 Production

The production of mixtures with RAP material starts with collecting the RAP material. Old and damaged pavement is milled from the road and taken to the asphalt plant (Daniel & Lachance, 2005). There, the incoming material is checked to make sure it is not contaminated with impurities (Devulapali et al., 2019). This can easily be done when the material comes from a sole source but it will take more time if the materials come from multiple sources. After that, the RAP aggregates will be crushed into smaller pieces. This is because the consistency of the material improves by this operation and more flexibility will be achieved in the mix design. However, care must be taken not to make the aggregates too small, because the final mix design may not be achieved if the proportion of small aggregates becomes too large. Moreover, the smaller particles hold more binder due to the relatively large surface area, which can lead to a too large amount of binder in the mixing process (Tarsi et al., 2020).

After the first steps, the RAP material can be further processed in the asphalt plant. The most widely used principle abroad is to overheat the virgin aggregates and add the RAP aggregates so that it dries and heat when they make contact with each other (Zaumanis & Mallick, 2014). The

advantage of this is that the RAP material is not directly exposed to the flame. This prevents the material from burning.

In a traditional drum plant, this principle is applied using an entrance in the middle. Here, the RAP material is put in the drum at the overheated virgin aggregates (Zaumanis & Mallick, 2014). In such drum asphalt plants, the maximum RAP content is limited to 50% approximately, because of restrictions related to overheating of the virgin aggregates (Devulapali et al., 2019). If higher percentages of RAP are applied, blue smoke may result due to volatilization of the aged binder (Lizárraga et al., 2018).

In the Netherlands, the most used principle is the usage of the parallel drum (Leysssens et al., 2013). The parallel drum is a separate drum for the RAP material, which is used to keep the new minerals and the old asphalt separate. In contrast to the primary drum, a parallel flow system is applied in the parallel drum. This means that the RAP material enters the drum at the location of the burner and the heat flow and the material flow follow the same way (Leysssens et al., 2013). In this parallel drum, the RAP material is heated to a temperature of 110 °C approximately. Higher temperatures are not possible because the bitumen in the RAP material may burn. At the same time, the virgin aggregates are overheated such that the final temperature of the whole will be around 160 °C (CROW, 2010). Then the two aggregate flows are mixed together with the preheated bitumen.

After the production process of the asphalt mixture is completed, the asphalt is transported to the construction site. There, the paving procedure is the same as for new asphalt, but it should be taken into account that workability and compatibility can be complicated when high percentages of RAP are applied (Zaumanis & Mallick, 2014).

Besides the production limitations, there are more reasons for limitations in the application of RAP: the quality of the RAP aggregate, the application of a new mix design and the quality of the asphalt mixture (Tarsi et al., 2020). Firstly, the quality of the recycled aggregates has to be guaranteed. Due to milling and crushing of the old pavement, the finer RAP aggregates have a higher share, which influences the quality and homogeneity. However, the aggregate size requirements do not change when RAP is applied, so this may lead to the problem that finer parts of the RAP material cannot be applied in the mixture (Zaumanis & Mallick, 2014). Secondly, the mix design has to be adapted to be able to meet the original performance with the use of RAP. This is because the recycling processes have to be taken into account (Tarsi et al., 2020). Further considerations about mix design are given in paragraph 2.2. Thirdly, there were questions on the actual quality and performance of the mixture when using RAP. This led to the fact that there were strong national norms for RAP which made it more difficult to implement very high RAP content in the mixture. The actual performance of mixtures with RAP material is discussed in paragraph 2.3.

2.1.2.3 Behaviour of asphalt mixtures with RAP

Applying RAP in asphalt mixtures may influence the mixture and performance reasonably (Yu et al., 2018). A major cause for this is the partial blending of the aged bitumen in the RAP and the virgin bitumen (Shirodkar et al., 2011). Due to this partial blending, a complicated binder system develops which is hard to predict (Devulapali et al., 2019). It is seen that the binder in the RAP material hardens during service life as a result of the oxidation process during this phase. The consequence is that the stiffness of the RAP mixtures is higher compared to new mixtures. This leads to the fact that the mixture may not be flexible enough anymore and that the mixture exhibits brittle behaviour. This has a negative effect on the cracking resistance (Hettiarachchi et al., 2019). This partial blending can thus be a problem when RAP is applied in the mixture. It is difficult to estimate how much aged binder can be reactivated and is able to coat the aggregates (Devulapali et al., 2019). It is often estimated that the aged binder and the virgin binder blend completely but this may not be the case (Shirodkar et al., 2011). The assumed performance then turns out to be incorrect, leading to overestimation of the mixture properties.

Three different blending scenarios can be distinguished: full blending between RAP binder and virgin binder, partial blending and no blending. The last scenario is also called black rock (Devulapali et al., 2019). In Figure 2.1, those three different blending scenarios can be seen. The blending exists of three different components: the RAP aggregates, RAP binder and the virgin binder. The extreme scenarios are shown on the left and right: on the left, the scenario is shown where no blending between aged binder and virgin binder takes place and on the right, the scenario is shown where full blending takes place (Al-Saffar et al., 2021). However, the scenario in the middle in Figure 2.1 is the most realistic (Devulapali et al., 2019). The RAP binder is not capable to blend fully with the virgin binder, leading to this partial blending scenario. The RAP binder is much stiffer than the virgin binder and therefore there is extra energy required to fully mobilize the RAP binder (Zhao et al., 2015).

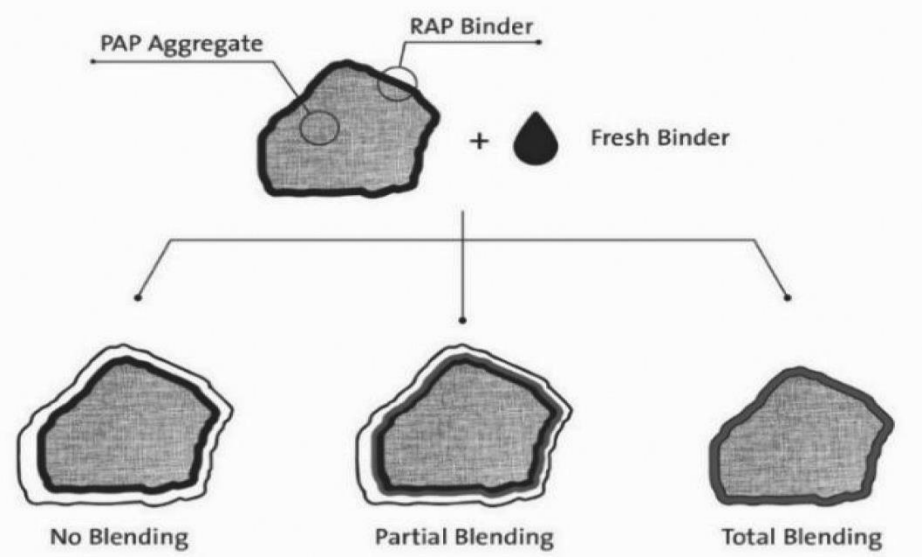

Figure 2.1: Three blending scenarios (Al-Saffar et al., 2021)

This partial blending influences the performance of the asphalt mixtures containing RAP material (Yu et al., 2018). Besides the negative effects on stiffness and cracking resistance, named at the first paragraph of this section, it influences the fatigue behaviour as well (Zaumanis et al., 2014). Multiple studies have shown that the fatigue resistance decreases when the percentage RAP material increases (Hettiarachchi et al., 2019). However, other studies claim the opposite, namely that the fatigue resistance increases when RAP material is used (Zaumanis et al., 2014). The performance of asphalt mixtures containing RAP material is further discussed in paragraph 2.4.

Dependent on the way the assumption of the blending of the RAP binder is done, material properties may change differently. If full blending was assumed, but in reality, this was not the case, it can result in mixtures with too little bitumen. This may have a negative effect on cracking resistance, raveling resistance and water sensitivity (Yu et al., 2018). However, if it was assumed as a black rock and in reality, the blending grade was higher, it can lead to mixtures with a too high bitumen content. Possible consequences are a mixture that is too soft and not enough resistance to permanent deformation (Zaumanis & Mallick, 2014).

So, the application of RAP material in asphalt mixtures has become increasingly popular in recent years because of the economic and environmental benefits. However, there are still some drawbacks which is why very high percentages of RAP towards 100 percent are still rarely applied. There are restrictions due to difficulties in the production, mostly caused by overheating the aggregates. Also, there are doubts about how well the aged and virgin binder blend together. Often, the estimation is that the aged binder and the virgin binder blend fully but it is more realistic that partial blending takes place. This has its influence on the performance of asphalt mixtures with RAP material.

2.2 Mix design of asphalt with RAP material

Besides the components themselves, they have to be properly implemented as well (Al-Qadi et al., 2012). This has to be done with the mix design. The mix design is a process in which the quantities and percentages of aggregates and binder are determined (CROW, 2010). This is because the optimal content of each ingredient is found so that the best mix composition is found for the specific final goal of the product (Bonaquist, 2011). This principle stays the same when RAP material is implemented instead of fresh asphalt concrete. However, the mix design method that is used, does change (Tarsi et al., 2020).

The mix design method changes because of the extra components that are added in the form of RAP. For example, the size fractions of the RAP aggregates have to be identified (Tarsi et al., 2020). Furthermore, it must be identified how much bitumen content is in the RAP material, because this bitumen contributes as well to the final mixture (Zaumanis & Mallick, 2014). How much this contributes, is difficult to estimate because of the partial blending, which has been addressed in paragraph 2.1.2. This makes it hard to do a proper mix design with RAP materials.

Another additional difficulty in the mix design are the possible additives in the form of rejuvenating agents. Those can be added in the application of RAP in HMA to meet the performance criteria, so the additives and rejuvenators need to be incorporated as well. This leads to an additional parameter in the mix design, both in the kind of rejuvenator as well in the optimum content (Tarsi et al., 2020).

Therefore, the current methods should be changed. Firstly, the binder content has to be determined. For this, the rheological properties of the RAP binder must be characterized. With that, the type and quantity of the virgin binder can be determined to obtain the desired grade (Al-Qadi et al., 2007). In general, this grade will be lower in comparison with aged binder to compensate for the ageing behaviour of the old binder.

Which bitumen grade to choose depends on the ratio between RAP binder and virgin binder and the penetration of the aged binder. In the European Standard NEN-EN 13108-1 (Nederlandse Norm (NEN), 2016a), it is described how the desired bitumen grade can be calculated (equation 2.1).

$$\mathbf{a} * \mathbf{log}(\mathbf{pen_1}) + \mathbf{b} * \mathbf{log}(\mathbf{pen_2}) = (\mathbf{a} + \mathbf{b}) * \mathbf{log}\,(\mathbf{pen_{mix}}) \quad (2.1)$$

where:	a	=	mass proportion RAP binder	[-]
	pen_1	=	penetration RAP binder	[0.1 * mm]
	b	=	mass proportion new binder	[-]
	pen_2	=	penetration new binder	[0.1 * mm]
	pen_{mix}	=	penetration mixture	[0.1 * mm]
	a + b	=	1	

The application of softer bitumen can mitigate the consequences of ageing of the bitumen to a certain level. The penetration rule in equation 2.1 can be used to estimate the limit of RAP content at which it is still feasible to apply a softer bitumen. This is detailed in Figure 2.2. In this figure, you can see the application of the penetration rule in equation 2.1 for different percentages of RAP material. It is shown what the penetration of the new binder should be to achieve a penetration value of 40 and 60. Those two values are based on the type of mixture chosen in this study. For these asphalt concrete mixtures, a penetration value between 40 and 60 is targeted. Thus, these two values are an upper and lower limit.

Furthermore, a constant value for the penetration of the RAP binder is estimated and applied in the figure. This is done to show a general picture of how the penetration rule works. This value is equal to 22 and can be considered an average value for RAP binders.

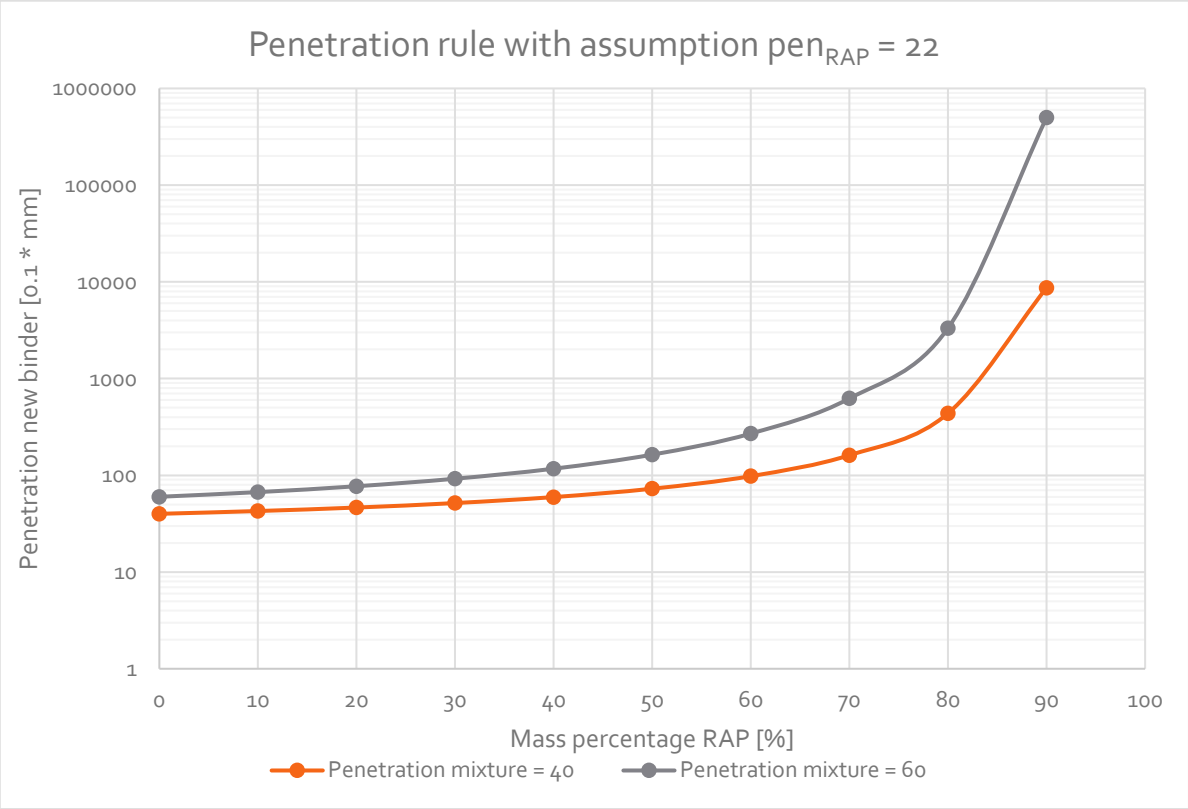

Figure 2.2: Estimation of penetration new binder according to the penetration rule

In Figure 2.2, it can be seen that the more RAP is applied, the softer the virgin bitumen should be. For lower percentages, this increase is small but for higher percentages of RAP the required penetration of the new binder increases significantly. The proportion of new binder is then so small that only a bitumen with an extremely high penetration grade can compensate for this.

In practice, the softest bitumen applied has a penetration grade of 160/220. From Figure 2.2 and equation 2.1, it becomes clear that with this bitumen grade it is possible to apply 55% to 70% RAP material so that the final penetration grade of bitumen in the mixture will be between 40 and 60. For higher percentages of RAP, it becomes infeasible to use a softer bitumen to soften the asphalt

mixture with RAP material such that a penetration between 40 and 60 is the end result. This corresponds to how the Netherlands deals with the application of RAP material as described in section 2.1.2. Until such time as it is practically feasible, it is preferable to use a softer bitumen to mitigate the effect of using RAP material. If this is not sufficient, a rejuvenator will be used in those cases. The point at which this is in Dutch practice corresponds to the point that emerged with the penetration rule.

Besides the type of bitumen, the quantity of the virgin binder has to be determined as well. For this, it is necessary to diminish the asphalt binder in the RAP materials from the virgin binder content (Al-Qadi et al., 2007). However, this can be difficult as it assumes how much old binder and new binder blend together. In the most mix design methods, a full blending scenario is assumed and the addition of new binder is thus assumed to be fully active (Tarsi et al., 2020).
Regarding the quantity of the rejuvenating additive, those are added according to the needed amount to the mixture. There is no standard procedure provided for mixing rejuvenating agent, but it is most common for it to be added directly to the hot mixture (Devulapali et al., 2019).

As for the RAP aggregates, they need to be heated to a lower temperature than the virgin aggregates in order to avoid burning of the aged binder. When the temperature of the virgin aggregates is namely applied, the binder around the recycled aggregates may burn. Furthermore, before applying the RAP aggregates in the mixture, the aggregates have to be examined for quality and gradations of the fractions. Also, the density of the aggregates has to be estimated to be able to determine the optimum proportion in the final mixture.

2.3 Performance of HMA mixtures containing RAP

The structural performance of asphalt mixtures can be influenced due to the application of RAP (Al-Qadi et al., 2012). Therefore, the performance of HMA mixtures containing RAP should be monitored. In general, asphalt with RAP materials has to meet the same requirements as new asphalt pavements (Tarsi et al., 2020). This means that the same performance criteria are set for the asphalt mixtures. Four different performance criteria are discussed: stiffness, resistance to fatigue, resistance to permanent deformation and water sensitivity.

2.3.1 Stiffness

The first material property that is influenced by using RAP instead of new asphalt concrete, is the stiffness of the final asphalt concrete mixture. This material property determines the load capacity of the asphalt. When applying RAP in the mixture, the stiffness will be higher because of the presence of aged binder in the asphalt concrete (Zaumanis et al., 2014). Because the binder is hardened over time, the RAP mixtures will have a higher stiffness. The ratio of asphaltenes to maltenes in the bitumen increases as the binder ages. As a result, the stiffness of the bitumen is higher (Zaumanis & Mallick, 2014).

The stiffness of the bitumen influences the stiffness of the final mixture containing RAP material and virgin material. How exactly the influence is, is still questioned. Some researches have shown

that there is a direct relation between RAP content and stiffness. However, other researches could not find such a direct relation (Tarsi et al., 2020).

According to Devulapali et al. (2019), the stiffness modulus will be higher when the RAP content is increased. However, more parameters may influence the stiffness modulus of the mixture. For example, a parameter which has a large influence on the stiffness increase, is the degree of blending between the virgin and aged bitumen as discussed in paragraph 2.1.2. Dependent on the blending rate, the variation of the increase in the stiffness of mixtures is great, especially for higher percentages of RAP material (Zaumanis & Mallick, 2014).

In general, the usage of RAP leads to a stiffness which is too high. A stiffness which is too high is undesirable because it could affect cracking resistance in a negative way (Al-Qadi et al., 2012; Milad et al., 2020). To mitigate the stiffness increase, there are mainly two options: the application of a softer binder or the application of a rejuvenating agent (Broere et al., 2016). Softer bitumen is mixed with the RAP binder, so that the desired hardness of the whole is obtained. However, this method is only applicable in mixtures till a certain percentage of RAP material (see paragraph 2.2). Rejuvenators have a softening effect on the asphalt mixtures. The rejuvenating agents can accelerate the diffusion of the aged binder in virgin binder, which leads to a lowering of the stiffness of the asphalt mixture with RAP material (Song et al., 2018). Earlier research of Dura Vermeer and KWS showed that for a mixture with 70% RAP the application of rejuvenators leads to lower stiffness values than a comparable asphalt mixture with softer bitumen (Van Oosterhout, 2017). Rejuvenators are further discussed in paragraph 2.4.

2.3.2 Resistance to fatigue

The fatigue resistance is the resistance to repetitive loading. Fatigue resistance is an important criterium in pavement design, because road structures are subjected to a repeated loading, such as traffic (Li et al., 2017). The influence on the fatigue resistance when using RAP and consequently a higher stiffness of the asphalt concrete is not fully clear. There are examples of researches that argue that the higher stiffness can cause fatigue damage, but other studies indicate that the fatigue resistance is higher when using RAP in the mixture (Zaumanis et al., 2014). The latter may be explained because the higher stiffness in the asphalt concrete leads to a decrease in tensile strain.

So, different studies show different results which makes it difficult to make clear the relation between usage of RAP and the fatigue resistance. Zaumanis and Mallick (2014) cite multiple studies for example that increasing the RAP content leads to a reduced fatigue cracking resistance of their asphalt mixture. This is explained by the fact that RAP leads to a more brittle behaviour of the mixture which may influence the fatigue resistance in a negative way. Devulapali et al. (2019) noted for example some decreasing results in the fatigue resistance of RAP mixtures.

Yousefi et al. (2021) claims however that RAP material increases the value of the release rate of critical strain energy which indicates a higher fatigue resistance. It is suggested that the RAP in

the mixture leads to a more elastic and stiffer behaviour which is positive for the fatigue resistance.
In the research of Farooq and Mir (2017) it is found that the fatigue resistance increases when the RAP content increases and it is claimed that asphalt mixtures with high levels of RAP show at least a similar performance of fatigue resistance in comparison with virgin mixtures. So, its conclusion is that fatigue needs not be a major problem when RAP is used.

The research of Lizárraga et al. (2018) confirms that the mixtures with RAP have a similar fatigue curve to mixtures with virgin materials, so fatigue can be monitored in the same way as it is done with virgin materials.

The application of rejuvenators leads to a slightly worse fatigue resistance than mixtures with the same RAP content but without rejuvenator according to the study of Dura Vermeer and KWS (Van Oosterhout, 2017). However, the ε_6-values suggested that the fatigue resistance is still high enough.

To summarize this performance criterium, inconsistent results have been reported regarding fatigue resistance for RAP mixtures. This is consistent with the conclusions of Al-Qadi et al. (2007).

2.3.3 Resistance to permanent deformation

The third performance indicator that is discussed, is the resistance to permanent deformation. This resistance is important because if this resistance would not be sufficient, it can lead to rutting behaviour of the pavement. This means that ruts in longitudinal direction can develop, leading to dangerous situations for the traffic.

Both the studies from Zaumanis et al. (2014) and from Tarsi et al. (2020), conclude that RAP in the asphalt mixture increases the rutting resistance of the pavement. This higher resistance is because of the aged binder. The binder hardens over age and is therefore harder than the virgin binder and less prone to rutting behaviour. However, recycling agents may be used in RAP pavements to soften the binder, so attention has to be paid that the binder does not soften too much because then rutting behaviour can still develop (Zaumanis et al., 2014).

Other researches confirm these aforementioned statements. The studies from Lu and Saleh (2016) and from Yousefi et al. (2021) show a positive correlation between rutting resistance and RAP content which is due to the high stiffness of the aged binder in the RAP. The increased stiffness in the mixture leads to a higher rutting resistance (Al-Qadi et al., 2007).

The resistance to permanent deformation can be negatively influenced by the binder content and the application of additives. Addition of extra binder to make the RAP mixture more workable leads to a decrease in rutting resistance, but the resistance is still higher in comparison with virgin mixtures (Lu & Saleh, 2016). The influence of additives is dependent on the kind of additives used. Some additives can have a positive effect on rutting resistance, while other have a negative effect

(Yousefi et al., 2021). So, this has to be monitored for the different additives. The research of Dura Vermeer and KWS showed that the rejuvenators soften the mixture leading to a lower rutting resistance (Van Oosterhout, 2017).

2.3.4 Water sensitivity

The last performance indicator that is discussed, is the water sensitivity. This indicator shows how sensitive the mixture is to water penetration. If this is the case, the water can cause severe damage to the mixture, named stripping. The bond between mastic and aggregate can namely weaken when water penetrates into the mixture between the mastic and the aggregate (Kandahl & Richards, 2001). If the resistance to water sensitivity is high enough, it means that the influence of water on the functional properties is small and the aforementioned internal bond stays strong enough. It is essential in pavement design, because it is directly related to the service-life of the pavement (Dinis-Almeida et al., 2016).

According to Lu and Saleh (2016), the water sensitivity in combination with RAP mixtures is something that is thought of differently. Some researchers argue that the water resistance increases when using RAP, while other researchers argue that the water resistance decreases when using RAP. In their own research, they concluded that the water sensitivity is decreased when RAP is applied.

However, in the study of Farooq and Mir (2017), it was found that the RAP material has a positive influence on the water sensitivity, but there are also some concerns. These are particularly in the use of additives. The application of additives may have a negative influence on the water sensitivity. Additives can also have a positive effect on the water resistance of the asphalt mixture. For example, the addition of rejuvenating agents led to a better water sensitivity in de study of Song et al. (2018). However, the research of Dura Vermeer and KWS showed that the water sensitivity is influenced negatively when rejuvenators are applied, which is because the rejuvenator softens the binder (Van Oosterhout, 2017).

In general, most studies conclude that penetration of water in the particles becomes less of a problem when RAP material is applied. This is because the RAP aggregates are already covered with asphalt, which minimizes the chance of penetration of water into the particles (Zaumanis & Mallick, 2014). Other studies (Al-Qadi et al., 2007) and (Devulapali et al., 2019) confirm that the performance of RAP mixtures regarding water sensitivity is at least equal to the performance of virgin mixtures.

2.3.5 Overview performance criteria

To conclude this paragraph, a brief summary is given of the findings regarding the performance of the HMA with RAP material considering the functional properties. The stiffness of the mixture increases when RAP material is applied. Because the binder is hardened over time, the RAP mixtures will have a higher stiffness. For fatigue behaviour, this relation is less clear. It seems that the RAP material has a positive influence on the fatigue resistance of the mixture but not all studies

are equivocal about this. The resistance to permanent deformation seems to retain good or even improve when RAP material is applied due to the aged binder. Regarding water sensitivity, the results are a little bit variable and ambiguous. Many parameters affect it, such as type and ageing of the binder and type and gradation of aggregates. However, multiple studies have shown that water sensitivity will not be a problem for RAP mixtures as the performance is at least equal to the performance of virgin mixtures.

Here, a nuance is needed because these statements are based on studies with different RAP content. Also, it depends on the bitumen parameters such as the penetration of the RAP binder, the penetration of the new binder and the bitumen content.

Because some material properties are influenced in a negative way, especially the stiffness increase, a search was made for alternatives that could eliminate these negative impacts. For that, additives are used to compensate those negative effects (Nazzal et al., 2015). In the following paragraph, this will be discussed.

2.4 Usage of additives/rejuvenators in asphalt mixtures with RAP material

Additives are essential in mixtures with high percentages of RAP, because they ensure that the rheological properties of the aged binder are restored (Al-Qadi et al., 2007). In particular, rejuvenators are often used in RAP mixtures abroad (Tran et al., 2012). This is because the old pavement is used, damaged and exposed to the natural environment. In this natural environment, the bitumen comes into contact with oxygen. Due to this contact, the oxidation process is initiated. This has as consequence that the bitumen in the pavement oxidizes over time. This means that the chemical composition of the bitumen changes (Tran et al., 2012). Chemically, bitumen consists of four main components: saturates, aromatics, resins and asphaltenes (SARA-fractions). Saturates, aromatics and resins can all be grouped in the maltenes fraction, so basically bitumen can be divided into two main groups: maltenes and asphaltenes (Hofko et al., 2015).

When the bitumen ages over time, it can be observed that the proportion of asphaltene fraction increases and that the proportion of maltene fraction decreases. Due to this relative change in asphaltene fraction and maltene fraction, the binder gets an increased gel structure (De Bock et al., 2020).

On binder level, the consequence is that the aged bitumen gets much stiffer compared with virgin bitumen (Yousefi et al., 2021). Moreover, the workability of the mixture decreases due to an increasing viscosity of the aged bitumen (Mogawer et al., 2012). As stated in paragraph 2.2, this can be countered by using a new softer bitumen to a certain limit. However, when using high levels of RAP, this may not be satisfied and the mixture stays too stiff and rejuvenators can be applied.

2.4.1 Operation and effect

Rejuvenators are additives from chemical or biological nature and those are added to the mixture aiming to rejuvenate the oxidized bitumen (Behnood, 2019). Then, the properties of the old bitumen are recovered in both physical and chemical way and are comparable with the original mixture (Tran et al., 2012). For example, the stiffness, which is increased due to ageing, decreases and the asphalt concrete will be more flexible again (Ongel & Hugener, 2015). However, the rejuvenator cannot undo the oxidation process of the bitumen, but it gives the opportunity to increase the RAP percentage in asphalt mixtures (Behnood, 2019). Further, it tries to make the bitumen more flexible again and improve the bonding between the binder and the aggregate (De Bock et al., 2020).

In general, there are three main effects of using rejuvenators that can be distinguished, based on the study of REjuveBIT (De Bock et al., 2020):

- Softening agent effect
- Effect of recycling in the chemical composition of the binder
- Effect of dispersant

Rejuvenating agents are commonly softening additives with a high content of light components (Behnood, 2019). Rejuvenators are mainly made of oils and due to the chemical composition of oil, rejuvenators will lower the viscosity of the aged binder to the desired value. The viscosity of the maltene fraction is lowered which leads to a lower viscosity of the binder as whole (Farooq et al., 2018). Thus, there occurs a softening effect, including a lubricating effect or a reduced friction and a wetting effect, leading to better workability.

The second distinguished effect is the effect of recycling in the chemical composition of the binder. This means that the share of SARA-fractions in the binder is redistributed. The maltenes fraction increases and the asphaltene fraction decreases so that the original balance returns. This can be done by rejuvenators because they have a lot of aromatics in it which are able to change the maltene fraction and asphaltene fraction (Brownridge, 2010).

The third effect is the effect of dispersant. This means that the rejuvenator is capable of breaking the bonds of asphaltenes as a consequence of oxidation. This leads to a mobilization of the aged bitumen (De Bock et al., 2020). The difference with the second mentioned effect is that that one changes the chemical composition of the bitumen while the last-mentioned effect reorders the components of the bitumen.

2.4.2 Categorization

To make a choice between all the different rejuvenators, it can be helpful to distinguish them in different groups. De Bock et al. (2020) has defined six different groups for rejuvenators, based on their source:

- aromatic extracts and naphthenic oils
- oils and fats from industrial activities
- oils and fats from food industry
- oils of organic origin
- engineered bio-based
- residual.

Those different groups are further explained below based on the study of De Bock et al. (2020). The first group is the aromatic extracts and naphthenic oils from the petrochemistry. This is gained by distillation of crude oil, which is the same as for the virgin bitumen itself. They are characterized by their presence of aromatics and decrease the viscosity of the aged binder. This may lead to a lower stiffness of the binder which is positive for the cracking resistance.

The second group is as well from the petrochemistry, but unlike the first group, this group is waste material from the industry instead of an originally manufactured agent, like group 1. Out of this waste material, some fractions can be recycled which are useful as rejuvenating agent. The function consists mainly of making the bitumen softer. The advantage of this group is that a waste product is used instead of a new product which is from a sustainability point of view valuable, because it cooperates in a circular economy.

The third group is waste group as well. The difference with group 2 is that this group is not derived from the petrochemistry but find their way out of vegetal or biological resources. Those are recycled cooking oils and fats from different categories, but they consist mainly of fatty acids. Its operations are mainly as a softener. The viscosity of the binder is decreased by applying this kind of rejuvenator. So, it does not rearrange the maltene and asphaltene fractions as described earlier.

The fourth group has the same kind of source as the third group, but it differs in the way that this group is not a waste group, but it is originally manufactured, just like group 1. This group finds its origin in the agriculture, which marks the difference with group 1. This group is not fossil, but it is renewable instead. These products consist mainly of fatty acids with biological origin. The agent acts primarily as a softener and lowers the viscosity of the binder. Furthermore, it can have a dispersant effect by which asphalt bonds are broken and the oxidation process is reversed.

The fifth group exists of bio-based engineered oils. So, it has a biological origin, just like group 3 and 4. However, this group finds its origin in tree woods and is made of crude tall oil. This exists of a mix of resin acids and fatty acids. The function is comparable with the fourth group. It acts as a softener and it has a dispersant effect on the aged binder.

The sixth and last group is a residual group. It is difficult to characterize this group because it exists of remaining agents which does not fit into one of the five previous groups. Due to this variety, it is hard to describe the function of this group uniformly, although the agents focus on softening the aged binder. Specific agents can have extra specifications but this is dependent on the agent.

To conclude the paragraph about additives and rejuvenating agents, it becomes clear that they can be useful in applying RAP material in asphalt mixtures. The RAP material consists of aged binder, which means that relative to the virgin bitumen, the asphaltene fraction in the binder has increased at the expense of the maltene fraction. The consequence on macro level is that the stiffness and viscosity increase and the workability decreases. The application of rejuvenators is an option to counteract this process so that the aged binder behaves like a virgin binder again. The rejuvenating agents focus on three different effects: softening effect, compensation effect and dispersant effect. Rejuvenators are available in a wide range. Therefore, it is important to categorize them in groups. This can be used to select the agent that is the most appropriate for the specific situation.

2.5 Micromechanical modelling of asphalt mixtures

To evaluate the functional properties of asphalt mixtures, laboratory tests are usually executed. The advantage of this is that these tests deliver reliable results, but it has as disadvantage that it is time consuming and labor intensive (Zhang et al., 2020a). Alternatively, models were developed to predict the functional properties of asphalt mixtures. A commonly used material parameter is the dynamic modulus. This indicates how stiff the material is and it is used in determining stress and strain. This means that it is an important parameter in designing pavements and can be related to the performance of the mixtures (Zhang et al., 2017). Therefore, the focus will be on micromechanical models predicting the mixture stiffness.

The advantage of micromechanical models is that besides the properties of the different parts in the mixture, also volumetric properties are considered. Because of this, the composite properties of the complete mixture can be better predicted. Furthermore, no calibration factor is needed which is a big advantage relative to other homogenization theories (Zhang et al., 2018a).

Different kind of models are available. Numerical models are based on finite element methods or discrete element methods and attempt to achieve the stress/strain field of each phase of the asphalt mixture (Zhang et al., 2020c). Those models can give reliable results, but a huge amount of finite or discrete elements are needed which requires powerful computational facilities and it takes a long time to get reliable results (Zhang et al., 2021b).

Analytical and semi-empirical micromechanical models can offer an alternative for this and can be of value in predicting properties of asphalt mixtures (Zhang et al., 2020a). Those models find their origin in the homogenization theory. This theory is discussed in the next section and after that, different types of micromechanical models are introduced.

2.5.1 Homogenization theory

Homogenization is the process where a composite mixture such as asphalt concrete with various parts in different phases, is homogenized to single effective properties (Zhang et al., 2018a). With the homogenization theory, the properties of the different composites are related to the properties of the mixture as whole. The input parameters for this theory are the mechanical properties of the different phases (aggregate, mastic and air voids) and the geometric properties or volume fractions of the different phases. A Representative Volume Element (RVE) is chosen which can describe the properties of the whole mixture. In this element, the volume fractions of the three phases sums up to unity.

Further, the average stress and average strain of the mixture can be determined with the average strain and average stress of each phase, as shown in equation 2.2-2.5 (Zhang et al., 2018a).

$$< \boldsymbol{\sigma} >_{\boldsymbol{m}} = \boldsymbol{C}^{*}_{\boldsymbol{m}} : < \boldsymbol{\varepsilon} >_{\boldsymbol{m}} \quad (2.2)$$

where: $<\sigma>_m$	=	average stress of the mastic phase	[N/mm²]
C^*_m	=	stiffness tensor of the mastic phase	[N/mm²]
$<\varepsilon>_m$	=	average strain of the mastic phase	[-]

$$< \boldsymbol{\sigma} >_{\boldsymbol{a}} = \boldsymbol{C}_{\boldsymbol{a}} : < \boldsymbol{\varepsilon} >_{\boldsymbol{a}} \quad (2.3)$$

where: $<\sigma>_a$	=	average stress of the aggregate phase	[N/mm²]
C_a	=	stiffness tensor of the aggregate phase	[N/mm²]
$<\varepsilon>_a$	=	average strain of the aggregate phase	[-]

$$< \boldsymbol{\sigma} >_{\boldsymbol{mix}} = \boldsymbol{f}_{\boldsymbol{m}} < \boldsymbol{\sigma} >_{\boldsymbol{m}} + \mathbf{f_a} < \boldsymbol{\sigma} >_{\boldsymbol{a}} + \mathbf{f_v} < \boldsymbol{\sigma} >_{\boldsymbol{v}} \quad (2.4)$$

where: $<\sigma>_{mix}$	=	average stress of the mix	[N/mm²]
f_m	=	volume fraction of the mastic phase	[-]
$<\sigma>_m$	=	average stress of the mastic phase	[N/mm²]
f_a	=	volume fraction of the aggregate phase	[-]
$<\sigma>_a$	=	average stress of the aggregate phase	[N/mm²]
f_v	=	volume fraction of the air void phase	[-]
$<\sigma>_v$	=	average stress of the air void phase	[N/mm²]

$$< \boldsymbol{\varepsilon} >_{\boldsymbol{mix}} = \boldsymbol{f_m} < \boldsymbol{\varepsilon} >_{\boldsymbol{m}} + \mathbf{f_a} < \boldsymbol{\varepsilon} >_{\boldsymbol{a}} + \mathbf{f_v} < \boldsymbol{\varepsilon} >_{\boldsymbol{v}} \quad (2.5)$$

where:	$<\varepsilon>_{mix}$	=	average strain of the mix	[-]
	f_m	=	volume fraction of the mastic phase	[-]
	$<\varepsilon>_m$	=	average strain of the mastic phase	[-]
	f_a	=	volume fraction of the aggregate phase	[-]
	$<\varepsilon>_a$	=	average strain of the aggregate phase	[-]
	f_v	=	volume fraction of the air void phase	[-]
	$<\varepsilon>_v$	=	average strain of the air void phase	[-]

Then, the effective stiffness tensor can be described by the average stress and average strain, shown in equation 2.6 (Zhang et al., 2018a).

$$< \boldsymbol{\sigma} >_{\boldsymbol{mix}} = \boldsymbol{C^*_{mix}} : < \boldsymbol{\varepsilon} >_{\boldsymbol{mix}} \quad (2.6)$$

where:	$<\sigma>_{mix}$	=	average stress of the mixture	[N/mm²]
	C^*_{mix}	=	stiffness tensor of the mixture	[N/mm²]
	$<\varepsilon>_{mix}$	=	average strain of the mixture	[-]

To determine the stiffness tensor, the strain localization tensors of the different phases are used. Those are defined in equation 2.7 - 2.9. (Zhang et al., 2018a).

$$< \boldsymbol{\varepsilon} >_{\boldsymbol{m}} = \boldsymbol{A_m} : < \boldsymbol{\varepsilon} >_{\boldsymbol{mix}} \quad (2.7)$$

where:	$<\varepsilon>_m$	=	average strain of the mastic phase	[-]
	A_m	=	strain localization tensor of the mastic phase	[N/mm²]
	$<\varepsilon>_{mix}$	=	average strain of the mixture	[-]

$$< \boldsymbol{\varepsilon} >_{\boldsymbol{a}} = \boldsymbol{A_a} : < \boldsymbol{\varepsilon} >_{\boldsymbol{mix}} \quad (2.8)$$

where:	$<\varepsilon>_a$	=	average strain of the aggregate phase	[-]
	A_a	=	strain localization tensor of the aggregate phase	[N/mm²]
	$<\varepsilon>_{mix}$	=	average strain of the mixture	[-]

$$< \boldsymbol{\varepsilon} >_{\boldsymbol{v}} = \boldsymbol{A_v} : < \boldsymbol{\varepsilon} >_{\boldsymbol{mix}} \quad (2.9)$$

where:	$<\varepsilon>_v$	=	average strain of the void phase	[-]
	A_v	=	strain localization tensor of the void phase	[N/mm²]
	$<\varepsilon>_{mix}$	=	average strain of the mixture	[-]

Combining equation 2.2-2.9, the stiffness tensor of the mixture can be determined according to equation 2.10.

$$\boldsymbol{C}^*_{\boldsymbol{mix}} = \boldsymbol{C}^*_{\boldsymbol{m}} + \boldsymbol{f}_{\boldsymbol{a}}(\boldsymbol{C}_{\boldsymbol{a}} - \boldsymbol{C}^*_{\boldsymbol{m}}) : \boldsymbol{A}_{\boldsymbol{a}} + \boldsymbol{f}_{\boldsymbol{v}}(-\boldsymbol{C}^*_{\boldsymbol{m}}) : \boldsymbol{A}_{\boldsymbol{v}} \quad (2.10)$$

where:	C^*_{mix}	=	stiffness tensor of the mixture	[N/mm²]
	C^*_m	=	stiffness tensor of the mastic phase	[N/mm²]
	f_a	=	volume fraction of the aggregate phase	[-]
	C_a	=	stiffness tensor of the aggregate phase	[N/mm²]
	A_a	=	strain localization tensor of the aggregate phase	[N/mm²]
	f_v	=	volume fraction of the air void phase	[-]
	A_v	=	strain localization tensor of the void phase	[N/mm²]

So, the strain localization tensor of the aggregate phase and the void phase are needed to determine the stiffness tensor of the asphalt mixture. Those two parameters are calculated using micromechanical models. Different types of those models are developed and this is discussed in the following section.

2.5.2 Types of micromechanical models

Micromechanical models to determine the mixture stiffness can mainly be divided into two different approaches: the geometry based approach and the bounds based approach (Zhang et al., 2020a). The bounds based approach is used to obtain a range of the stiffness with an upper bound and a lower bound. In this approach, there is no specific geometry of the composite in contrary to the geometry based approach. With this approach, the arrangements of the different phases are predefined. This can be done in two different ways: an arrangement of the phases in series and parallel or inclusions embedded into a matrix (Zhang et al., 2020a).

The models existing of a matrix and several types of inclusions embedded into this matrix are based on the Eshelby's solution. Examples of those continuum-based micromechanical models are the Dilute model, Mori-Tanaka model, Self-consistent model and the generalized self-consistent model (Zhang et al., 2021b). The advantage of this kind of models is that calibration factors are not required, but the Eshelby's solution is used to obtain the stiffness of the mixture (Zhang et al., 2020a).

Calibration factors are required in the type of models which exist of an arrangement of the phases in series and parallel. Examples of those models are Reuss model and the Hirsch model (Zhang et al., 2020a). The Hirsch model is a commonly used empirical model, which can easily be derived and implemented (Zhang et al., 2021a). This is because the application of the model requires only a few constituent properties (Zhang et al., 2018b).

Because of those advantages and that it is one of the most popular models for predicting the dynamic modulus, there is chosen to apply the Hirsch model in this study. Therefore, this model will be discussed in the next section.

2.5.3 Hirsch model

The Hirsch model is based on the law of mixtures which states that the stiffness of the composite is made up of the individual stiffnesses of each phase, taking into account the volume fractions and arrangement of each phase (Christensen Jr et al., 2003).

According to Christensen and Bonaquist (2015), the Hirsch model can be applied on mixtures with RAP material. However, as input it is necessary to know the modulus of the effective binder. This means that the modulus of the combined binder has to be measured. In this measurement, only the active binder that actually mixes with the RAP material is included.

2.5.3.1 Description of the Hirsch model

The Hirsch model assumes three different volume fractions to model the mixture: aggregates, mastic and air voids. Those volume fractions have their own material properties such as stiffness. Some of those volume fractions are in series and some are in parallel. So, for the case of asphalt concrete, there are aggregates, mastic and air voids in parallel and there are aggregates, mastic and air voids in series. This idea of volume fractions in parallel and series is schematically shown in Figure 2.3. In subfigure a, the parallel part can be seen and in subfigure b, the series part can be seen. This combined gives the basis for the Hirsch model in subfigure c.

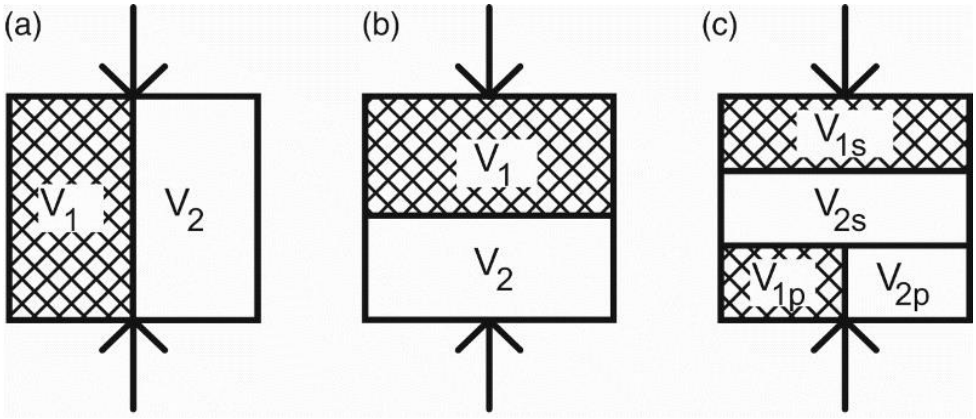

Figure 2.3: Schematic figure of parallel, series and combined model (Zhang et al., 2020b).

In a parallel system, the modulus of the system can be determined by summing the two moduli of each phase, as it can be seen in equation 2.11 (Zhang et al., 2020b).

$$\boldsymbol{E_c = \nu_1 * E_1 + \nu_2 * E_2} \quad (2.11)$$

where:	E_c	=	system modulus	[N/mm²]
	ν_1	=	volume fraction phase 1	[-]
	E_1	=	modulus phase 1	[N/mm²]
	ν_2	=	volume fraction phase 2	[-]
	E_2	=	modulus phase 2	[N/mm²]
	$\nu_1 + \nu_2$	=	1	

In a series system, the modulus of the system can be determined by taking the inverse of the sum of the inverses of the two moduli of each phase, as it can be seen in equation 2.12 (Zhang et al., 2020b).

$$\frac{\mathbf{1}}{\boldsymbol{E_c}} = \frac{\boldsymbol{\nu_1}}{\boldsymbol{E_1}} + \frac{\boldsymbol{\nu_2}}{\mathbf{E_2}} \tag{2.12}$$

where: E_c	=	system modulus	[N/mm²]
ν_1	=	volume fraction phase 1	[-]
E_1	=	modulus phase 1	[N/mm²]
ν_2	=	volume fraction phase 2	[-]
E_2	=	modulus phase 2	[N/mm²]
$\nu_1 + \nu_2$	=	1	

Zhang et al. (2020b) combined equation 2.11 and 2.12 to predict the modulus of the combined system as shown in Figure 2.3(c). This is given in equation 2.13.

$$\frac{\mathbf{1}}{\boldsymbol{E_c}} = \frac{\boldsymbol{\nu_{1,s}}}{\boldsymbol{E_1}} + \frac{\boldsymbol{\nu_{2,s}}}{\mathbf{E_2}} + \frac{\left(\boldsymbol{\nu_{1,p}} + \boldsymbol{\nu_{2,p}}\right)^{\mathbf{2}}}{\boldsymbol{\nu_{1,p}} * \boldsymbol{E_1} + \boldsymbol{\nu_{2,p}} * \boldsymbol{E_2}} \tag{2.13}$$

where: E_c	=	system modulus	[N/mm²]
$\nu_{1,s}$	=	volume fraction phase 1 series	[-]
E_1	=	modulus phase 1	[N/mm²]
$\nu_{2,s}$	=	volume fraction phase 2 series	[-]
E_2	=	modulus phase 2	[N/mm²]
$\nu_{1,p}$	=	volume fraction phase 1 parallel	[-]
$\nu_{2,p}$	=	volume fraction phase 2 parallel	[-]
$\nu_{1,s} + \nu_{2,s} + \nu_{1,p} + \nu_{2p}$	=	1	

The combination of different phases in series and parallel arrangement form the basis of the Hirsch model. Christensen Jr et al. (2003) adapted the elastic Hirsch model and made the best combination of series and parallel, making it appropriate for asphalt mixtures. This original Hirsch model shows pretty accurate results (Zhang et al., 2018b). The original Hirsch model is shown in Figure 2.4.

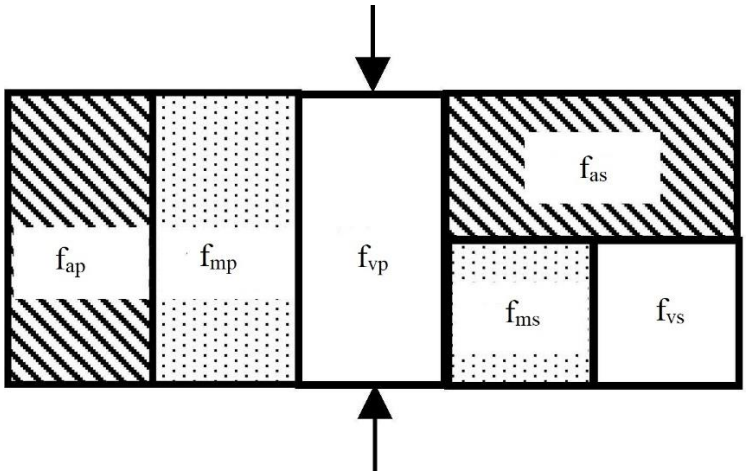

Figure 2.4: Schematic figure of the original Hirsch model (Zhang et al., 2020b)

In Figure 2.4, it can be seen that the model exists of three phases: aggregate, mastic and air voids. Those three phases have its own stiffness and occur partly in series and partly in parallel.

The matching equation for the model in Figure 2.4 is a combination of the above mentioned equations (equation 2.11 – 2.13) and is given in equation 2.14 (Christensen Jr et al., 2003).

$$|\boldsymbol{E}^*|_{\boldsymbol{mix}} = \mathbf{f_{ap}} * \mathbf{E_a} + \mathbf{f_{mp}} * \mathbf{E_m} + (\mathbf{f_{as}} + \mathbf{f_{ms}} + \mathbf{f_{vs}})^{\mathbf{2}} * (\frac{\mathbf{f_{as}}}{\boldsymbol{E_a}} + \frac{(\boldsymbol{f_{ms}} + \boldsymbol{f_{vs}})^{\mathbf{2}}}{\boldsymbol{f_{ms}} * \boldsymbol{E_m}}) \quad (2.14)$$

where: $\lvert E^*\rvert_{mix}$	=	dynamic complex modulus of the mixture	[N/mm²]
f_{ap}	=	volume fraction aggregate parallel	[-]
E_a	=	modulus of aggregate	[N/mm²]
f_{mp}	=	volume fraction asphalt mastic parallel	[-]
E_m	=	modulus of mastic	[N/mm²]
f_{as}	=	volume fraction aggregate series	[-]
f_{ms}	=	volume fraction asphalt mastic series	[-]
f_{vs}	=	volume fraction air voids series	[-]

However, it is difficult to determine the parallel and series volume fractions of the individual phases by material tests (Zhang et al., 2018b). Therefore, the model is modified by the introduction of a contact factor (P_c), which describes the ratio of the parallel volume fraction to the whole volume fraction (Christensen Jr et al., 2003). This factor is a critical parameter in the model and it determines which part best can described in parallel (P_c) and which part best can described in series (1-P_c) (Zhang et al., 2018b). The value of P_c is the same for all phases, so it is assumed that the ratio of parallel volume fraction and series volume fraction is the same for all three phases in the model.

Further, the mastic phase is replaced by a binder phase. This should almost give the same results (Zhang et al., 2020b). Then, the Young's modulus of the binder can be replaced by the dynamic

shear modulus of the binder, making use of Poisson's ratio. This has the advantage that the shear modulus can be easily determined with the dynamic shear rheometer during material testing.

Those two modifications have been implemented, which is shown in equation 2.15 (Christensen Jr et al., 2003).

$$|E^*|_{mix} = P_c * \left[29400 * \left(1 - \frac{VMA}{100}\right) + 3 * |G^*|_{binder} * \left(\frac{VFA * VMA}{10000}\right)\right] + (1 - P_c) * \left(\frac{1 - \frac{VMA}{100}}{29400} + \frac{VMA}{3 * VFA * |G^*|_{binder}}\right)^{-1} \quad (2.15)$$

where: $|E^*|_{mix}$ = dynamic complex modulus mixture [N/mm²]
P_c = contact factor [-]
VMA = voids in mineral aggregate [%]
$|G^*|_{binder}$ = dynamic complex modulus binder [N/mm²]
VFA = voids filled with asphalt [%]

In equation 2.15, P_c is used. A empirically found expression for P_c, which provide the best results, is shown in equation 2.16 (Christensen Jr et al., 2003).

$$P_c = \frac{\left(0.138 + \frac{VFA * 3 * |G^*|_{binder}}{VMA}\right)^{0.58}}{36.2 + \left(\frac{VFA * 3 * |G^*|_{binder}}{VMA}\right)^{0.58}} \quad (2.16)$$

where: P_c = contact factor [-]
VMA = voids in mineral aggregate [%]
$|G^*|_{binder}$ = dynamic complex modulus binder [N/mm²]
VFA = voids filled with bitumen [%]

From equation 2.15 and 2.16, it becomes clear how the dynamic complex modulus is predicted based on the Hirsch model. For this, only three parameters of the mixture are needed: the dynamic complex modulus of the binder, the percentage voids in mineral aggregate (VMA) and the percentage voids filled with bitumen (VFA).
The VMA and VFA can be calculated using equation 2.17 and 2.18.

$$VMA = 100 - \frac{\rho_{mb} * P_s}{\rho_{sb}} \quad (2.17)$$

where: VMA = voids in mineral aggregate [%]
ρ_{mb} = bulk density mixture [kg/m³]
P_s = mass percentage aggregate [%]
ρ_{sb} = bulk density aggregate [kg/m³]

$$VFA = 100 * \frac{VMA - V_a}{VMA} \quad (2.18)$$

where: VFA = voids filled with bitumen [%]
VMA = voids in mineral aggregate [%]
V_a = volume percentage air voids [%]

Equation 2.17 and 2.18 show that to calculate the VFA and VMA, the volume of the air voids, the bulk density of the mixture, the mass proportion of the aggregate and the bulk density of the aggregate must be known.

2.5.3.2 Simplified Hirsch model

Equation 2.14 can be modified for simplicity and practically reasons. It was found that the influence of the phases in series is much smaller than the influence of the phases in parallel. Therefore, Christensen and Bonaquist (2015) proposed a simplification in which only the parallel part is included. This simplified model is shown in Figure 2.5.

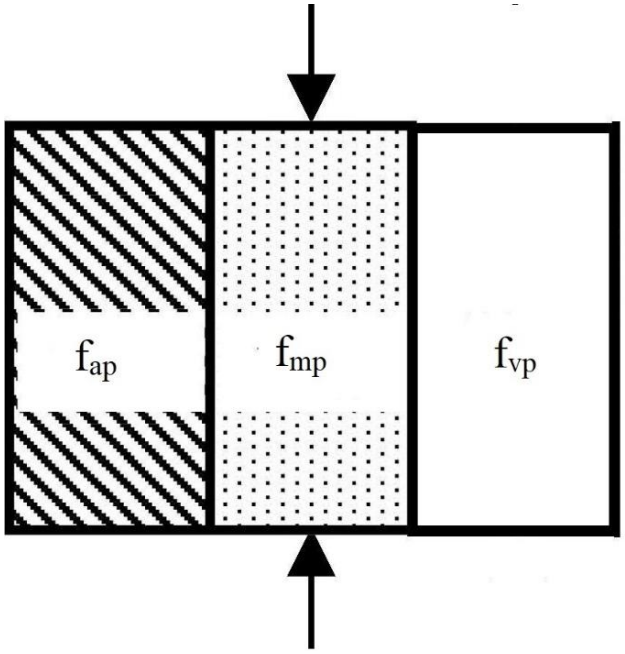

Figure 2.5: Schematic figure of the simplified Hirsch model

Neglecting the series part of the model and replacing the mastic phase with the binder phase leads to a simplification of equation 2.14. This simplified equation is shown in equation 2.19.

$$|\boldsymbol{E^*}|_{\boldsymbol{mix}} = \boldsymbol{f_{ap}} * \boldsymbol{E_a} + \boldsymbol{f_{bp}} * \mathbf{2} * (\mathbf{1} + \boldsymbol{\nu}) * |\boldsymbol{G^*}|_{\boldsymbol{binder}}$$

(2.19)

where:	$\lvert E^* \rvert_{mix}$	=	dynamic complex modulus of the mixture	[N/mm²]
	f_{ap}	=	volume fraction aggregate parallel	[-]
	E_a	=	modulus of aggregate	[N/mm²]
	f_{bp}	=	volume fraction asphalt binder parallel	[-]
	ν	=	Poisson's ratio binder	[-]
	$\lvert G^* \rvert_{binder}$	=	complex shear modulus binder	[N/mm²]

Likewise the original Hirsch model, P_c is introduced and equation 2.19 has been adapted. The result is shown in equation 2.20.

$$|\boldsymbol{E^*}|_{\boldsymbol{mix}} = \boldsymbol{P_c} * (\boldsymbol{f_a} * \boldsymbol{E_a} + \boldsymbol{f_b} * \mathbf{2} * (\mathbf{1} + \boldsymbol{\nu}) * |\boldsymbol{G^*}|_{\boldsymbol{binder}})$$

(2.20)

where:	$\lvert E^* \rvert_{mix}$	=	dynamic complex modulus of the mixture	[N/mm²]
	P_c	=	contact factor	[-]
	f_a	=	volume fraction aggregate	[-]
	E_a	=	modulus of aggregate	[N/mm²]
	f_b	=	volume fraction asphalt binder	[-]
	ν	=	Poisson's ratio binder	[-]
	$\lvert G^* \rvert_{binder}$	=	complex shear modulus binder	[N/mm²]

Since the behaviour of asphalt concrete is dependent on frequency/temperature, the ratio of parallel volume fraction and series volume fraction is dependent on frequency/temperature as well (Zhang et al., 2018b). At lower temperature, the stiffness of the binder increases. This leads to a higher value of P_c. Then, the system behaves mostly as a parallel system. At higher temperatures, the binder will be more viscous and the stiffness will be lower. This leads to a lower value of P_c and the system behaves mostly as a series system. The aggregates and the binder behave next to each other and there is little interaction between the two parts.

2.5.3.3 Modified Hirsch model with inclusion of aggregate organization factor

A modified version has been proposed with the introduction of the aggregate organization factor (P_a), as alternative for P_c (Zhang et al., 2018b). This is because it is difficult to interpret P_c physically and the aggregate contact interaction is not taken into account in an appropriate manner. P_a describes the input to the mixture stiffness from the arrangement of the aggregate particles (equation 2.21).

Figure 2.6 shows the corresponding model. It is similar to the simplified Hirsch model in Figure 2.5, except that instead of parallel volume fractions, the full volume fraction is applied.

$$|E^*|_{mix} = P_a * f_a * E_a + f_b * 2 * (1 + \nu) * |G^*|_{binder} \quad (2.21)$$

where: $|E^*|_{mix}$ = dynamic complex modulus mixture [N/mm²]
P_a = aggregate organization factor [-]
f_a = volume fraction aggregate [-]
E_a = Young's modulus aggregate [N/mm²]
f_b = volume fraction binder [-]
ν = Poisson's ratio binder [-]
$|G^*|_{binder}$ = complex shear modulus binder [N/mm²]

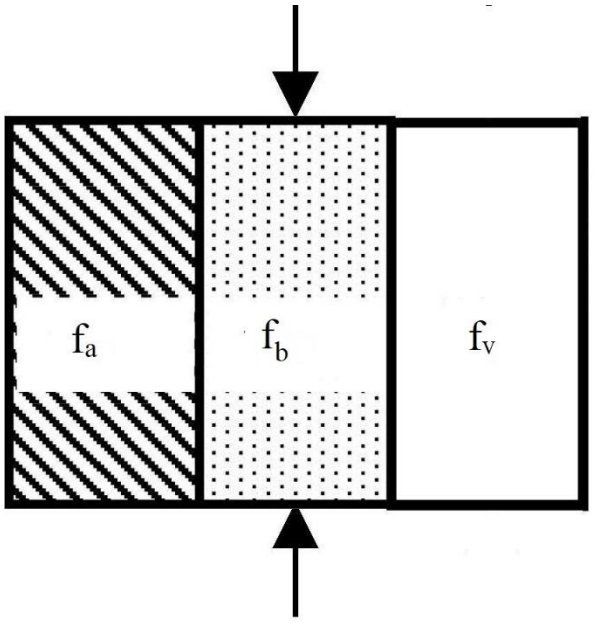

Figure 2.6: Simplified Hirsch model with inclusion of P_a

P_a indicates the structure of the aggregates in the mixture. A higher value suggests that the entire structure will cooperate in the bearing capacity due to a stiff asphalt binder which is able to properly bond the particles to each other. A lower value suggests that the asphalt binder will not participate, because the binder would be too soft to bind the particles to each other and the mixture has a low bearing capacity.

In the study of Zhang et al. (2018b), a function of was determined to calculate P_a. A sigmoidal curve was assumed and the parameters a, b, c and d were used to fit the function to the test results. The expression of P_a is given in equation 2.22 and the fitted parameters are given in Table 2.1 (Zhang et al., 2018b).

$$P_a = a + (1 - a) * \frac{e^{b+c*ln\left(\frac{f_b}{f_b+f_v}*|G^*|_b\right)+d*(f_b+f_v)}}{1 + e^{b+c*ln\left(\frac{f_b}{f_b+f_v}*|G^*|_b\right)+d*(f_b+f_v)}} \quad (2.22)$$

where: P_a = aggregate organization factor [-]
f_b = volume fraction binder [-]
f_v = volume fraction air voids [-]
$|G^*|_b$ = complex shear modulus binder [N/mm²]
a, b, c, d = fitting parameters [-]

Table 2.1: Fitting parameters (Zhang et al., 2018b)

Parameters	a	b	c	d
Values	0.0017	0.62	0.72	-0.17

Equation 2.22 was fitted into the test results of an open graded mixture without RAP. This means that the fitting parameters made the model suitable for open graded mixtures. The obtained expression for P_a can only be applied on mixtures for which is it calibrated (Zhang et al., 2018b). Because the used asphalt mixtures in this study differ in gradation and the usage of RAP and rejuvenator with the used mixture for fitting the parameters, it can be expected that the values for the fitting parameters in Table 2.1 do not satisfy. Then, the model may be less accurate.

3 Materials and Methodology

In this chapter, the materials and methodology are considered. Firstly, the used materials are discussed and then the composition of the tested mixtures is addressed. After that, the methodology of this research is explained and the functional tests are described.

3.1 Used materials

3.1.1 RAP material

The RAP material is extracted by milling old asphalt. This old asphalt is transported from the site towards the factory where it is processed. RAP material can vary greatly in material properties, composition and density. To exclude this influence, it is decided to work with a single batch of RAP material. Then, the different mixtures can easier be compared with each other.

Once the RAP material is arrived at the asphalt production site, it is fully dried before it can be processed further. After it is dried, it can be used for testing. A sample of the material is used for the binder research to characterize the aged binder. For this purpose, the aged bitumen is extracted from the RAP material. The bitumen content of the RAP material can then be determined as well. The used batch of RAP material has a bitumen content of 4.9%.

All other RAP material can be used to produce asphalt mixtures. Before the samples can be prepared, which is explained in paragraph 3.1.4, the material must first be sieved. The material is divided into three different fractions: larger than 16 mm, between 8 and 16 mm and smaller than 8 mm.

As indicated in the introduction, mixtures with two different percentages of RAP material are studied. Firstly, a mixture with 65% RAP is used as reference, because of the wide experience with this content. Secondly, mixtures with 80% RAP are tested to study the possibilities to increase the rate of reuse with the application of rejuvenators.

3.1.2 Bitumen

The bitumen that is used in the mixtures and the binder tests, is a combination of aged bitumen from the RAP material and virgin bitumen. The goal for the mixture is to have a penetration value between 40 and 60. To achieve this for the mixture with 65% RAP without rejuvenator, a very soft binder is used, namely with grade 160/220. This is based on the penetration rule (equation 2.1). Using this equation with the assumption that the penetration of the RAP binder is 22 and using 190 as value for the penetration of the new binder, the result is a penetration for the mixture of 46.8. This value satisfies the criterium for the penetration of the mixture between 40 and 60.

A lower viscosity is expected for the mixtures with rejuvenators. Therefore, for those mixtures, a more common bitumen is used, namely grade 70/100. For the 80% RAP mixture without rejuvenators, this bitumen grade is used as well. This is because then a good comparison can be

made between the mixtures to evaluate the influence of the rejuvenator. It should be noted that the penetration rule is thus not applied to the 80% RAP mixture without rejuvenator. On this basis, a very soft bitumen should be added. However, the preference is given to make such a pure comparison between the 80% RAP mixture without and with rejuvenator. Therefore, the mixture is kept the same in all other respects.

The proportion of new bitumen is small, because the proportion of RAP material, and therefore the amount of aged binder, is very high in this study. In addition, the RAP material has a higher bitumen content than the desired bitumen content of the final mixture. So, to reach this desired bitumen content, only a small percentage new binder has to be added. The compositions at the binder level for the different variants are shown in Appendix A and the composition at mixture level is shown in Appendix B. The exact mixture composition is further discussed in paragraph 3.1.4.

3.1.3 Rejuvenators/additive

For the selection of the rejuvenators, it is considered that the rejuvenating agent is available so that it can be applied in the mixtures. Further, it is taken into account that the rejuvenators are not too similar. This is to make clear the differences between the rejuvenators and its operation. So, a choice is made for rejuvenators which work all differently. Three different rejuvenators and one viscosity reducing additive are chosen to apply on binder level. Those rejuvenators and additive are addressed below and their application is explained.

3.1.3.1 Regenis 50

Regenis 50 is a rejuvenator supplied by Total (Total Nederland N.V., 2008). Using the categorization in paragraph 2.4.2, it is placed in the group of aromatic extracts and naphthenic oils, because it is extracted in a similar way to bitumen. It is directly added in the bitumen tank. After that, it is mixed with the bitumen and then it is further processed in the asphalt mixture. According to Van den Bergh et al. (2021a), the rejuvenator leads to an increase in workability. Furthermore, the asphalt mixture becomes softer and the water sensitivity increases. This improved performance is gained without compromising on resistance to permanent deformation and stiffness. Van den Bergh et al. (2021a) reported that the added quantity of this rejuvenator is around 0.65 %, which is significantly higher than the other rejuvenators. This is because Regenis 50 is a quite viscous rejuvenator in comparison with others.

3.1.3.2 Ravasol RAP-5V

Ravasol RAP-5V is a rejuvenator supplied by Ravago Chemicals (Ravago Chemicals, 2021). It is vegetal based, so it is placed in one of the bio-based categories. This rejuvenator is added directly to the bitumen tank and then mixed with the bitumen before it is mixed with the asphalt mixture. The added quantity of the Ravasol RAP-5V is between 0.05% and 0.1% of the mixture. Application of this rejuvenator leads to an improvement of the workability of the mixture (Van den Bergh et al., 2021b). The authors also reported that the overall stiffness of the mixture marginally decreased. Other performance indicators such as water sensitivity, resistance to fatigue and resistance to permanent deformation, did not change.

3.1.3.3 Neomex HR

Neomex HR is a rejuvenator supplied by Latexfalt (Latexfalt, 2022). It exists of biological components, so it is categorized in one of the bio-based groups. Unlike the two previously mentioned rejuvenators, this agent is not added via the bitumen tank. Instead, it is directly added via a tube in the mixer. This has the consequence that the amount of rejuvenator was added on top of the amount of virgin bitumen and that this amount was not deducted from the new bitumen, as had been done for the previous two rejuvenators. The relevant amount of Neomex HR is between 0.1% and 0.15% of the mixture. Furthermore, Van den Bergh et al. (2021c) reported that the workability of the mixture increases when the rejuvenator was added. Furthermore, it is concluded that the ITS value decreases for both conditions when applying the rejuvenating agent. The water sensitivity, measured with ITSR value, stays the same. This is also the case for the resistance to permanent deformation.

3.1.3.4 Cecabase RWI

Cecabase RWI is a viscosity reducing additive supplied by the chemical company Arkema (Arkema, 2022). Adding this additive to the asphalt mixture, is possible in different ways. An option is to add it to the bitumen tank and then mix it with the bitumen. The other option is to add the agent at the mixing part by injecting into the bitumen in line or spraying it on the RAP. Regarding the dose, it depends on the specific case, but as guidance a range can be taken between 0.15% and 0.20% (Arkema, 2021).

This additive should increase the workability of the mixture. Furthermore, it performs better in terms of cracking resistance and other performance indicators are not influenced negatively (Arkema, 2021). This indicates that Cecabase RWI is an additive indeed and not a true rejuvenator. It acts as a softening agent which leads to a better workability. However, the influence of the additive on material properties seems small.

3.1.4 Mixture Composition

For the mixture, it is chosen to focus on the base/binder layer of an asphalt pavement. Those mixtures are less critical, which makes it easier to apply higher percentages of RAP material. Furthermore, a choice has been made for a densely graded asphalt mixture, because for this type of mixture, a higher percentage of RAP can be applied.
In a short way, there is chosen for AC 16 Bin/Base 40/60, where

AC	=	Asphalt Concrete	
16	=	the upper limit of the applied aggregate size	[mm]
bin/base	=	binder or base layer	
40/60	=	range of penetration of the bitumen	[0.1 * mm]

The desired bitumen content of this mixture is 4.3% (m/m) and the target density is 2390 kg/m^3. Furthermore, the focus is on hot mix asphalt, so the mixing temperature is set on 165 °C.
On the base of those requirements, the optimal mix composition is determined. This also incorporates the fact that the bitumen content of the RAP material is 4.9%, which means that less

new bitumen is added to achieve the desired bitumen content. For all four tested mixtures, the used mix composition is shown in Appendix B.

It becomes clear that the mixture does not vary in essence because the same mix design is applied on all mixtures. The variation between the mixtures is in the amount of RAP applied and the rejuvenating additive used. Furthermore, the dosage of the additives, 0.16%, is kept as similar as possible in order to be able to make a good comparison between the different mixtures.

3.1.4.1 Sample preparation

The starting point for making the samples is the mix design, as discussed in the previous section. Firstly, the new aggregates and RAP aggregates are sieved so that the proper proportions of each fraction can be weighed. After that, all the components are heated to the right temperature. For this, the standard temperatures are used. This means that the aggregates are heated to the mixing temperature of 165 °C and the bitumen is brought up to temperature depending on the grade (145 °C for bitumen 160/220 and 165 °C for bitumen 70/100). According to the procedure standard, the RAP material has to be heated for 4 hours.

After this heating time, the components are put together in the mixer, starting with the new aggregates, followed by the first half of the RAP material, the filler and the second half of the RAP material. Finally, the bitumen and the rejuvenating agent are added. After mixing for 6 minutes, the mixture is compacted to a square plate of 500 mm length and width and a height of 90 mm. For this, a slab compactor is used. An example of such a compactor is shown in Figure 3.1.

Figure 3.1: Example of a slab compactor (Mastrad Limited, n.d.)

After the slab is cooled down, it can be used to cut out the samples: beams for the four point bending test and cylindrical specimens for the cyclic indirect tensile test. The dimensions of the

beams are 50 mm x 50 mm x 450 mm. The dimensions of the cylindrical specimens are 40 mm height and 100 mm diameter.

For the indirect tensile test and the triaxial cyclic compression test, gyratory specimens are used. The same mixer is used as when making plates, but in this case the gyratory machine is used as compactor. This machine is shown in Figure 3.2.

Figure 3.2: Gyratory machine

Eight samples are made for measuring water sensitivity, six samples are made for the triaxial cyclic compression test and four samples are made for fracture toughness. The diameter of those specimens is 100 mm and they are compacted with a gyratory until the height is equal to 77 mm. After that, the specimens are cut and polished to the right height: 50 mm for the indirect tensile test and 60 mm for the triaxial cyclic compression test.

3.2 Research methodology

The research methodology is summarized in a flow chart shown in Figure 3.3. The research starts with an identification of the functional tests to characterize asphalt mixtures with high RAP percentages, split in binder level and mixture level. The test at binder level is also used to select and reject the rejuvenators which are applied at mixture level. The results of the tests are evaluated and from that, a coupling is made with the micromechanical model to make a prediction.

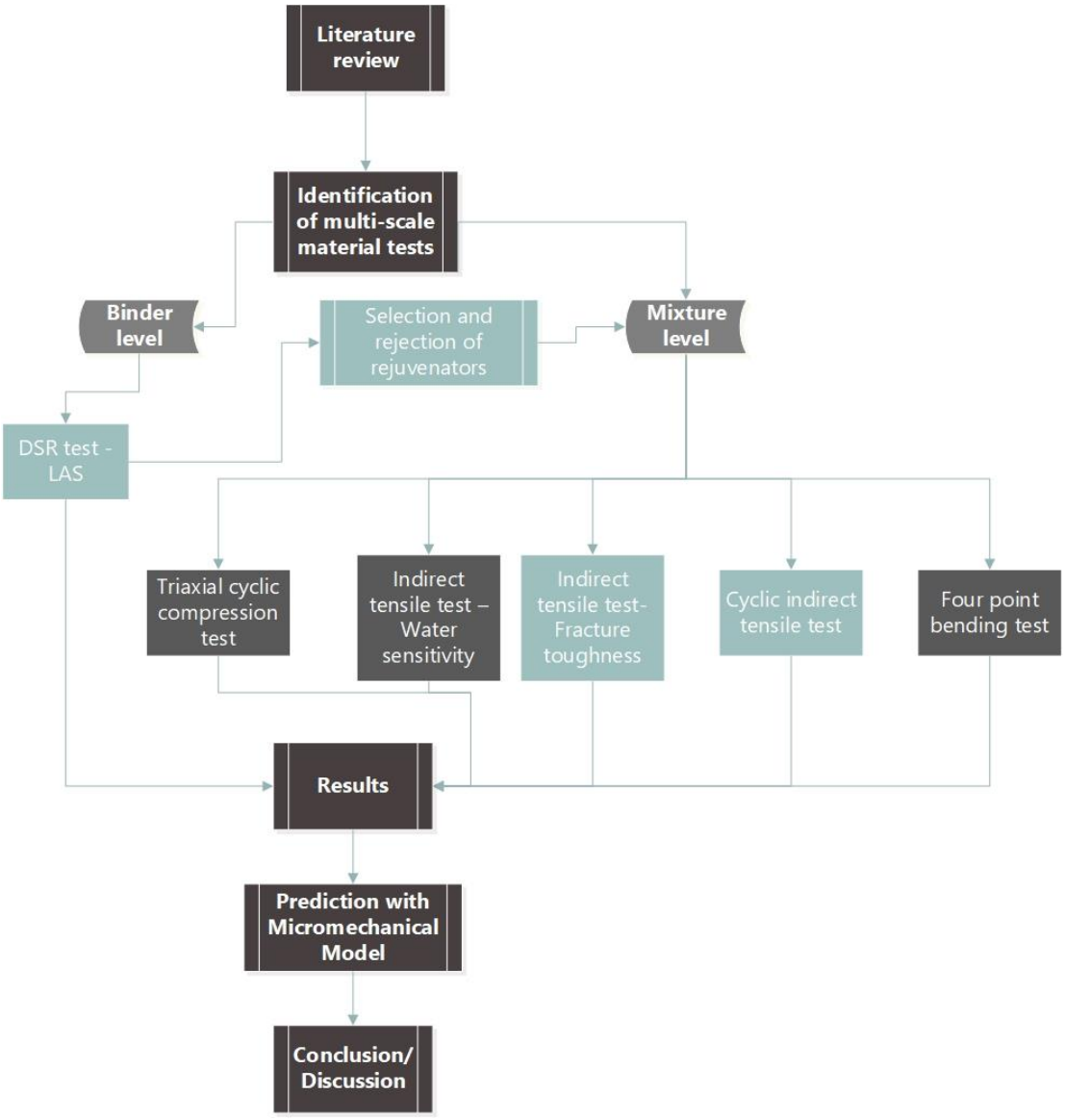

Figure 3.3: Flow chart of research methodology

3.2.1 Experimental campaign

The experimental campaign exists of two different levels of scale. A start is made with the test at bitumen level so that it can yield as selection moment for the rejuvenators. Six different binder compositions are tested as this level. These compositions vary in the added rejuvenator and a reference is tested without RAP binder. The variants are given in Table 3.1.

Table 3.1: Variants of bitumen tests

Variant	RAP [%]	Rejuvenator/additive
1	0	No
2	80	No
3	80	Regenis 50
4	80	Cecabase RWI
5	80	Neomex HR
6	80	Ravasol RAP-5V

At mixture level, only two rejuvenators are tested because there is limited time and preference is given to evaluate the mixtures on multiple material properties. The selection of the rejuvenators is based on the results of the bitumen tests. The additives that show the best results based on the bitumen tests are included for the mixture tests.

In chapter 4, the results of the bitumen tests are discussed, which means that the results are unknown at this point. The chosen rejuvenators are applied to the mixtures with 80% RAP. Besides that, a reference mixture will be tested with 65% RAP and a reference mixture of 80% RAP. All variants can be found in Table 3.2. With those variants, the functional tests at mixture level are done.

Table 3.2: Variants of mixture tests

Variant	RAP [%]	Rejuvenator/additive
1	65	No
2	80	No
3	80	Yes, rejuvenator 1
4	80	Yes, rejuvenator 2

The experimental campaign is graphically shown in Figure 3.4. Here, a detailed flow chart of all the executed experiments is shown, split in binder level and mixture level. At binder level, a dynamic shear rheometer (DSR) device will be used to determine the stiffness and fatigue resistance of the binder. The linear amplitude sweep (LAS) method is used for this purpose. The test is done multiple times when simulating short-term ageing with rolling thin film oven test (RTFOT) and long-term ageing with the pressure ageing vessel (PAV)-test.

At mixture level, the functional tests for the type test are done: the triaxial cyclic compression test to determine the resistance to permanent deformation, the indirect tensile test (ITT) to determine water sensitivity, and the four point bending test to determine the stiffness of the mixture. Regarding the four point bending test, the fatigue test is excluded. This is because this test is time intensive for which there is not enough time. Further, additional tests are done to gain extra information about the behaviour of the asphalt mixtures. Those tests are the cyclic indirect tensile test to determine stiffness and fatigue resistance and the ITT to determine fracture toughness.

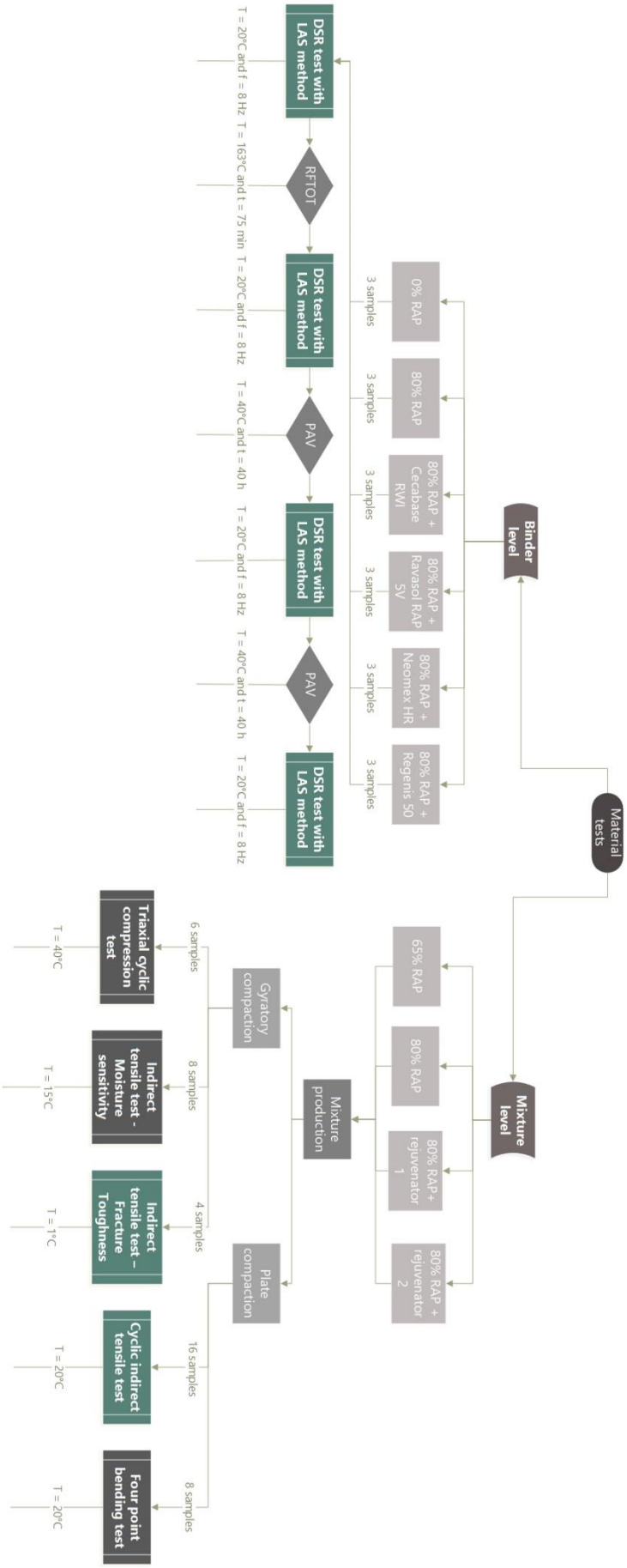

Figure 3.4: Flow chart experimental campaign

Table 3.3 shows which mixtures are executed for which tests and how many specimens are used for them. From the table, it should be noted that the 80% RAP mixture without additive is not tested with the four point bending test, which is due to material limitations. Due to execution conditions, the number of samples tested is divergent for the 80% RAP mixture regarding the cyclic ITT measuring the stiffness and for the 65% RAP mixture regarding the four point bending test.

Table 3.3: Experimental campaign mixture level

RAP percentage Rejuvenator	65 % No	80 % No	80 % Rejuvenator 1	80 % Rejuvenator 2
Triaxial cyclic compression test	✓	✓	✓	✓
Number of samples	4	4	4	4
Indirect tensile test – Moisture sensitivity	✓	✓	✓	✓
Number of samples	8	8	8	8
Indirect tensile test – Fracture toughness	✓	✓	✓	✓
Number of samples	4	4	4	4
Cyclic indirect tensile test – Stiffness	✓	✓	✓	✓
Number of samples	9	8	9	9
Cyclic indirect tensile test – Fatigue	✓	✓	✓	✓
Number of samples	9	9	9	9
Four point bending test – Stiffness	✓	×	✓	✓
Number of samples	7	-	8	8

3.2.2 Functional Tests

To evaluate the material properties of asphalt mixtures with high RAP percentages, performance based tests are done. A lot of different functional tests are possible to test the asphalt mixture. As earlier discussed, the functional tests for the type tests are done and some additional tests to gain extra information about the behaviour of the asphalt mixtures. All tests are executed following the European Standards and procedure 62 out of the Standaard RAW bepalingen 2020.
In this section, all used functional tests are described.

3.2.2.1 Dynamic Shear Rheometer (DSR)

The Dynamic Shear Rheometer (DSR) is a device which can measure the rheological properties of the bitumen. The used device can be seen in Figure 3.5.

Figure 3.5: DSR device

With this device it is possible to determine the complex shear modulus ($|G^*|$) of the binder. This is the ratio of the peak stress to the peak strain. Besides that, the phase angle (δ) can be determined. This is defined as the phase difference between stress and strain.

The test procedure is described in the European standard NEN-EN 14770:2012 (2012). A schematic layout of the test can be seen in Figure 3.6. It can be seen that a small amount of bitumen is placed between two parallel circular plates. The lower plate is fixed while the upper plate is loaded with a torque leading to shear stress in the bitumen.

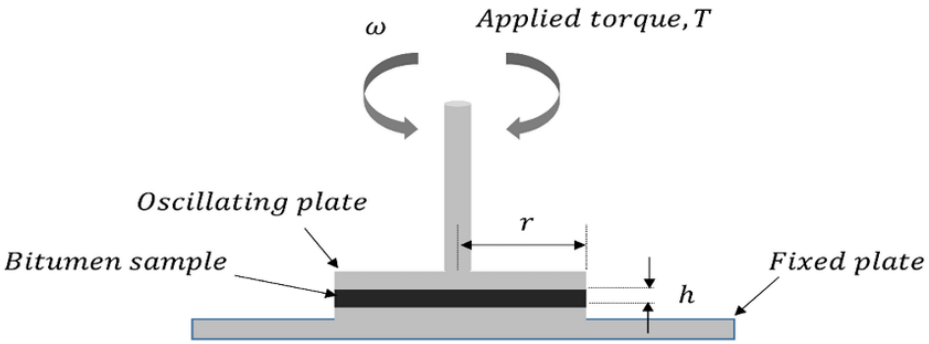

Figure 3.6: Schematic layout of DSR test (Subhy, 2017)

The relation between torque and shear stress is also expressed in equation 3.1.

$$\boldsymbol{\tau_{max} = \frac{2 * T}{\pi * r^3}} \quad (3.1)$$

where: τ_{max} = maximum shear stress [N/mm²]
T = applied torque [N*mm]
r = radius [mm]

Then, the response of the bitumen is measured in terms of its shear strain. The angular deflection is measured by the DSR with which the shear strain can be expressed according to equation 3.2.

$$\boldsymbol{\gamma_{max} = \frac{\theta * r}{h}} \quad (3.2)$$

where: γ_{max} = maximum shear strain [-]
θ = deflection angle [rad]
r = radius of the sample [mm]
h = height of the sample [mm]

With those two parameters, it is possible to determine the complex shear modulus. The applied shear stress is divided by the measured shear strain, as can be seen in equation 3.3.

$$\boldsymbol{|G^*| = \frac{\tau_{max}}{\gamma_{max}}} \quad (3.3)$$

where: $|G^*|$ = complex shear modulus [N/mm²]
τ_{max} = maximum shear stress [N/mm²]
γ_{max} = maximum shear strain [-]

The phase angle can be determined as well with this test. This can be determined by multiplying the phase lag with the angular frequency as can be seen in equation 3.4.

$$\boldsymbol{\delta = \omega * \Delta t} \quad (3.4)$$

where: δ = phase angle [°]
ω = angular frequency [rad/s]
Δt = phase lag between stress and strain [s]

In Figure 3.7, the phase lag is shown in a graphical way. It can be seen that there is a delay in the response relative to the loading. This delay is defined as the phase lag between stress and strain.

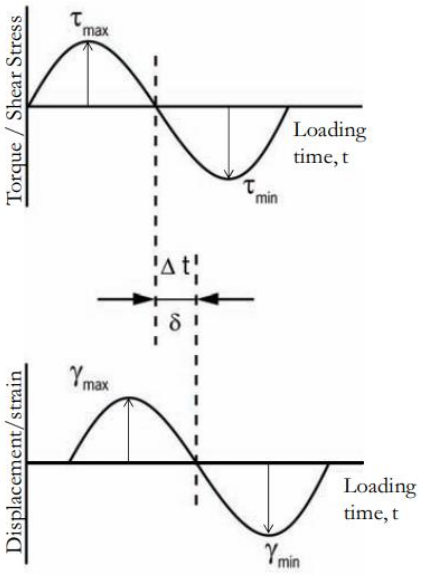

Figure 3.7: Stress-strain response of DSR (Van den Bergh, 2011)

In Figure 3.7, it can also be seen that the applied loading follows a sine curve, because the bitumen specimen is subjected to a cyclic loading at multiple frequencies.

The two parameters of this test reflect two important material properties of the bitumen. The complex shear modulus shows how much resistance the bitumen has to overall deformation. The phase angle shows the extent to which the bitumen behaves elastically or viscously. A phase angle of 0° suggests that the bitumen behaves fully elastically and a phase angle of 90° suggests that the bitumen behaves fully viscously. In reality, this value will somewhere in between due to the viscoelastic behaviour of bitumen (Van den Bergh, 2011).

Linear Amplitude Sweep (LAS)

In this study, the DSR device is used for executing the LAS method. With this method, the fatigue resistance of the bitumen can be estimated. Firstly, the rheological properties are determined with the DSR device. After that, frequency sweep and amplitude sweep are applied on those results and then with the continuum damage approach, the fatigue resistance of the binder can be estimated. The LAS test is based on the American standard AASHTO: T 391-20 (AASHTO, 2020).

In fact, the test exists of two different parts. The first part agrees with the execution of the DSR test which is described above. The complex shear modulus and phase angle of the bitumen are determined for frequencies with a range of 0.2 Hz to 30 Hz. The second part is used to measure the damage characteristics of the bitumen. Unlike the first part, which is frequency sweep, the second part is amplitude sweep. The frequency is kept constant at 10 Hz and the bitumen specimen is subjected to a strain control test. Every 10 seconds, the strain is increased with 1 % and during those 10 seconds, the strain is kept constant. The end of the test is when the strain reaches a value of 30 %. The testing temperature is 20 °C.

The frequency sweep is used to determine the rheological properties of the binder and the amplitude sweep is used to determine the damage accumulation in the binder, which can be used to determine the fatigue resistance.

In this study, the research of material properties at binder level is limited. Therefore, the following parameters are reported: the stiffness at 8 Hz and the strain level at which the mixture would fail after 1 million load repetitions (ε_6). These two parameters are plotted against each other on a graph. Using this graph, the various binders can then be compared and analyzed.

To study the change of the material properties of the bitumen due to ageing, two tests are developed to simulate the ageing of the bitumen. Both tests are outlined below.

Rolling Thin Film Oven Test (RTFOT)

The Rolling Thin Film Oven Test (RTFOT) is a test which simulates the ageing in the short-term. This simulation refers to the hardening in the production process in the asphalt plant and the paving in the construction process.

This test is described in European Standard NEN-EN 12607-1:2014 (2014). A thin film of bitumen is placed in an oven while it is rotating. This specimen is exposed to hot air for 75 minutes at 163 °C. An example of a device used to perform this test is shown in Figure 3.8.

Figure 3.8: RTFOT device

After this test, the bitumen specimens have been subjected to short-term ageing and can be further researched as if the bitumen has undergone the ageing process of the part in the production process.

Pressure Ageing Vessel (PAV) test

The Pressure Ageing Vessel (PAV) test is used for long-term ageing. With this test, the ageing during the service life is simulated. Because this is normally a long-time phase, it simulates the long-term ageing in an accelerated way.

The test is described in European Standard NEN-EN 14769:2012 (2012). Just like the RTFOT test, a thin film of bitumen is used. The bitumen is placed inside a vessel. In this vessel, the specimen is subjected to a pressure of 2.1 MPa for 40 hours at 90 °C. An example of a device used to perform the test is shown in Figure 3.9.

Figure 3.9: PAV device

After the PAV-test, the bitumen has undergone the long-term ageing process. In the 40 hours that is needed to execute the test, the ageing of multiple years in the user phase has been simulated and thus highly accelerated. Hereafter, the properties of the bitumen can be evaluated with other devices as if the bitumen aged multiple years.

To be able to monitor the ageing of the bitumen, the LAS analysis starts with a reference group of unaged bitumen. Then, the RTFOT is done once to simulate short-term ageing. After that, a new LAS analysis is done. For the long-term ageing, the bitumen specimens undergo the PAV test once. This is then again analyzed with the LAS test and for full ageing/end of service-life, the PAV test is done for the second time. Then, this set of specimens is analyzed for the last time with LAS to monitor the ageing at the end of service-life. The result of this is a complete picture of the fatigue behaviour and stiffness behavior of the binder throughout its service life.

3.2.2.2 Four point bending test (4PB-PR)

On mixture level, the four point bending test on prismatic specimens (4PB-PR) is a standard function test which can be used to determine fatigue behaviour and stiffness of the asphalt mixture. In this study, the beams are only used to determine the stiffness. The fatigue test is excluded because it takes a lot of time and therefore does not fit into the testing plan. A beam specimen is clamped at four distinct positions and at the two inner clamps, the beam is loaded by a sine shaped deformation. Because this loading is repeated many times, information is gained about the stiffness and the phase angle.

In Figure 3.10, an example of the device is shown that is used to execute the four point bending test.

Figure 3.10: Four point bending test device (Shafabakhsh et al., 2020)

The four point bending test is described in European Standard NEN-EN12697-26:2018 [Annex B] (2018) for the stiffness measurement. The beam specimen has fixed dimensions following the European Standard. Those dimensions are: 450 mm length, 50 mm width and 50 mm height. At 1/3 of 2/3 of the length, the inner clamps are placed. This can be seen in a schematic layout of the test in Figure 3.11. The distance between the clamps is 118.5 mm.

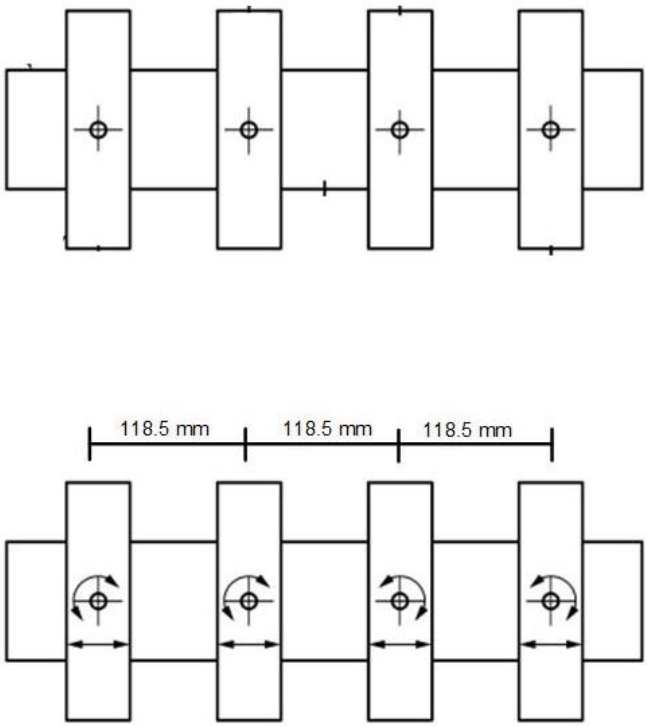

Figure 3.11: Schematic layout four point bending test (Nederlandse Norm (NEN), 2018c)

The two outer clamps are fixed while the at the two inner clamps are loaded by a sinusoidal deformation. This leads to a constant bending moment between the two inner clamps and a linear bending moment from the inner clamps to zero bending moment at the outer clamps.

Then, at mid-span, the deflection is measured using Linear Variable Differential Transformer (LVDT). Furthermore, the force needed to reach the applied deformation is reported. With the force and deflection, it is possible to determine the stiffness of the asphalt mixture. This can be done by calculating the tensile stress and tensile strain in the specimen.
The tensile stress is calculated using equation 3.5.

$$\sigma_t = \frac{M}{W} = \frac{\frac{F}{2} * A}{\frac{1}{6} * w * h^2} = \frac{3 * F * A}{w * h^2} \quad (3.5)$$

where: σ_t = tensile stress [N/mm^2]
F = total force [N]
A = length between inner and outer clamps [mm]
w = width of the beam [mm]
h = height of the beam [mm]

The tensile strain is calculated using equation 3.6.

$$\boldsymbol{\varepsilon_t = \frac{12 * \delta * h}{23 * A^2}} \quad (3.6)$$

where: ε_t = tensile strain [-]
δ = mid-span deflection [mm]
h = height of the beam [mm]
A = length between inner and outer clamps [mm]

With those parameters, it is possible to determine the flexural stiffness of the asphalt concrete (equation 3.7).

$$\boldsymbol{S_{mix} = \frac{\sigma_t}{\varepsilon_t}} \quad (3.7)$$

where: S_{mix} = stiffness modulus [N/mm^2]
σ_t = tensile stress [N/mm^2]
ε_t = tensile strain [-]

The stiffness measurement is displacement controlled. This means that a constant strain is imposed of 50 μm/m. Then, the force required to reach this strain is reported and from this force the stress can be calculated (equation 3.5). Furthermore, the phase angle is determined at each frequency to determine the proportion to which the material responds elastically and the proportion to which the material responds viscously.

The stiffness test is executed with 8 beam specimens at a temperature of 20 °C and at a range of frequencies of 0.1, 0.2, 0.5, 1, 2, 5, 8, 10, 20 and 30 Hz. After that, the test at 0.1 Hz is repeated. This is done to verify that no fatigue has occurred during the stiffness test.

The number of load repetitions is dependent on the frequency. For low frequencies, the number of load repetitions is lower than for high frequencies. The exact number of load repetitions per frequency is shown in Table 3.4.

Table 3.4: Number of load repetitions per frequency for four point bending test

Frequency [Hz]	Number of load repetitions [-]
0.1	25
0.2	25
0.5	50
1	50
2	50
5	100
8	100
10	100
20	200
30	200

The measurement of the stiffness value is determined on basis of an average of the last five repetitions. Then, it may be expected that all parameters are set in a constant way to make a reliable measurement. Furthermore, the stiffness at 8 Hz is explicitly reported because this is the standard value for type tests.

3.2.2.3 Indirect Tensile Test (ITT)

The indirect tensile test (ITT) is a test which gives information about the tensile strength of the asphalt mixture. This test can be done in a static way and in a dynamic way. With the latter, the resilient modulus of the material can be determined. Firstly, the static variant will be discussed. After that, the execution of the cyclic variant is addressed.

ITT

With the ITT, it is possible to determine the tensile strength of the asphalt mixture. This is done by loading the material with a compressive force along its vertical axis. As a consequence, there will develop a tensile stress along the horizontal axis.

In contrast to the four point bending test, a cylindrical specimen is used for the ITT. This specimen has a diameter of 100 mm and a height of 50 mm. It is placed between two loading strips, which can be seen in a schematic way in Figure 3.12. In Figure 3.13, a device which is used for the ITT can be seen.

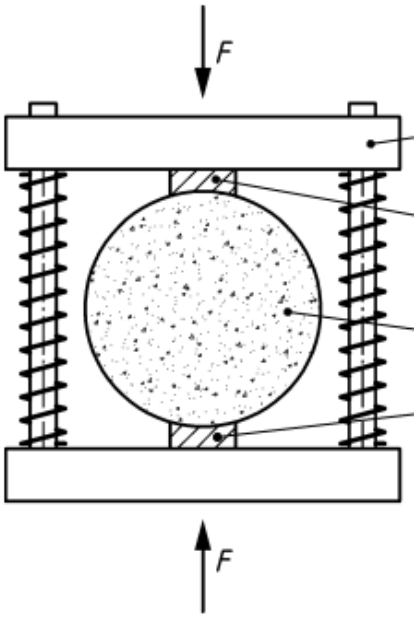

Figure 3.12: Schematic layout ITT (Nederlandse Norm (NEN), 2017)

Figure 3.13: ITT device

The ITT is described in European Standard NEN-EN12697-23:2017. A vertical deformation which increases with a constant speed of 50 mm/min, is applied on the specimen. The specimen is continuously loaded by a vertical deformation until the specimen fails. During this loading, the vertical force and the vertical deformation are measured. After failure, the numerical results of those parameters are reported. With equation 3.8, it is then possible to calculate the horizontal stress in the specimen.

$$\sigma_{xx} = \frac{2 * F}{\pi * h * D} \quad (3.8)$$

where:	σ_{xx}	=	horizontal stress	[N/mm^2]
	F	=	peak force	[N]
	h	=	thickness of the specimen	[mm]
	D	=	diameter of the specimen	[mm]

When the maximum force is used in equation 3.8, the horizontal stress is equal to the indirect tensile strength (ITS) of the asphalt mixture.

Besides the indirect tensile strength, it is also possible to measure the water sensitivity with the ITT. This is described in European Standard NEN-EN 12697-12:2018. It states that the ITT will be done on two sets of four specimens. One set of specimens maintains dry while the other set is vacuumed for 30 minutes and then placed in a water bath at 40 °C for 72 hours. Then, the ITT will be done with both sets of specimens and the indirect tensile strength is measured. The ratio of the wet and dry specimens determines the water sensitivity, expressed as indirect tensile strength ratio (ITSR) (equation 3.9).

$$\mathbf{ITSR} = \mathbf{100} * \frac{\mathbf{ITS_w}}{\mathbf{ITS_d}} \quad (3.9)$$

where:	ITSR	=	indirect tensile strength ratio	[%]
	ITS_w	=	indirect tensile strength wet	[N/mm^2]
	ITS_d	=	indirect tensile strength dry	[N/mm^2]

Regarding water sensitivity, the test is conducted at a temperature of 15 °C.

Lastly, the fracture toughness of the material can be measured with this test. Regarding this test, the test is conducted at a temperature of 1 °C with four specimens. This property can be expressed in either the fracture toughness until the point of maximum force or the total fracture toughness. The former option is given in equation 3.10 and the latter option is given in equation 3.11.

$$\textbf{Fracture toughness until maximum force} = \frac{\mathbf{W_s}}{\mathbf{h} * \mathbf{D}} \quad (3.10)$$

where:	W_s	=	split energy	[J]
	h	=	thickness of the specimen	[m]
	d	=	diameter of the specimen	[m]

$$\textbf{Total fracture toughness} = \frac{\mathbf{W_s + W_p}}{\mathbf{h * D}} \quad (3.11)$$

where: W_s = split energy [J]
W_p = fail energy [J]
h = thickness of the specimen [m]
d = diameter of the specimen [m]

In equation 3.10 and 3.11, the parameters split energy and fail energy are used. The split energy is defined as the integral of the force-deflection line until the maximum force (equation 3.12) and the fail energy is defined as the integral of the force-deflection line from the maximum force until the end of test (equation 3.13). This is graphically shown in Figure 3.14.

$$\mathbf{W_s} = \int_{\mathbf{0}}^{\mathbf{u_{F_{max}}}} \mathbf{F du} \quad (3.12)$$

where: W_s = split energy [J]
F = force [N]
$u_{F_{max}}$ = displacement at maximum force [mm]

$$\mathbf{W_p} = \int_{\mathbf{u_{F_{max}}}}^{\mathbf{u_{end}}} \mathbf{F du} \quad (3.13)$$

where: W_p = fail energy [J]
F = force [N]
$u_{F_{max}}$ = displacement at maximum force [mm]
u_{end} = displacement at end of the test [mm]

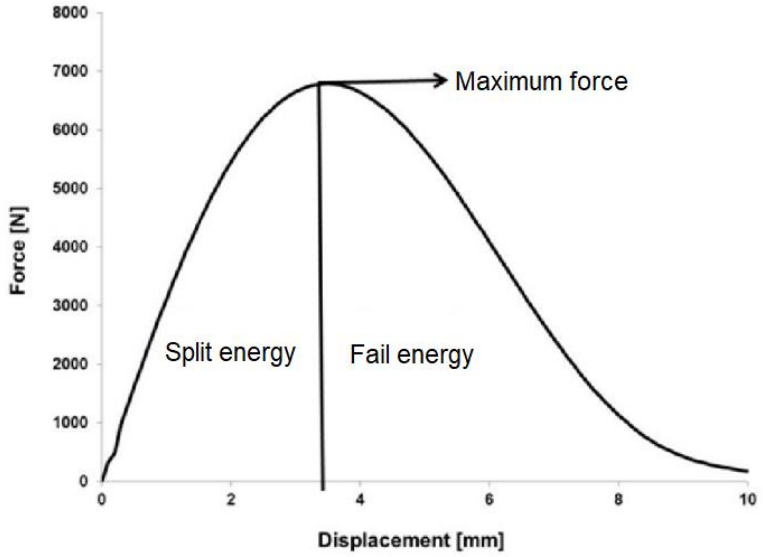

Figure 3.14: Typical force-displacement curve for monotonic ITT (Reyes-Ortiz et al., 2011) (adapted)

Cyclic ITT

With the cyclic ITT, the cylindrical specimen is loaded with a cyclic force instead of a continuously increasing force. Also, the dimensions are different. The diameter is 100 mm and the height is 40 mm. However, the principle stays the same. A vertical compressive force is placed on a cylindrical specimen which leads to a tensile stress along the horizontal axis. An example of the used device is shown in Figure 3.15. The test is conducted at 20 °C.

Figure 3.15: Cyclic ITT device (Mullapudi et al., 2020)

The cyclic ITT is described in European Standard NEN-EN12697-24:2018 [Annex F] (2018) and NEN-EN12697-26:2018 [Annex F] (2018). The former describes the resistance to fatigue and the latter describes the stiffness measurement. The difference with the stiffness measurement of the four point bending test is that the cyclic ITT is stress-controlled instead of strain-controlled.

For determining the fatigue resistance, three sets of three specimens are used. Those three sets are subjected to a low load level, medium load level and high load level.

The applied force is described in the European Standard and can be found in equation 3.14.

$$\mathbf{F(t) = F_m + F_a * \sin(2\pi * f * t)} \quad (3.14)$$

where:	F(t)	=	applied vertical force	[kN]
	F_m	=	minimum force	[kN]
	F_a	=	force amplitude	[kN]
	f	=	frequency	[1/s]
	t	=	time	[s]

The minimum force is kept constant for all specimens and has a value which results in a stress level of 0.035 MPa. The force amplitude is used to subject the specimens to the intended load level. The frequency is kept constant at 30 Hz.

During the fatigue test, the horizontal deformation is measured with which the strain can be determined according to equation 3.15.

$$\boldsymbol{\varepsilon_a = \frac{2 * u_a}{d} * \frac{1 + 3 * \nu}{4 + \pi * \nu - \pi}} \quad (3.15)$$

where:	ε_a	=	maximum horizontal strain amplitude	[-]
	u_a	=	horizontal displacement amplitude	[mm]
	d	=	diameter of the specimen	[mm]
	ν	=	Poisson's ratio	[-]

Furthermore, the force is measured with which the stress can be determined according to equation 3.16.

$$\boldsymbol{\sigma_a = \frac{2 * F_a}{\pi * h * d}} \quad (3.16)$$

where:	σ_a	=	horizontal tensile stress amplitude	[N/mm^2]
	F_a	=	vertical force amplitude	[N]
	h	=	height of the specimen	[mm]
	d	=	diameter of the specimen	[mm]

Then, the stiffness modulus can be determined by dividing the stress by the strain (equation 3.17).

$$\mathbf{S_{mix}} = \frac{\boldsymbol{\sigma_a}}{\boldsymbol{\varepsilon_a}} * (\mathbf{1} + \mathbf{3} * \boldsymbol{\nu}) \tag{3.17}$$

where:	S_{mix}	=	stiffness modulus	[N/mm²]
	σ_a	=	horizontal tensile stress amplitude	[N/mm²]
	ε_a	=	maximum horizontal strain amplitude	[-]
	ν	=	Poisson's ratio	[-]

With the stiffness modulus, the fracture life can be determined. For this, the energy ratio is used (equation 3.18).

$$\mathbf{ER(n)} = \mathbf{n} * \mathbf{S_{mix,n}} \tag{3.18}$$

where:	ER(n)	=	energy ratio at number of cycle *n*	[N/mm²]
	n	=	number of cycles	[-]
	$S_{mix,n}$	=	stiffness modulus at number of cycle *n*	[N/mm²]

The fracture life is equal to the number of cycles when the energy ratio reaches its maximum. Then, the initial tensile strain can be plotted against the number of cycles of the fracture life for the obtained test results. With these points, the fatigue line can be fitted to the data. Furthermore, the ε_6-value can be determined, which is the strain level at which the mixture would fail after 1 million load repetitions.

For the stiffness test, a sinusoidal load is placed on the specimen with different loading frequencies, according to the following range: 30, 10, 8, 5, 2, 1, 0.5, 0.2 and 0.1 Hz. After that, the test at 30 Hz is repeated. This is done to verify that no fatigue has occurred during the stiffness test.

The stiffness of the specimen can then be calculated using equation 3.19.

$$|\mathbf{E}| = \frac{\mathbf{F}}{\boldsymbol{\Delta d}} * \frac{\boldsymbol{\upsilon} + \mathbf{0.274}}{\mathbf{h}} \tag{3.19}$$

where:	|E|	=	stiffness modulus	[N/mm²]
	F	=	force	[N]
	Δd	=	force amplitude	[mm]
	ν	=	Poisson's ratio	[-]
	h	=	thickness of the specimen	[mm]

The number of load repetitions is dependent on the frequency. For low frequencies, the number of load repetitions is lower than for high frequencies. The exact number of load repetitions per frequency is shown in Table 3.5.

Table 3.5: Number of load repetitions per frequency for cyclic ITT

Frequency [Hz]	Number of load repetitions [-]
30	100
10	30
8	25
5	20
2	15
1	15
0.5	15
0.2	10
0.1	10
30	100

The measurement of the stiffness value is determined as an average of the last five repetitions. Then, it may be expected that all parameters are set in a constant way to make a reliable measurement. Furthermore, the stiffness at 8 Hz is explicitly reported because this is the standard value for the stiffness tests.

3.2.2.4 Triaxial cyclic compression test

The triaxial cyclic compression test is used to measure the resistance of the asphalt mixtures to permanent deformation. The distress phenomenon rutting is linked to this permanent deformation, so the resistance must be enough to prevent this distress to happen.

The test exists of a cylindrical specimen which is uniformly confined. Thereafter, a uniaxial stress is repeatedly applied. Then the axial displacement is measured and with this the axial permanent strain is determined. A schematic layout of this test is shown in Figure 3.16. There, a sealed specimen in an airtight cell can be seen which is uniformly confined using a compressor. In Figure 3.17, an example of the device which executes the triaxial cyclic compression test, is shown. The diameter of the specimen is 100 mm and its initial height is 60 mm.

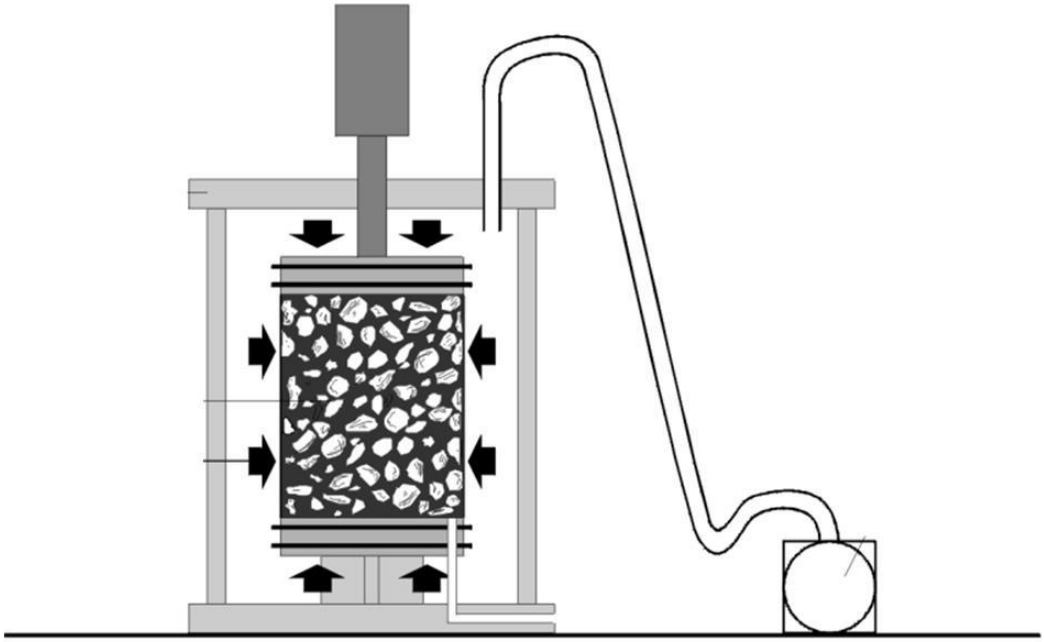

Figure 3.16: Schematic layout triaxial cyclic compression test (Nederlandse Norm (NEN), 2016b)

Figure 3.17: Triaxial cyclic compression test device (Wang et al., 2015)

The triaxial cyclic compression test is described in European Standard NEN-EN 12697-25:2016. The testing temperature for the binder and base layer is 40 °C.

The load exists of multiple parts. At the whole surface of the specimen a uniaxial confining pressure is applied. This simulates the horizontal stress in the pavement and has a value of 0.05 MPa. For the vertical stress, two extra components are added to this uniaxial confining pressure. These is a static part which simulates the difference between vertical and horizontal overburden stress and a cyclic part which simulates the traffic loading. This cyclic part is repeated 10000 times and has the form of a haversine and its equation is shown in equation 3.20.

$$\boldsymbol{\sigma_a(t) = \sigma_v * (1 + \sin(2\pi * f * t))} \quad (3.20)$$

where:	σ_a	=	vertical cyclic stress	[N/mm²]
	σ_v	=	amplitude axial stress	[N/mm²]
	f	=	frequency loading pulse	[Hz]
	t	=	time	[s]

The total vertical stress is then expressed in equation 3.21.

$$\boldsymbol{\sigma_1(t) = \sigma_a(t) + \sigma_c + \sigma_s} \quad (3.21)$$

where:	σ_1	=	total axial stress	[N/mm²]
	σ_a	=	vertical cyclic stress	[N/mm²]
	σ_c	=	uniaxial confining stress	[N/mm²]
	σ_s	=	static overburden stress	[N/mm²]

An example of the course of stress can be seen in Figure 3.18. Here, a static part of the stress and a haversine part with a certain loading time (t_{load} =0.4 s) and a certain rest time (t_{rest} =0.6 s) are shown.

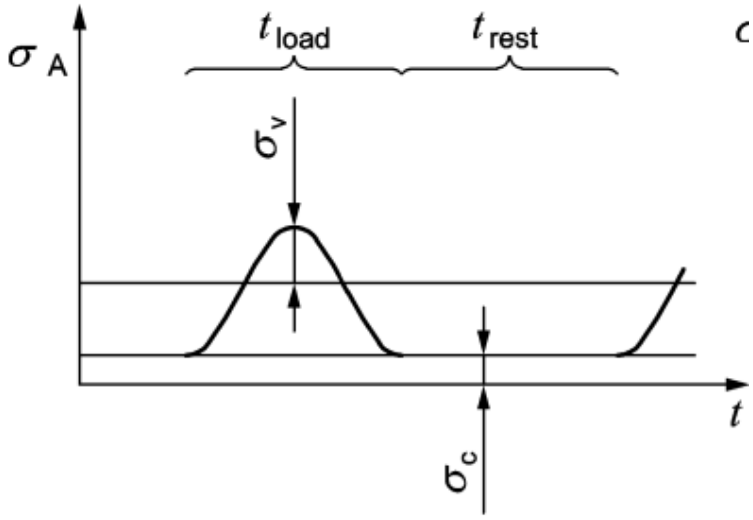

Figure 3.18: Loading signal (Nederlandse Norm (NEN), 2016b)

During the test, the vertical axial displacement is measured with LVDT displacement transducers. With those measurements, it is possible to determine the cumulative axial strain of the specimen. First, the cumulative permanent deformation is determined with equation 3.22 and then this parameter is used to determine the cumulative axial strain (equation 3.23).

$$\mathbf{u_n = |h_0 - h_n|} \tag{3.22}$$

where: u_n =cumulative permanent deformation after n loading cycles [mm]
h_0 =mean vertical position of the upper loading plate at start of the test [mm]
h_n =mean vertical position of the upper loading plate after n loading cycles [mm]

$$\boldsymbol{\varepsilon_n = 100 * \frac{u_n}{t_i}} \tag{3.23}$$

where: ε_n = cumulative axial strain after n loading cycles [%]
u_n = cumulative permanent deformation [mm]
t_i = initial thickness of the specimen [mm]

To determine the resistance to permanent deformation, the cumulative axial strain has to be plotted as a function of the number of cycles. In Figure 3.19, a typical result of this plot is shown, also called the creep curve. In this plot, three different parts can be distinguished: stage 1, stage 2 and stage 3.

Stage 1 is characterized by a decreasingly increasing line, when the number of cycles is rising. The second stage is characterized by quasi-linear part where the slope is quasi constant. The parameter creep rate (f_c) is equal to this slope. Stage 3 is the last stage and is characterized by the fact that the slope is not constant anymore, but the line increasingly increases. This is when the resistance of the specimen decreases drastically.

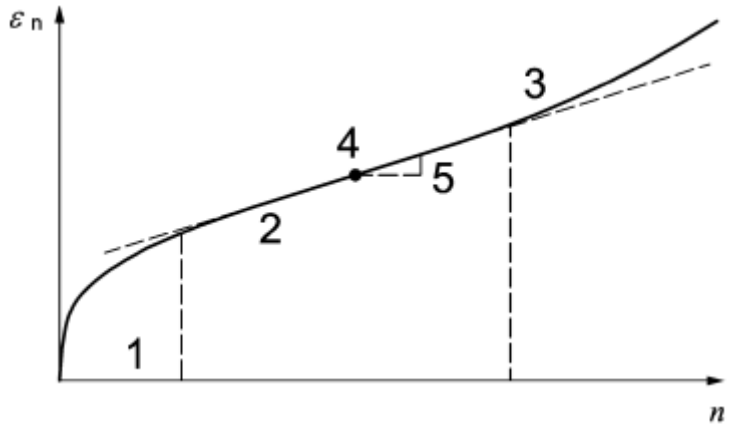

Figure 3.19: Example of plot of cumulative axial strain as a function of number of cycles (Nederlandse Norm (NEN), 2016b)

The creep rate gives information about the resistance to permanent deformation of the mixture and this makes it essential to determine this parameter during this test. For doing this, different options are given in the European Standard. The most used option in the Netherlands is to make a linear regression of stage 2 of the creep curve with equation 3.24. A linear line is usually fit between 4000 and 10000 cycles.

$$\boldsymbol{\varepsilon_n = A_1 + B_1 * n} \tag{3.24}$$

where: ε_n	=	cumulative axial strain after n loading cycles	[%]
A_1	=	intercept from the least square linear fit	[%]
B_1	=	slope from the least square linear fit	[%]
n	=	number of loading cycles	[-]

Then the creep rate f_c can be calculated by multiplying the constant B_1 with 10^4. The result is the creep rate in μstrains/loading cycle.

4 Results

In this chapter, the results of the functional tests are shown. Firstly, the results of the DSR on binder level are presented. After that, the results of the tests on mixture level are given.

4.1 Results on binder level

4.1.1 DSR - LAS

The final results of the LAS test method are given in terms of stiffness and fatigue resistance. The stiffness of the bitumen is measured at a frequency of 8 Hz and a temperature of 20 °C. The fatigue resistance is represented by the parameter ε_6, which is the strain level at which the mixture would fail after 1 million load repetitions. Per binder composition, four different points are determined. Those are the unaged bitumen, after applying RTFOT, after applying PAV and after applying 2 times PAV.

The results are graphically shown in Figure 4.1. In this figure, the different steps can be recognized as follows: square for unaged bitumen, circle for RTFOT, triangle for 1x PAV and diamond for 2x PAV. The numerical values can be found in Table 4.1 and Appendix C. All tests were executed three times, so those values are an average of three different specimens.

Symbol	Step
■	Unaged
●	RTFOT
▲	PAV
♦	2x PAV

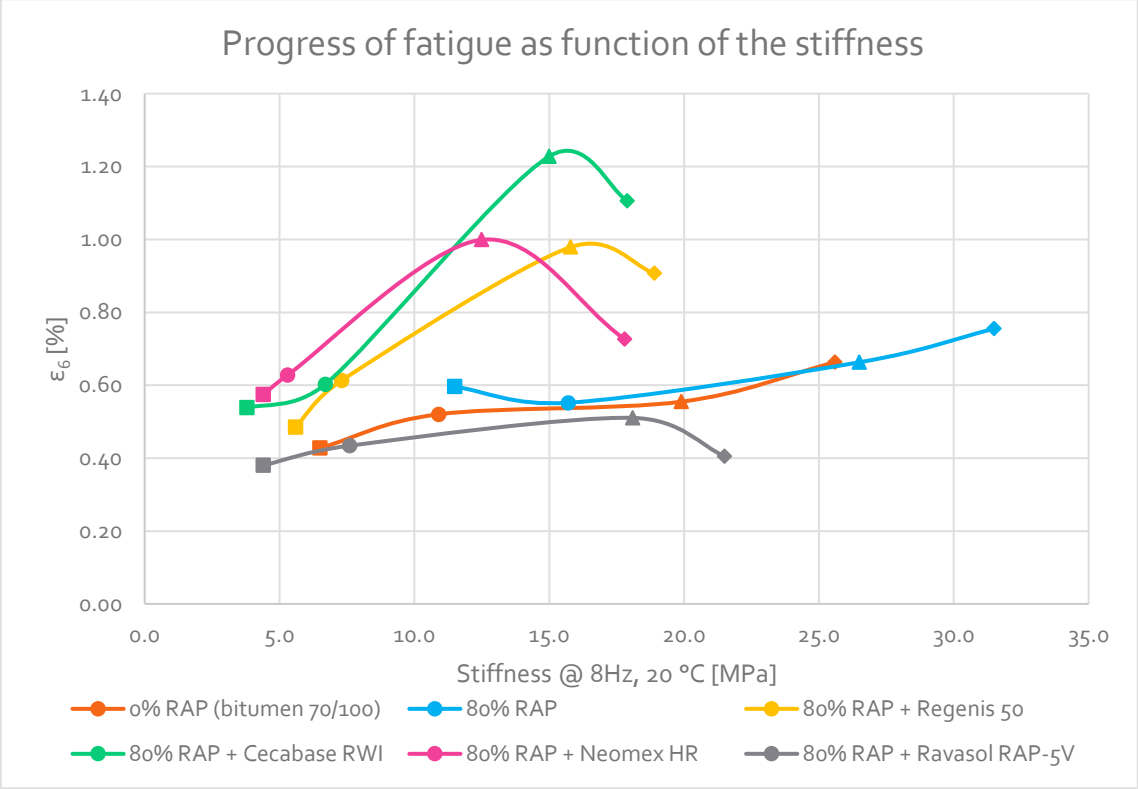

Figure 4.1 : Fatigue values as function of the stiffness for 6 binder compositions

Table 4.1: Numerical values LAS results

		0% RAP (bit 70/100)	80% RAP	80% RAP + Regenis50	80% RAP + Cecabase RWI	80% RAP + Neomex HR	80% RAP + Ravasol RAP-5V
Unaged	Stiffness [MPa]	6.5	11.5	5.6	3.8	4.4	4.4
	ε_6 [%]	0.428	0.596	0.485	0.538	0.574	0.380
After RTFOT	Stiffness [MPa]	10.9	15.7	7.3	6.7	5.3	7.6
	ε_6 [%]	0.520	0.552	0.613	0.603	0.628	0.434
After PAV	Stiffness [MPa]	19.9	26.5	15.8	15.0	12.5	18.1
	ε_6 [%]	0.555	0.663	0.979	1.228	0.999	0.510
After 2x PAV	Stiffness [MPa]	25.6	31.5	18.9	17.9	17.8	21.5
	ε_6 [%]	0.663	0.755	0.907	1.106	0.726	0.405

In Figure 4.1, it can be seen that for all binder compositions, the RTFOT and PAV test lead to a strong increase in stiffness and an increase as well in the fatigue resistance. After applying the PAV for the first time, the highest increase in stiffness can be seen.

The stiffness increases strongly when 80% RAP is applied in comparison to the unaged bitumen. The fatigue resistance is increased as well, albeit to a lesser extent.

Application of rejuvenating additives leads to the undoing of the increase. The stiffness values for all samples with rejuvenating additives are significantly lower than the 80% RAP sample without additive. The stiffness values are comparable with the unaged bitumen. For the fatigue resistance, this is less straightforward. For the unaged samples, the specimen with 80% RAP without additive shows a slightly better fatigue resistance than the specimens with additives. However, after ageing is simulated with RTFOT and PAV, the fatigue resistance of the specimens with additives is higher than the specimen with 80% RAP, except for the additive Ravasol RAP-5V. This fatigue resistance stays lower towards the specimen without additive. Ravasol appears to best return the binder to its original stiffness and fatigue resistance.

Furthermore, the fatigue results of 2x PAV are notable, because these results are different from the previous steps. Instead of an increase in the fatigue resistance, it decreases for the specimens with rejuvenating additives. With this last step, the specimens with additives show another progress than the specimens without. The stiffness of the specimens does continue to increase similarly to the reference.

This deviating fatigue behavior of these specimens might be the result of the addition of rejuvenators. The fatigue resistance decreases for all specimens with rejuvenators and increases for all specimens without rejuvenator after 2x PAV.

However, the fatigue resistance values belonging to 2x PAV, are still relatively high, except for the Ravasol. The values are quite higher than the values of the unaged specimens and after applying RTFOT. So, despite the decrease after the second time PAV, ageing in general still leads to a higher fatigue resistance. From that perspective, the decrease in fatigue resistance may not be a problem.

So, in general, it yields that the application of 80% RAP leads to a strong increase in stiffness and a slight increase in fatigue resistance. The stiffness increase can be undone by applying rejuvenating additives. This application leads also to a higher fatigue resistance in comparison with unaged bitumen, except for the Ravasol RAP-5V. This one approximates the unaged bitumen best.

Besides the evaluation of the binder properties, the tests at binder level are used as well to choose the rejuvenating additives that are applied on mixture level. The limited time gives the opportunity to test two mixtures with a rejuvenator. Firstly, there is chosen for Cecabase RWI, because this rejuvenator shows a very improved fatigue resistance on binder level in comparison with the virgin bitumen and it has the highest ε_6-value of all binder compositions. This makes it interesting to test this additive also at mixture level. Furthermore, Cecabase RWI is the only additive used which strictly speaking cannot be described as a rejuvenator (see chapter 3.1), which is an extra reason to study this additive on mixture level.

The second choice was made based on limitations and availability. Ravasol RAP-5V was poorly supplied which made it difficult to apply this rejuvenator on mixture level. For Regenis 50, it should have a higher dosage than the other three because it is more viscous than the rest. In order to compare the rejuvenators with each other, the same dose is used as much as possible. This leads to Neomex HR being preferred over Regenis 50. So, in a short way, there is chosen to apply Cecabase RWI and Neomex HR on mixture level.

4.2 Results on mixture level

All mean results of the ITT, cyclic ITT, four point bending test and the triaxial cyclic compression test are shown. The error bars in the figures indicate the standard deviation.

4.2.1 Indirect tensile test

4.2.1.1 Water sensitivity

Figure 4.2 shows the mean results of the ITT regarding water sensitivity. The test was done four times. These results can be found in Appendix D.

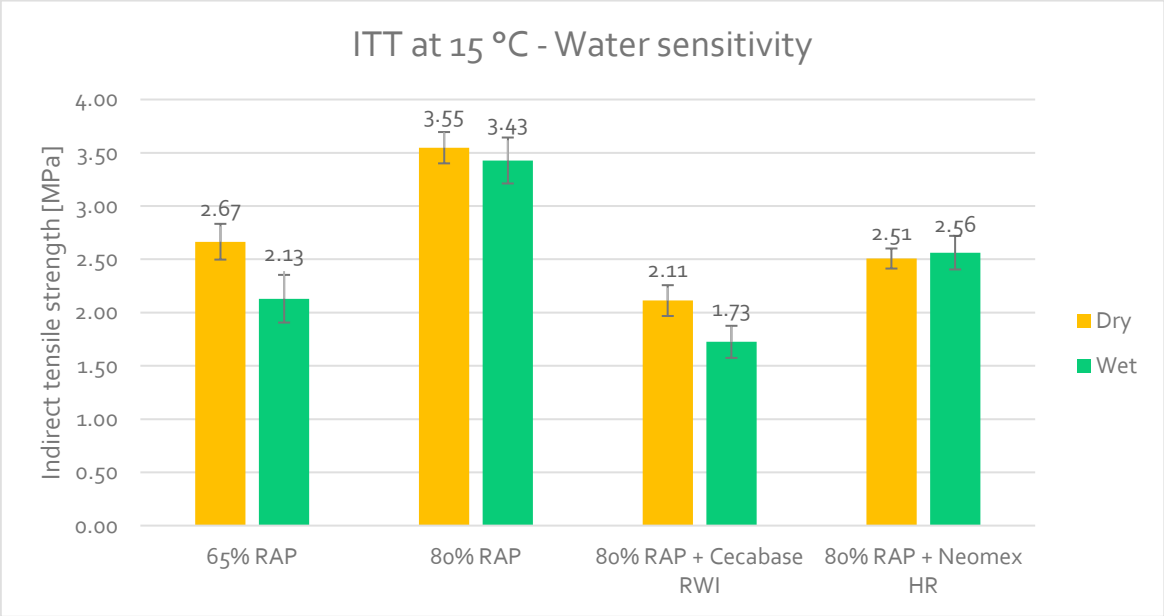

Figure 4.2: Results of ITT for water sensitivity

From the ITT results in Figure 4.2, it becomes clear that the indirect tensile strength (ITS) is the highest for the mixture with 80% RAP regarding both the dry and wet specimens. The increase in RAP content from 65% to 80% leads to a 33% increase in the ITS of the dry specimens and 61% increase in the ITS of the wet specimens. The application of rejuvenating additives leads to a decrease in ITS, with the maximum decrease for the mixture with Cecabase RWI. In comparison with the 80% RAP mixture, the ITS-value for dry specimens decreases with 40% and for the wet specimens with 50%. The decrease in the ITS-value for the mixture with Neomex is smaller with 29% and 25% for dry specimens and wet specimens respectively.

The water sensitivity is expressed as ITSR-value, shown in Table 4.2, as ratio between ITS-values of the wet specimens and the dry specimens.

Table 4.2: ITSR results

Mixture	ITSR [%]
65% RAP	80 %
80% RAP	97 %
80% RAP + Cecabase RWI	82 %
80% RAP + Neomex HR	102%

The minimum requirement for the ITSR-value for base and binder layers is 70% (CROW, 2020). It is clear that all mixtures are well above this requirement. It can be seen that the increase in RAP content from 65% to 80% leads to an increase in the ITSR-value of 17 percentage points. Thus, increase in RAP content has a positive effect on the water sensitivity. The application of rejuvenating additives has not led to a uniform effect. The addition of Cecabase leads to a reduction in the ITSR-value of 15 percentage points while the addition of Neomex HR leads to an increase in the ITSR-value of 5 percentage points. The ITSR-value of the mixture with Neomex HR is even above 100%, which implies that water has no negative effect on the strength of this mixture. So, for the 80% RAP mixture and the mixture with Neomex HR, water has practically no effect on the ITS of the mixture.

4.2.1.2 Fracture toughness

Figure 4.3 shows the overall results of the ITT regarding fracture toughness. The test was done four times. These results can be found in Appendix D.

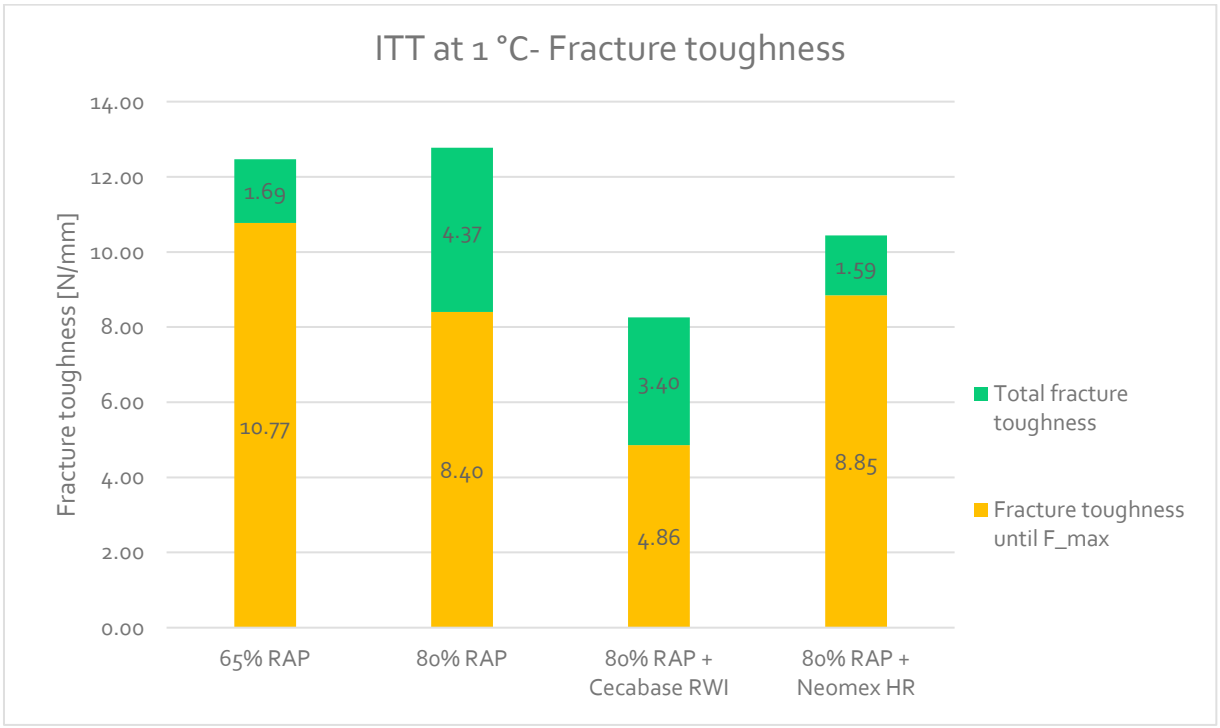

Figure 4.3: Results of ITT for fracture toughness

The mixture with 80% RAP has the highest total fracture toughness, 2% higher than the fracture toughness of the 65% RAP mixture. Thus, the increase in RAP content from 65% to 80% hardly affects the total fracture toughness. However, the addition of rejuvenating additives does have influence on the total fracture toughness. The mixture with Cecabase RWI shows 35% decrease relative to the 80% RAP mixture without additive. For the mixture with Neomex HR, a decrease of 18% of the total fracture toughness was observed. So, the rejuvenating additives lead to a large decrease in total fracture toughness. In addition, there is also a clear mutual difference between the two additives. The total fracture toughness of the mixture with Cecabase RWI is 21% lower than the total fracture toughness of the mixture with Neomex HR. So, applying Cecabase leads to a higher decrease in fracture toughness than applying Neomex.

The ratio between the fracture toughness until F_{max} and the total fracture toughness varies greatly for the different mixtures. The proportion of the fracture toughness until F_{max} is much higher for the 65% RAP mixture and the mixture with Neomex HR than the proportion for the mixture with Cecabase RWI and the 80% RAP mixture. This means that almost all of the required crack energy is expressed as split energy and there is only a small proportion of fail energy. For the mixture with Cecabase and 80% RAP, this is better distributed and this leads to a more gradual failure.

However, it is hard to interpret the results regarding the proportion of fracture toughness until F_{max} and the total fracture toughness. This is because it is sometimes difficult to identify a maximum force because there is more of a plateau in the force-displacement diagram instead of a single maximum. In such cases, the value of the fracture toughness until F_{max} becomes inaccurate and it is difficult to compare the values with each other. As the individual results in Appendix D show, there is indeed a large inaccuracy, except for the mixture with Cecabase. So apart from the mixture with Cecabase it is difficult to draw conclusions from this.

4.2.2 Cyclic indirect tensile test

4.2.2.1 Stiffness

Figure 4.4 shows the overall results of the cyclic ITT regarding stiffness. The test was done nine times. These results can be found in Appendix E.

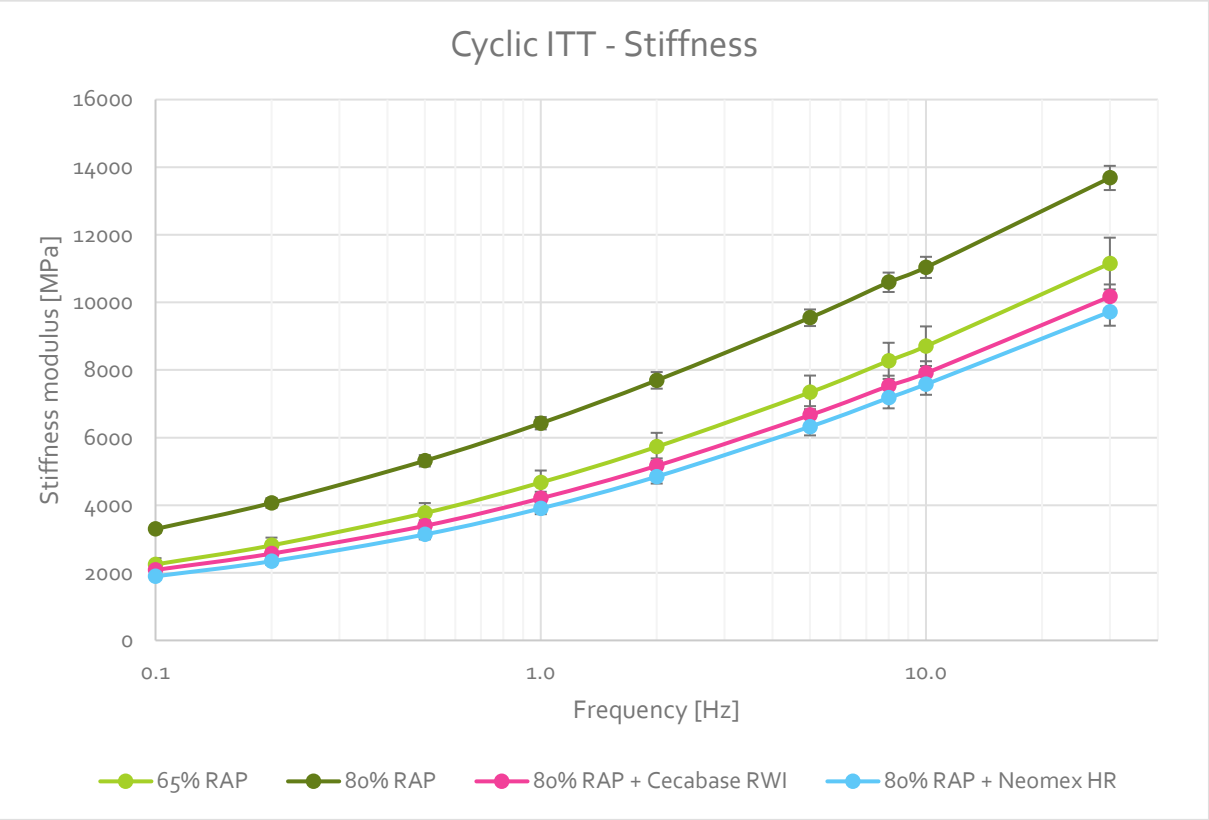

Figure 4.4: Results of cyclic ITT for stiffness

In Figure 4.4, it can be seen that the increase in RAP content from 65% to 80% leads to an increase in stiffness. For small frequencies, the increase is 45% and for high frequencies the increase is

around 25%. Thus, the influence of increasing the RAP content is higher for low frequencies than for high frequencies. It is further found that the stiffness of the mixture with 80% RAP changes less at different frequency than the stiffness of the mixture with 65% RAP.

The application of rejuvenating additives leads to a large decrease in stiffness values. Relative to the mixture with 80% RAP, the stiffness values are 26% to 42% lower. The mixture with Neomex has a slightly lower stiffness than the mixture with Cecabase.

The application of rejuvenating additives undoes the stiffness increase due to the increase in RAP content. Both mixtures with rejuvenating additives show also lower stiffness values than the 65% RAP mixture. The stiffness of the mixture with Cecabase is for all frequencies almost 10 % lower than the mixture with 65% RAP. The stiffness of the mixture with Neomex HR is relatively lower for small frequencies (approximately -16%) than for high frequencies (approximately -13%) in comparison with the mixture with 65% RAP.

The stiffness values for a frequency of 8 Hz are used in pavement design and are therefore important. It should be noted that this yields for the stiffness values obtained by the four point bending test. But it may still be interesting for the stiffness values of the cyclic ITT. They are reported in Table 4.3.

Table 4.3: Stiffness results cyclic ITT for frequency = 8 Hz

Mixture	S_{mix} [MPa]	Standard deviation [MPa]
65% RAP	8271	534
80% RAP	10595	287
80% RAP + Cecabase RWI	7528	305
80% RAP + Neomex HR	7176	310

The results in Table 4.3 confirm the picture outlined above. The increase in RAP content leads to a 28% increase in stiffness at f = 8 Hz. This increase can be reversed by applying rejuvenators. The application of Cecabase RWI leads to a decrease of 29% relative to the 80% RAP mixture and the application of Neomex HR leads to a decrease of 32% relative to the 80% RAP mixture.

This decrease even leads to a lower stiffness than the 65% RAP mixture. The stiffness at f = 8Hz of the mixture with Cecabase is 9% lower and the mixture with Neomex is 13% relative to the 65% RAP mixture.

During the stiffness measurement, the phase angle is measured as well. The overall results are given in Figure 4.5. The test was done nine times. Those results can be found in Appendix E.

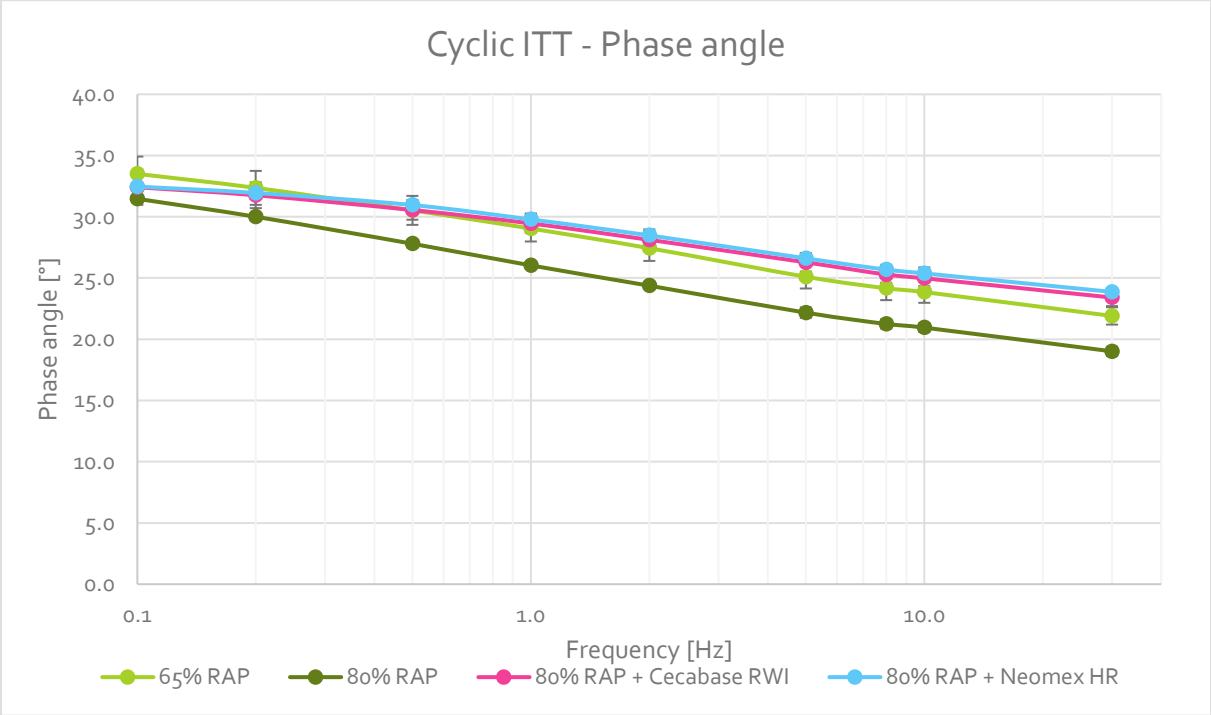

Figure 4.5: Results of cyclic ITT for phase angle

In Figure 4.5, it can be seen that the increase in RAP content leads to a lower phase angle. This is the case for all frequencies, but the difference is larger for higher frequencies than for smaller frequencies.

Furthermore, it can be seen that the application of rejuvenating additives leads to a higher phase angle. Both mixtures with rejuvenators show the comparable values and hardly any difference can be noticed. Relative to the 80% RAP mixture without additive, the phase angle values for both mixtures with rejuvenator are higher for all frequencies. For small frequencies, this difference is relatively small (less than 10%), but for higher frequencies this difference is larger (up to 20%). Relative to the 65% RAP mixture, the values are similar for lower frequencies and for the lowest frequency the phase angle of the 65% RAP mixture is even higher. For higher frequencies, the difference becomes larger and the mixtures with rejuvenator show higher phase angle values compared to the 65% RAP mixture.
In Table 4.4, the phase angle results for the frequency of 8 Hz are given.

Table 4.4: Phase angle results cyclic ITT for frequency = 8 Hz

Mixture	δ [°]	Standard deviation [°]
65% RAP	24.2	1.0
80% RAP	21.2	0.4
80% RAP + Cecabase RWI	25.3	0.7
80% RAP + Neomex HR	25.7	0.4

From Table 4.4, it becomes clear that the phase angle for the frequency of 8 Hz decreases with 12% when the RAP content is increased from 65% to 80%. Furthermore, it can be seen that the application of Cecabase and Neomex leads to a 19% and 21% increase respectively, compared to the 80% RAP mixture without additive. Lastly, it can be noted that the phase angle values of the mixtures with rejuvenator are also higher than the 65% RAP mixture. The phase angle of the mixture with Cecabase RWI is 5% higher and the phase angle of the mixture with Neomex HR is 6% higher.

4.2.2.2 Fatigue resistance

Figure 4.6 shows the overall results of the cyclic ITT regarding fatigue resistance. More detailed results can be found in Appendix E.

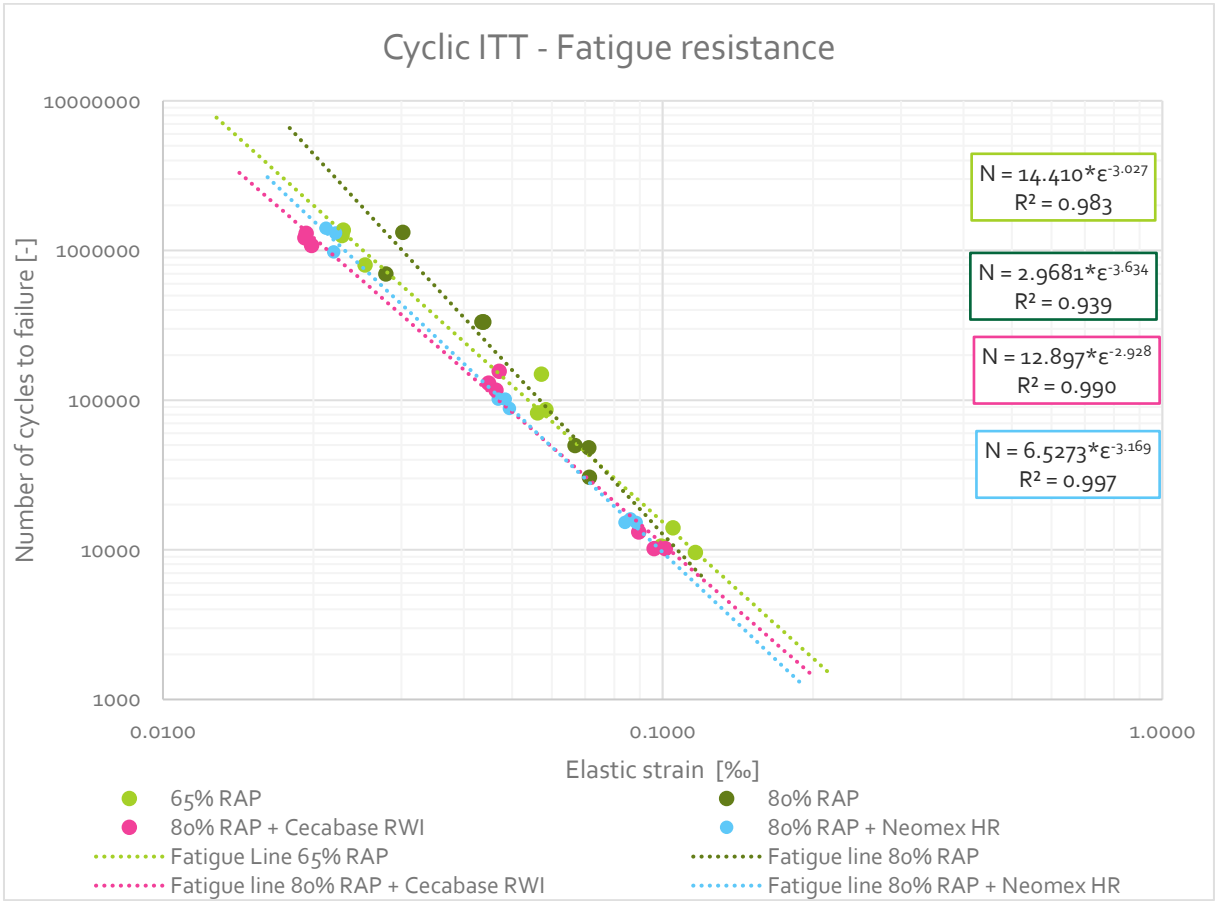

Figure 4.6: Results of cyclic ITT for fatigue resistance

In Figure 4.6, it can be seen that the 80% RAP mixture shows the best fatigue resistance for low and medium strain levels. For high strain levels the 65% RAP mixture shows the best fatigue resistance.

The application of rejuvenating additives leads to a decrease in fatigue resistance. For all strain levels, the number of cycles to failure is the lowest for the mixtures with Cecabase and Neomex. Compared with each other, both mixtures with rejuvenating additive show a similar fatigue resistance. For lower strain levels, the mixture with Neomex HR shows a slightly better fatigue

resistance, while for higher strain levels, the mixture with Cecabase RWI has a slightly better fatigue resistance.

In pavement design, the ε_6-value is used to express fatigue resistance. This value is based on the fatigue line and indicates the strain level at which the mixture would fail after 1 million load repetitions. Those values are given in Table 4.5. It should be noted that the ε_6-value for pavement design is based on the four point bending test. These values are not comparable with the fatigue test of the cyclic ITT. However, the values can mutually be compared to determine which mixture has the best fatigue resistance

Table 4.5: ε_6-value cyclic ITT

Mixture	ε_6 [‰]
65% RAP	0.0252
80% RAP	0.0301
80% RAP + Cecabase RWI	0.0214
80% RAP + Neomex HR	0.0231

The ε_6-values in Table 4.5 confirm that an increase in RAP content leads to a higher fatigue resistance. The ε_6-value of the 80% RAP mixture is 19% higher than the ε_6-value of the 65% RAP mixture. The application of rejuvenating additives leads to a reduction in the ε_6-value. Relative to the 80% RAP mixture, the ε_6-value of the mixture with Cecabase is 29% lower and the ε_6-value of the mixture with Neomex is 23% lower.

Furthermore, it can be seen that the reduction due to the rejuvenating additive is higher than the increase due to the RAP content. The ε_6-value of the mixture with Cecabase is 15% lower and the ε_6-value of the mixture with Neomex is 8% lower compared with the 65% RAP mixture.

4.2.3 Triaxial cyclic compression test

Figure 4.7 shows the average results of the triaxial cyclic compression test. The test was done four times. These results can be found in Appendix F.

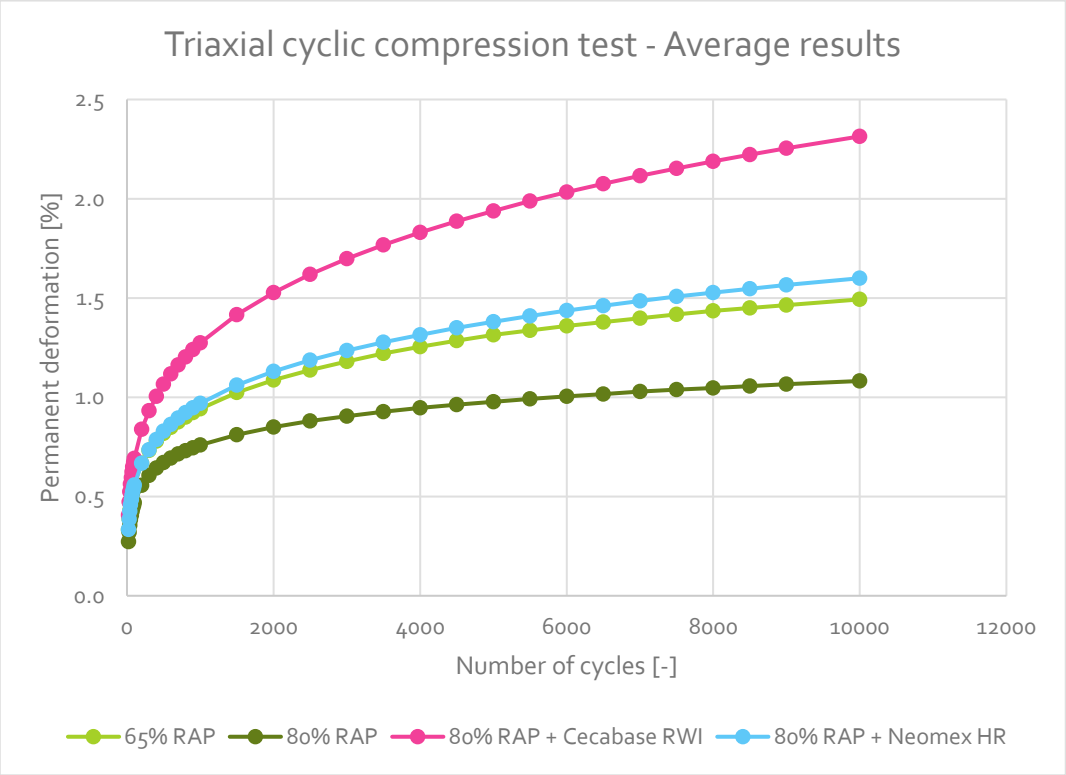

Figure 4.7: Results of the triaxial cyclic compression test

In Figure 4.7, the permanent deformation is given as function of the number of cycles. Here, it turns out that the mixture with 80% RAP has the best resistance to permanent deformation. The total permanent deformation is the lowest and the slope between the 4000th and 10000th cycle is the smallest. Thus, the increase in RAP content leads to an increase in resistance to permanent deformation.

The application of rejuvenating additives leads to a reduction in the resistance to permanent deformation. The mixtures with the rejuvenating additives show much higher permanent deformation and the slope of those mixtures are higher as well.

However, there is also a big difference between the two mixtures with rejuvenator. The mixture with Cecabase shows very high permanent deformation while the mixture with Neomex shows comparable permanent deformation with the 65% RAP mixture. So, the increase in permanent deformation due to Neomex HR is approximately equal to the decrease achieved by the higher RAP content. With the mixture with Cecabase this is not the case. The influence due to Cecabase is much higher than the influence due to the increase in RAP content.

In Table 4.6, the numerical results of the triaxial cyclic compression test are given. The best linear fit of the line describing the permanent deformation between the 4000th and 10000th cycle is

given. The creep rate is given as well. This parameter is the most common to express the resistance to permanent deformation.

Table 4.6: Triaxial cyclic compression test results

	65% RAP	80% RAP	80% RAP + Cecabase RWI	80% RAP + Neomex HR
Intercept linear fit mean [%]	1.115	0.865	1.536	1.144
Standard deviation of the intercept linear fit [%]	0.248	0.046	0.059	0.085
Creep rate mean [µstrains/loading cycle]	0.39	0.23	0.81	0.47
Standard deviation of the creep rate [µstrains/loading cycle]	0.12	0.01	0.06	0.03

Table 4.6 confirms the statements based on Figure 4.7. Both the intercept and the slope of the linear fit of the 80% RAP mixture are the lowest, suggesting that this mixture has the highest resistance to permanent deformation. The increase in RAP content from 65% to 80% leads to a decrease in creep rate of 41%.

Also, the influence of rejuvenating additives is clear. When applying rejuvenating additives, the creep rate increases. For the mixture with Cecabase yields that the creep rate is 3.5 times higher than the creep rate of the 80% RAP mixture without additive. The same kind of influence is seen with the mixture with Neomex, albeit to a lesser extent. The creep rate is doubled compared to the 80% RAP mixture without additive.

Furthermore, it can be seen that the increase due to the rejuvenator is higher than the reduction due to the increase in RAP content. For the Neomex, it is the case that the impact is slightly higher. The creep rate is 21% higher than the 65% RAP mixture. This is not the case with the mixture with Cecabase. The creep rate of this mixture is more than doubled in comparison with the 65% RAP mixture.

4.2.4 Four point bending test

Figure 4.8 shows the overall results of the four point bending test regarding stiffness. The test was done eight times. These results can be found in Appendix G. The 80% RAP mixture is missing due to practical reasons.

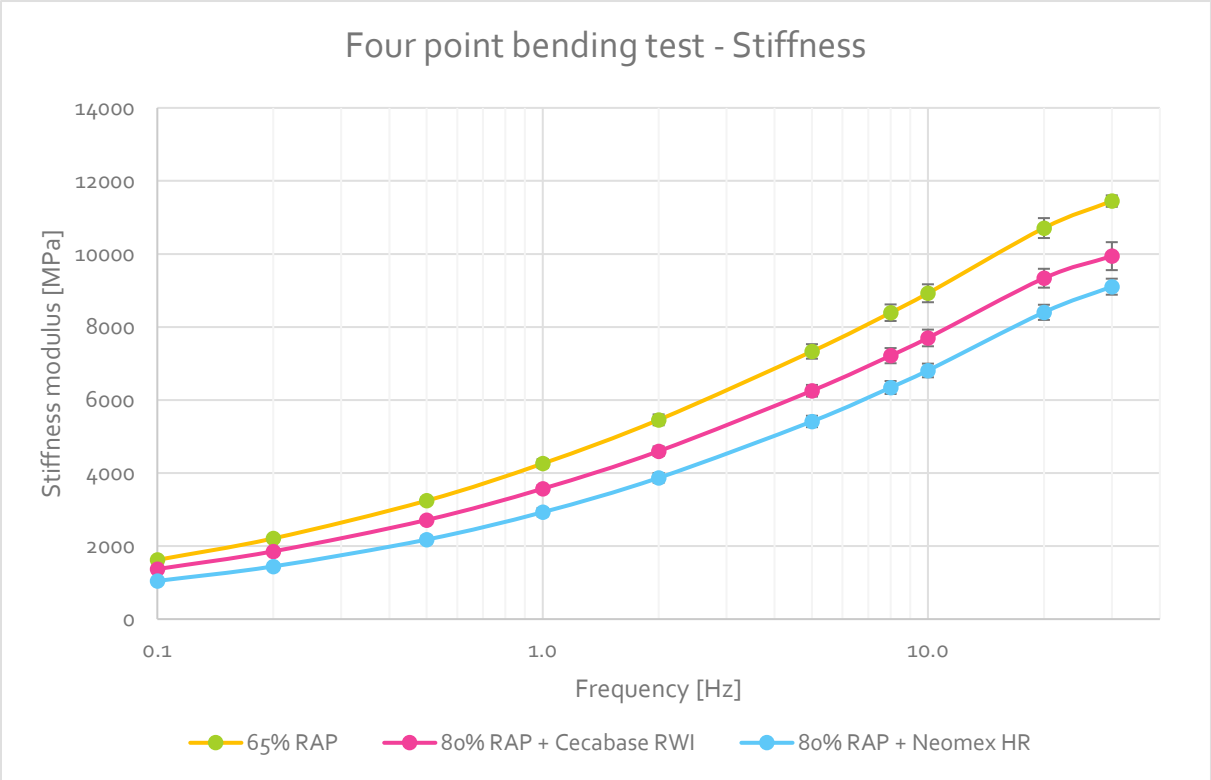

Figure 4.8: Results of the four point bending test for stiffness

The four point bending test is only used for the stiffness measurement, due to time limitations. From Figure 4.8, it can be seen that the stiffness is lower for the 80% RAP with Cecabase RWI and Neomex HR in comparison with the mixture with 65% RAP.

The mixtures largely follow the same course. All stiffness values of the mixture with Cecabase are around 15% lower in comparison with the 65% RAP mixture. So, frequency does not have any influence on the difference in stiffness values between the 65% RAP mixture and the mixture with Cecabase RWI. Regarding the mixture with Neomex HR, the stiffness values are 35% lower for low frequencies and around 23% lower for high frequencies, in comparison with the 65% RAP mixture. So, for small frequencies, the difference is higher than for high frequencies.

Regarding the mutual difference between Cecabase RWI and Neomex HR, the stiffness for the mixture with Neomex HR is much lower than for the mixture with Cecabase RWI. Especially for small frequencies, the difference is high (above 20%). For larger frequencies, this difference is decreasing (approximately 10%).

Like the stiffness measurement of the cyclic ITT, the stiffness values of the four point bending test are reported for the frequency of 8 Hz. Those values are given in Table 4.7.

Table 4.7: Stiffness results four point bending test for frequency = 8 Hz

Mixture	S_{mix} [MPa]	Standard deviation [MPa]
65% RAP	8391	226
80% RAP + Cecabase RWI	7215	208
80% RAP + Neomex HR	6343	177

From Table 4.7, it becomes clear that the application of rejuvenators leads to a lower stiffness, although the RAP content is increased. The stiffness of the mixture with Cecabase measured at a frequency of 8 Hz is 14% lower and the stiffness of the mixture with Neomex is 24% lower in comparison with the 65% RAP mixture.

During the stiffness test, in addition to stiffness, the phase angle is also measured. Figure 4.9 shows the overall results of the four point bending test regarding phase angle. More detailed results can be found in Appendix G. The 80% RAP mixture is missing due to practical reasons.

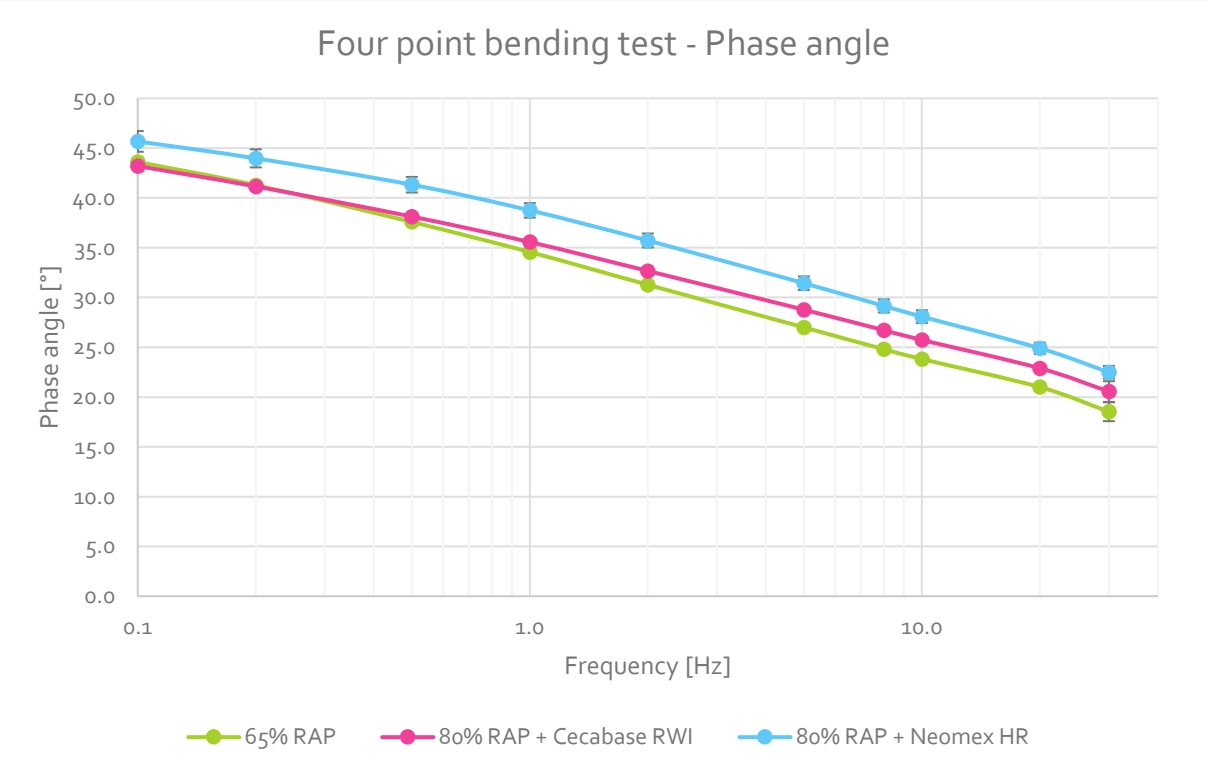

Figure 4.9: Results of the four point bending test for phase angle

For small frequencies, the phase angle is almost the same for the 65% RAP mixture and the mixture with Cecabase. However, for high frequencies there is a difference. The 80% RAP mixture with Cecabase RWI shows higher phase angle values than the mixture with 65% RAP (up to +10%). This means that the behaviour of the mixture with Cecabase RWI regarding phase angle is less dependent on the frequency than the 65% RAP mixture is. The mixture with Neomex HR shows the highest phase angle values for all frequencies. The deviation relative to the 65% RAP mixture becomes higher for larger frequencies. The difference is between 5% and 10% for small frequencies and 21% for the highest frequency.

Regarding the mutual difference between Cecabase RWI and Neomex HR, it can be seen that the mixture with Neomex HR has higher values for all frequencies. Moreover, they largely follow both the same course, but the mixture with Neomex shows for all frequencies around 9% higher values.

Like the stiffness values, the phase angle values are also reported for a frequency of 8 Hz. The results are shown in Table 4.8.

Table 4.8: Phase angle results four point bending test for frequency = 8 Hz

Mixture	δ [°]	Standard deviation [°]
65% RAP	24.8	0.2
80% RAP + Cecabase RWI	26.7	0.1
80% RAP + Neomex HR	29.1	0.7

From Table 4.8, it becomes clear that the phase angle value at 8 Hz is higher for the mixtures with rejuvenator than the value for the 65% RAP mixture. The increase of the mixture with Cecabase is limited: the phase angle value is 8% higher relative to the 65% RAP mixture. The increase of the mixture with Neomex is higher. Relative to the 65% RAP mixture, the phase angle value of the mixture with Neomex is 17% higher.

4.2.5 Compactability

Besides the functional properties, the compactability of the mixture is also considered. The application of high RAP percentages may lead to a decrease in workability, resulting in insufficient compaction of the asphalt mixture. The compactability of the mixture is determined by the number of gyrations when making the gyratory specimens. In total, 18 gyratory specimens per mixture were made to do the material tests. The gyratory performed gyrations until the height of the specimen equaled 77 mm. The number of gyrations needed is reported and its average, rounded to integers, is shown in Figure 4.10. More details can be found in Appendix H.

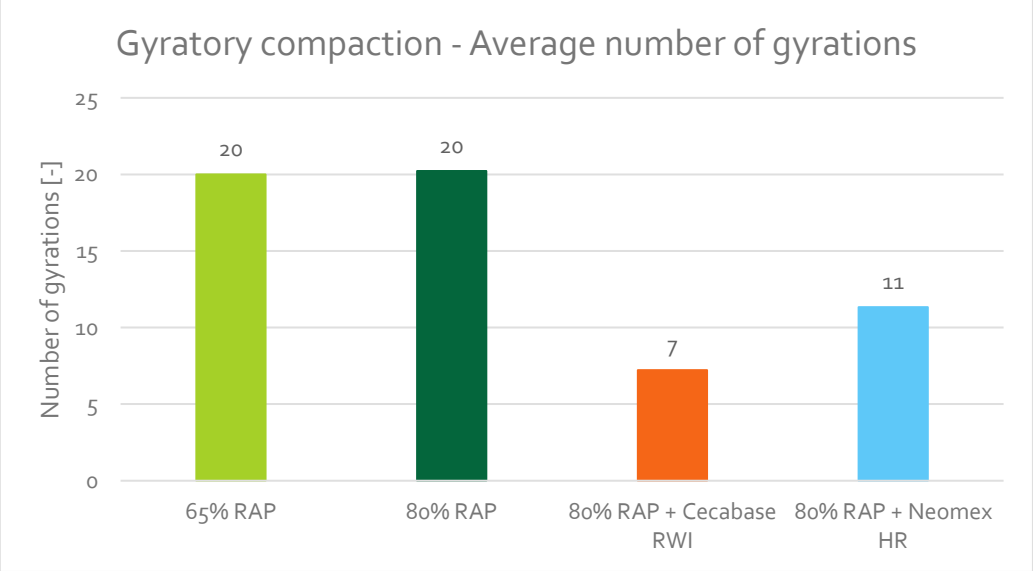

Figure 4.10: Average number of gyrations

From Figure 4.10, it turns out that the number of gyrations is almost the same for the mixture with 65% RAP and the mixture with 80% RAP. So, the increase in RAP content from 65% to 80% does not lead to a decrease in workability. Also, it appears that the application of a softer binder in the 65% RAP mixture does not change the number of gyrations in comparison with the 80% RAP mixture.

Further, the application of a rejuvenating additive leads to a big decrease in the number of gyrations. This means that the mixtures with a rejuvenator can be compacted more easily than the mixtures without a rejuvenator. The number of gyrations required for the mixture with Neomex HR is almost halved compared to the mixture without additive and for the mixture with Cecabase RWI the number of gyrations required is more than halved.

4.2.6 Overview results on mixture level

This section gives an overview of all results on mixture level as presented in the previous sections (4.2.1-4.2.4). The four discussed performance indicators are summarized in Table 4.9 with the parameter describing each performance criterium.

Table 4.9: Overview test results on mixture level

Mixture	ITSR [%]	$S_{mix,cyclic\ ITT}$ [MPa]	$\varepsilon_{6,\ cyclic\ ITT}$ [‰]	f_c [µstrains/ loading cycle]	$S_{mix,4pb}$ [MPa]
65% RAP	80%	8271	0.0252	0.39	8391
80% RAP	97%	10595	0.0301	0.23	-
80% RAP + Cecabase RWI	82%	7528	0.0214	0.81	7215
80% RAP + Neomex HR	102%	7176	0.0231	0.47	6343

A remark has to be made that on the base of Table 4.9, the mixture with 80% RAP without additive shows the best overall performance. However, the ε_6-value describes only partly the fatigue behaviour of the mixture. The results in section 4.2.2.2 shows that the increase in RAP content leads to a better fatigue resistance for the lower and medium strains and a worse fatigue resistance for the highest strains.

4.2.7 Comparison stiffness values of cyclic ITT and four point bending test

Because the stiffness of the mixtures is determined in two ways, the test methods can be compared to each other. Because the mixture with 80% RAP without rejuvenator is excluded from the four point bending test, only a comparison is made between the other three mixtures. This is shown in Figure 4.11, Figure 4.12 and Figure 4.13.

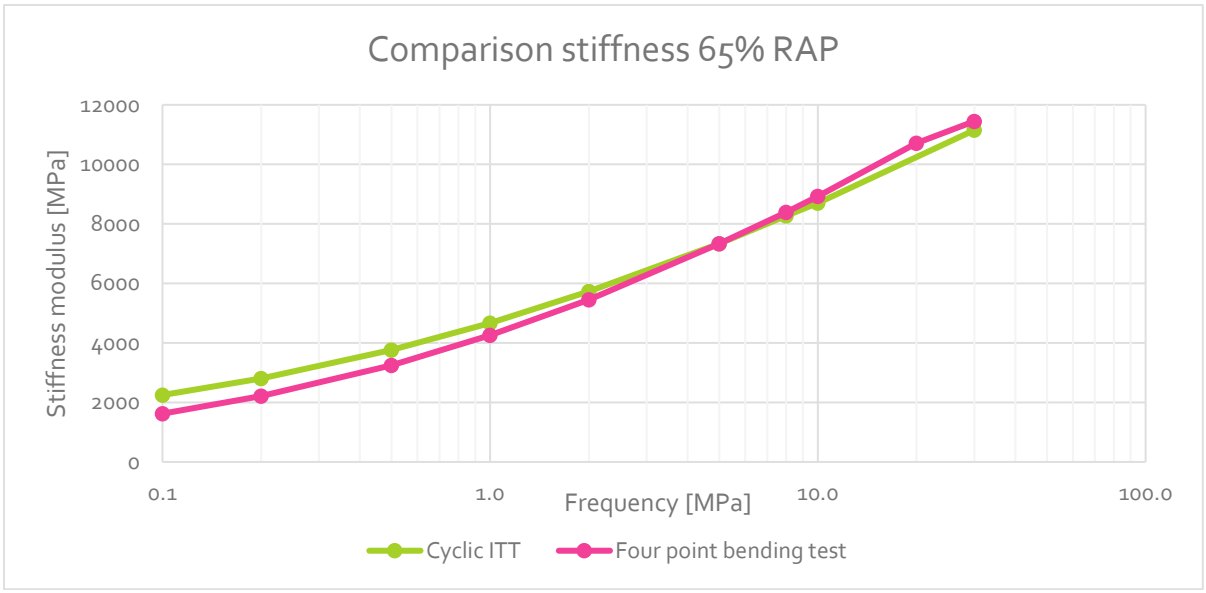

Figure 4.11: Comparison stiffness of cyclic ITT and four point bending test- 65% RAP

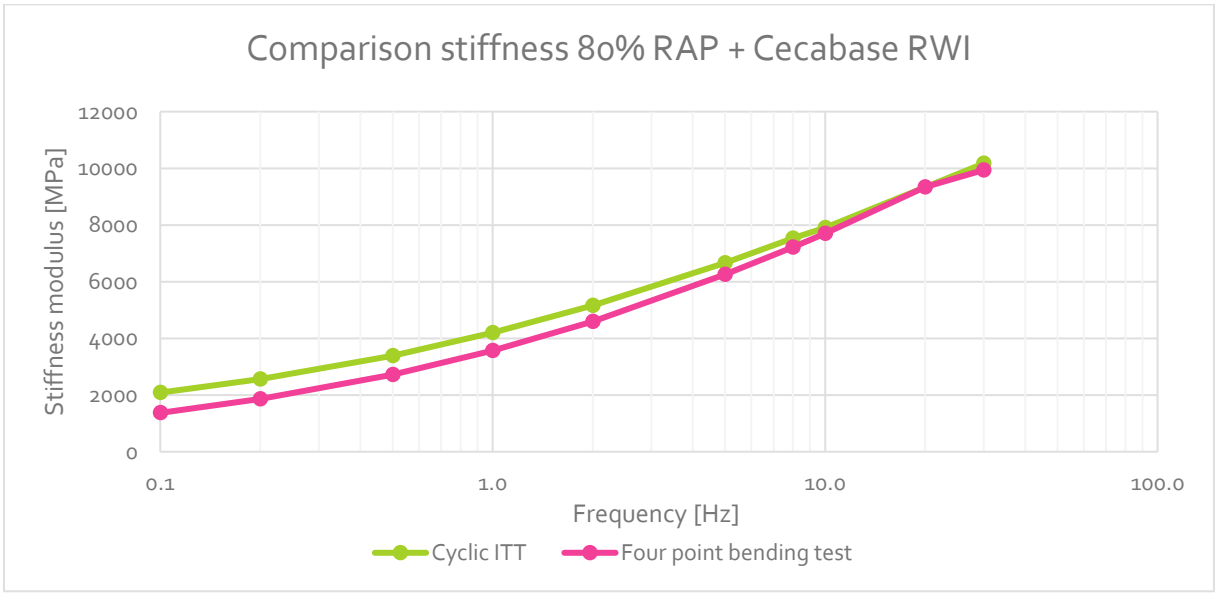

Figure 4.12: Comparison stiffness of cyclic ITT and four point bending test- 80% RAP + Cecabase RWI

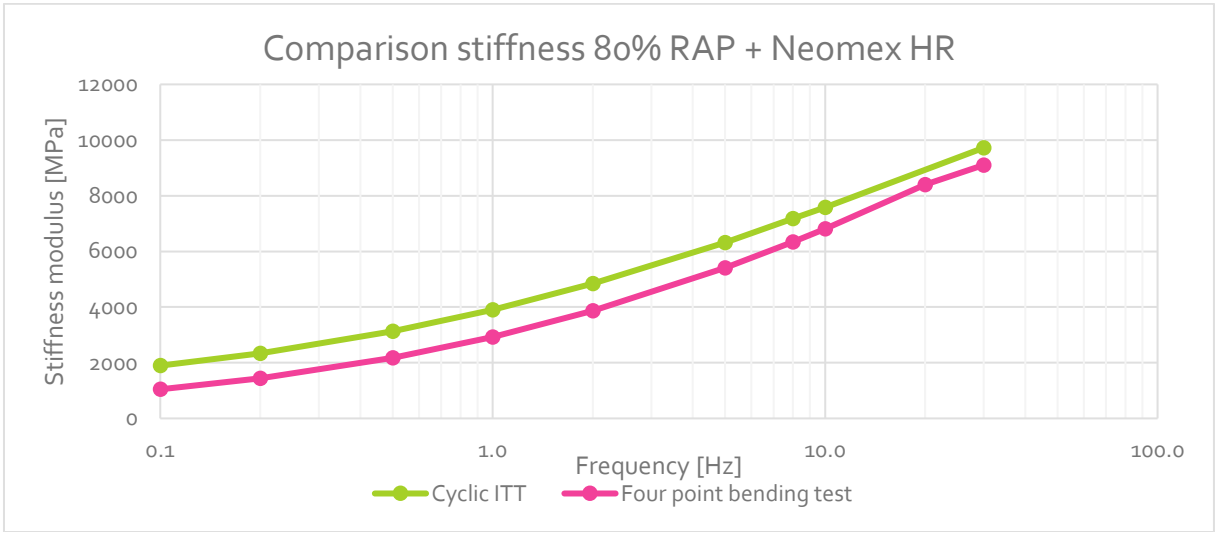

Figure 4.13: Comparison stiffness of cyclic ITT and four point bending test- 80% RAP + Neomex HR

In general yields for the three mixtures that the cyclic ITT shows higher stiffness results than the four point bending test for the lower frequencies. For higher frequencies, the differences are smaller.

For the 65% RAP mixture, the results are the closest to each other. For frequencies of 2 Hz and higher, the deviation is smaller than 5%. For the lowest frequencies, the stiffness results of the cyclic ITT are higher than the results of the four point bending test.
For the mixture with Cecabase RWI, it is the case that the deviation is smaller than 5% for frequencies of 8 Hz and higher. For frequencies below 1 Hz, the deviation is above 25%.

The highest deviations are found for the mixture with Neomex HR. For this mixture, the stiffness results of the cyclic ITT are quite a bit higher than the stiffness results of the four point bending test, especially for the lower frequencies.

It is noticeable that for all three mixtures, the line of the four point bending test is steeper than the line of the cyclic ITT. Over the different frequencies, the stiffness change is higher for the four point bending test than for the cyclic ITT. The stiffness values of the four point bending test increase faster with an increasing frequency than the stiffness values of the cyclic ITT.

In Table 4.10, the stiffness results of both tests for the frequency of 8 Hz are given.

Table 4.10: Stiffness results cyclic ITT and four point bending test for frequency = 8 Hz

Mixture	S_{mix} cyclic ITT [MPa]	S_{mix} 4 point bending test [MPa]
65% RAP	8271	8391
80% RAP + Cecabase RWI	7528	7215
80% RAP + Neomex HR	7176	6343

It confirms that with the mixture with Neomex HR the greatest difference is observed. Relative to the stiffness of the cyclic ITT, the stiffness measured by the four point bending test is 12% lower. For the mixture with Cecabase, the difference is 4% and for the 65% RAP mixture, the difference is just 1%. Considering the standard deviation, which is smaller in the four point bending test than in the cyclic ITT, the differences are within the error margins for the 65% RAP mixture and the mixture with Cecabase. For the mixture with Neomex this is not the case, which means that the stiffness value of the cyclic ITT is significantly higher than the stiffness value of the four point bending test.

4.2.8 Comparison results of binder level and mixture level

Because the tests are executed at both binder level and mixture level, the results at both levels regarding stiffness and fatigue resistance can be compared to each other. Regarding to the binder level, both the results of the unaged binder and the results after RTFOT are included, because the specimens the specimens were not aged on mixture level. Therefore, only the results of the unaged binder and after RTFOT will be considered. Regarding the mixture level, the stiffness results of the

cyclic-ITT are chosen to be able to compare the 80% RAP mixture without additive. This mixture was excluded for the four point bending test.

Because the 65% RAP mix composition is not tested on binder level, it is excluded in this comparison. The comparison is given in Table 4.11 for stiffness and Table 4.12 for fatigue resistance.

Table 4.11: Stiffness results binder level and mixture level for frequency = 8 Hz

Mix composition	Binder level		Mixture level
	G^*_{unaged} [MPa]	G^*_{RTFOT} [MPa]	$S_{mix,\ cyclic\ ITT}$ [MPa]
80% RAP	12.3	16.3	10595
80% RAP + Cecabase RWI	4.2	7.2	7528
80% RAP + Neomex HR	4.8	5.6	7176

Table 4.12: Fatigue resistance results binder level and mixture level for frequency = 8 Hz

Mix composition	Binder level		Mixture level
	$\varepsilon_{6,unaged}$ [%]	$\varepsilon_{6,RTFOT}$ [%]	ε_6 [‰]
80% RAP	0.596	0.552	0.0301
80% RAP + Cecabase RWI	0.538	0.603	0.0214
80% RAP + Neomex HR	0.574	0.628	0.0231

Regarding the stiffness results in Table 4.11, it can be seen that the higher stiffness value of the 80% RAP at bitumen level is also found at mixture level. For the mixtures with rejuvenators, it is difficult to draw a conclusion based on the stiffness results. Using the results of the unaged binder, the values are close to each other, which is also the case for the stiffness values at mixture level. However, on binder level, the mixture with Neomex has a higher stiffness value, but on mixture level it is the other way around.

Using the results after RTFOT, the ranking of the mix compositions on binder level is the same as on mixture level. The 80% RAP mixture shows the highest value, followed by the mixture with Cecabase and Neomex. However, the difference between the stiffness values of the compositions with rejuvenators at bitumen level suggests that there is a greater stiffness difference at mixture level than it ultimately turns out to be.

Regarding the fatigue resistance results in Table 4.12, it seems that the unaged results of the binder better match the results of the mixture than the RTFOT results. Looking at the results of the unaged binder, the ranking of the three mixture compositions corresponds to the ranking on mixture level. With the RTFOT results, this is not the case. The mix composition of 80% RAP shows the lowest ε_6-value after RTFOT but scores the highest at mixture level. Based on that, the fatigue resistance results of the unaged binder are more consistent with the mixture level results.

In conclusion, with this limited number of results, it is difficult to make a link between the results at binder level and at mixture level. Based on the fatigue results, the unaged binder results seem to agree best with the mixture results, at least on ranking. However, based on the stiffness results, this does not seem to hold true. There, the ranking is correct if the RTFOT results are used.

5 Micromechanical prediction of the stiffness of mixtures with high RAP percentages

In this chapter, micromechanical models are used to predict the stiffness of the tested asphalt mixtures. As indicated in section 2.5.2, only the Hirsch model will be applied due to time constraints. Multiple proposed modifications of the Hirsch model are included to examine their applicability to mixtures with high RAP percentages. Firstly, the original Hirsch model proposed by Christensen Jr et al. (2003) is applied and after that the proposed simplified Hirsch model with inclusion of the factor P_a by Zhang et al. (2018b) model is used to predict the stiffness of mixtures with high RAP percentages. In the first place, the proposed expression of P_a is used to predict the stiffness of the mixtures. Afterwards, an alternative expression of P_a is determined using the mixture results of the 80% RAP mixture and then this P_a is used to predict the stiffness of the two mixtures with additive. The 65% RAP mixture is excluded in this chapter because this composition is not tested at binder level.

The models are applied according to the following steps:

1. Determination of volume fractions of different phases
2. Calculation of the contact factor P_c / aggregate organization factor P_a
3. Calculation of the stiffness values

5.1 Application of the original Hirsch model

At first, the original Hirsch model is applied. This model should be applicable to mixtures containing RAP material (Christensen & Bonaquist, 2015). It is unclear if this also yields for mixtures with very high RAP percentages and the application of rejuvenating additives. Further, the used expressions are empirically found, so depending on what mixtures were used to calibrate, the predicted values may or may not be accurate.

5.1.1 Determination of the volume fractions of the different phases

The determination of the volume fractions is based on the mixture density of the cylindrical drill core specimens, because those specimens give the most representative results. The volume fraction of the air voids is determined with equation 5.1.

$$\mathbf{f_v = \frac{\rho_{max} - \rho_{mix}}{\rho_{max}}} \quad (5.1)$$

where: f_v = volume fraction air voids [-]
ρ_{max} = maximum density [kg/m³]
ρ_{mix} = mixture density [kg/m³]

The volume fraction of the bitumen is determined using equation 5.2. For the mass percentage of the binder, the target percentage is used as follows from the mix design, which is equal to 4.3 %. The density of the binder is 1025 kg/m³.

$$\mathbf{f_b = \frac{m_{\%,binder}}{100} * \frac{\rho_{mix}}{\rho_b}} \quad (5.2)$$

where: f_b = volume fraction binder [-]
$m_{\%,binder}$ = mass percentage binder [%]
ρ_{mix} = mixture density [kg/m³]
ρ_b = binder density [kg/m³]

After determining the volume fraction of air voids and the binder, the volume fraction of the aggregate can be easily determined on the condition that $f_a + f_b + f_v$ is equal to 1.

Equations 2.17 and 2.18 are used to determine VMA and VFA. For the density of the aggregate, a value of 2648 kg/m³ is used. Detailed calculations can be found in Appendix I.

5.1.2 Calculation of the contact factor P_c

For the calculation of P_c, equation 2.16 is used. Besides the calculated VMA and VFA from the previous section, the dynamic shear modulus of the binder is needed. Those values are given in Appendix C. The unaged results are used because the resulting mixture stiffness being compared to is also unaged. The calculated P_c values are shown in Figure 5.1. The detailed calculation of the contact factor can be found in Appendix I.

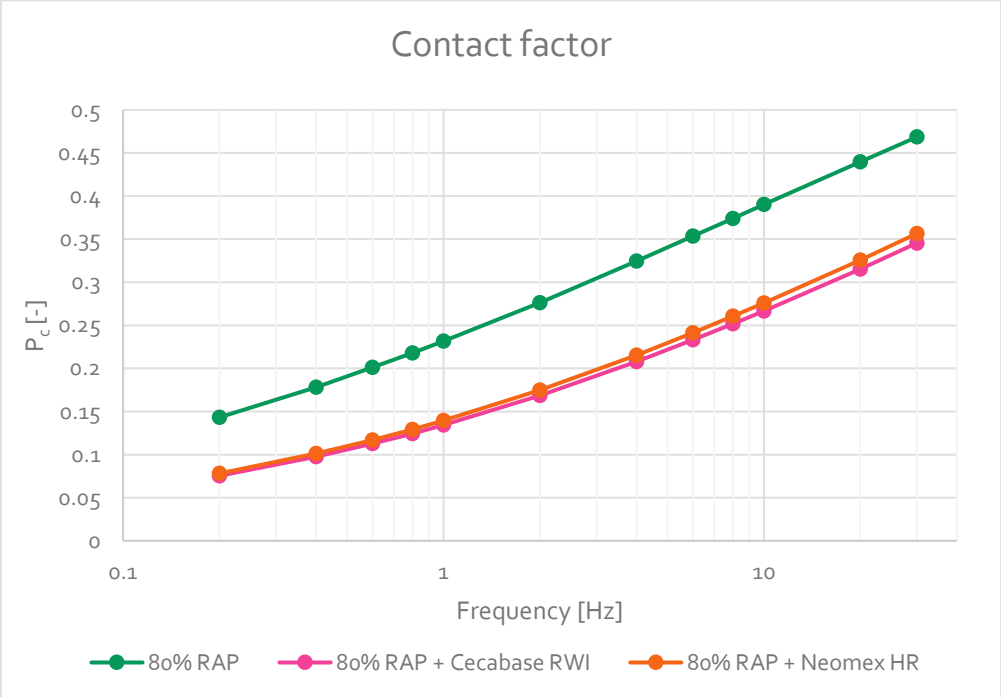

Figure 5.1: P_c values for original Hirsch model

In Figure 5.1, it can be seen that the 80% RAP mixture shows the highest value for P_c. This suggests that the prediction of the stiffness of the 80% RAP mixture is higher than the two mixtures with rejuvenating additive. Further, the P_c for the mixtures with rejuvenator is almost the same, so a comparable prediction of the stiffness may be expected.

5.1.3 Calculation of the stiffness values

For the calculation of the stiffness values of the asphalt mixtures, equation 2.15 is used. Detailed calculations can be found in Appendix I.

The predicted stiffness values can be compared with the measured stiffness values presented in chapter 4. The comparison is made with the results from the cyclic ITT, because the 80% RAP mixture without additive is not tested with the four point bending test. Further, the density used for the determination of the volume fractions is based on the cyclic ITT specimens.

The comparisons for the three mixtures are given in Figure 5.2, Figure 5.3 and Figure 5.4. The magenta colored line represents the line of equality. The closer the points are to this line, the better the prediction.

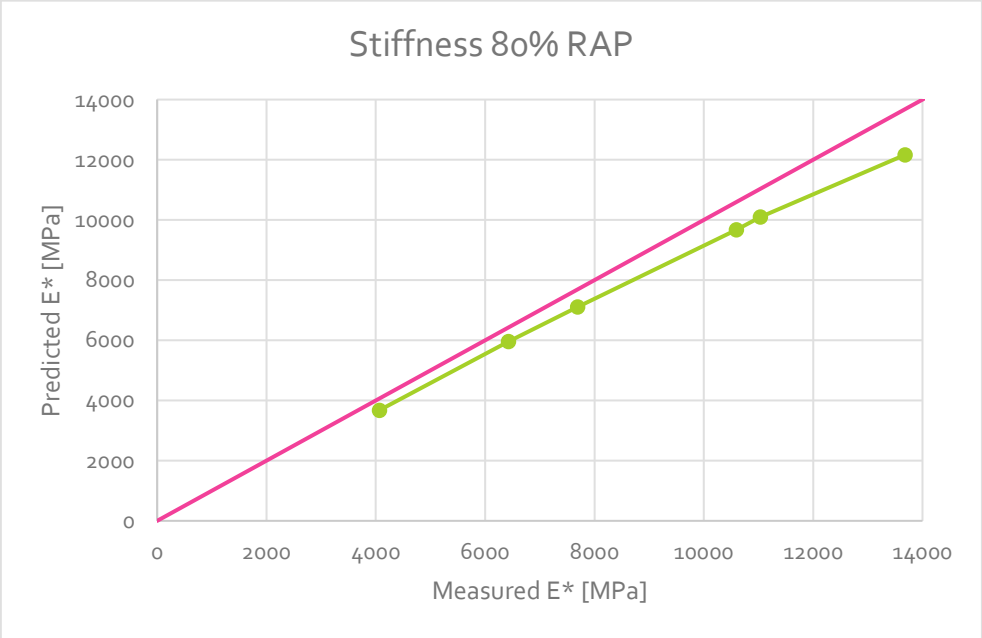

Figure 5.2: Comparison between measured stiffness and predicted stiffness using original Hirsch model – 80% RAP

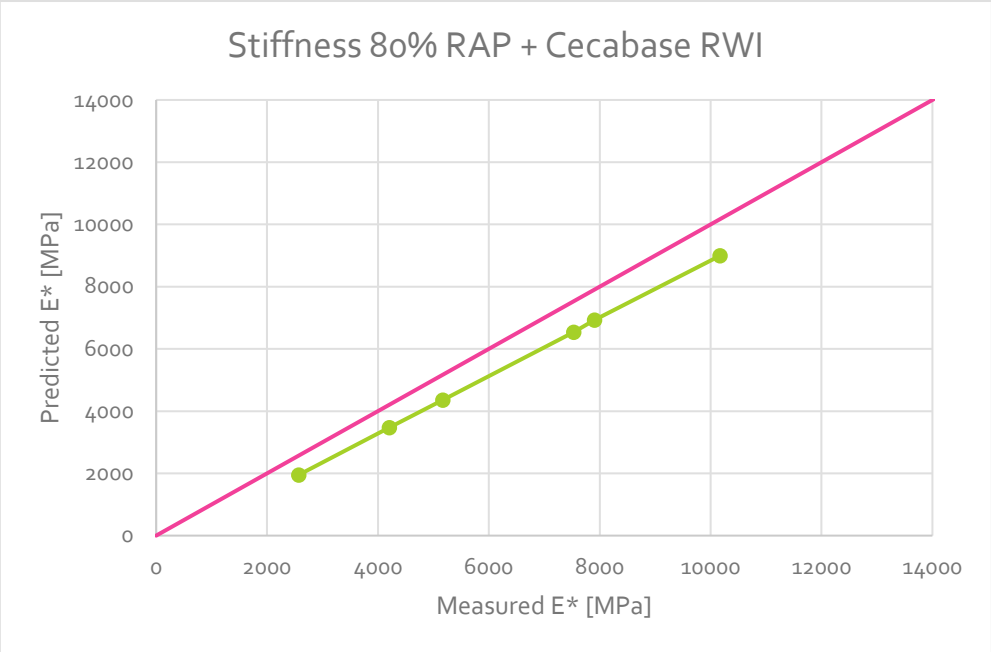

Figure 5.3: Comparison between measured stiffness and predicted stiffness using original Hirsch model – 80% RAP + Cecabase RWI

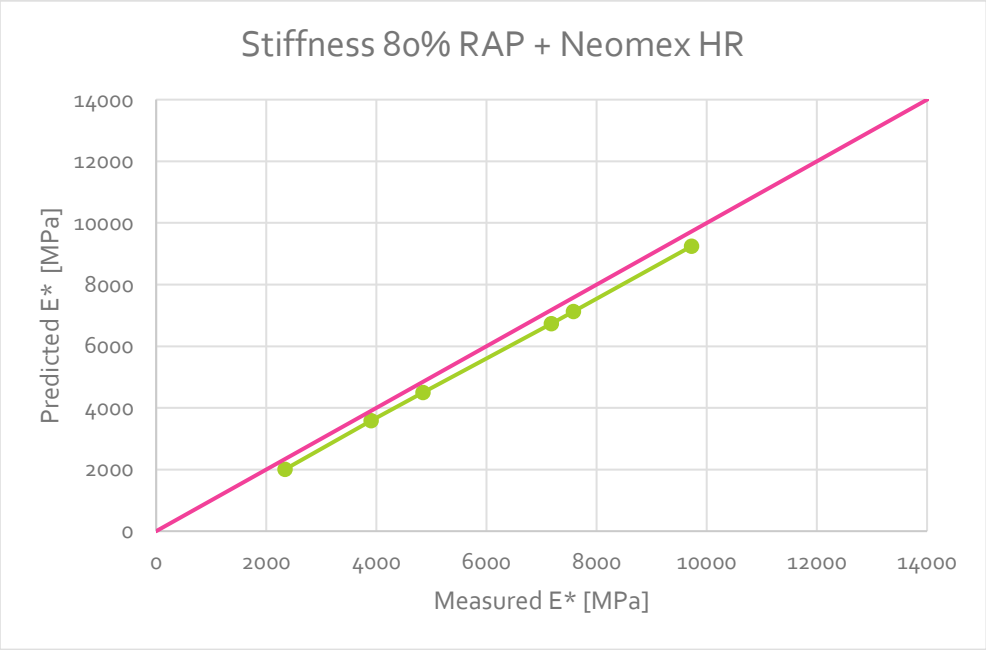

Figure 5.4: Comparison between measured stiffness and predicted stiffness using original Hirsch model – 80% RAP + Neomex HR

From Figure 5.2, Figure 5.3 and Figure 5.4, it turns out that the original Hirsch model shows reasonably accurate results. Further, all predicted stiffness values are lower than the measured stiffness values. This means that the original Hirsch model underestimates the mixture stiffness for all frequencies.

For the two mixtures with rejuvenator, the accuracy is similar for all frequencies. For the mixture without rejuvenator, it can be seen that the highest deviation is found for the highest frequency. Thus, it becomes clear that the original Hirsch model with the applied model coefficients can be

applied on mixtures with high RAP percentages. Further, it becomes clear that the application of rejuvenating additives does not lead to a lower accuracy.

To assess the accuracy of the predicted stiffness values, the root mean squared error is determined. The result is given in Table 5.1.

Table 5.1: Root mean squared error for stiffness predictions using original Hirsch model

Mixture	Root mean squared error [MPa]
80% RAP	951.2
80% RAP + Cecabase RWI	903.1
80% RAP + Neomex HR	399.0

From Table 5.1, it turns out that the mixture with Neomex HR shows the smallest error. The errors for the 80% RAP mixture and the mixture with Cecabase RWI are comparable and substantially higher than the error for the mixture with Neomex HR.

The error values in Table 5.1 can be compared with the standard deviation values for the measured stiffness results in Table 4.3. It turns out that the values are of similar order of magnitude for the mixture with Neomex. For the other two mixtures yields that the root mean squared error is around three times higher than the standard deviation of the measured stiffness values.

5.2 Application of the simplified Hirsch model with inclusion of P_a

As second, the simplified Hirsch model with inclusion of the factor P_a proposed by Zhang et al. (2018b), as presented in paragraph 2.5.1, is applied. This is applied twice: once with the proposed P_a values by Zhang et al. (2018b) and once with alternative fitting parameters based on the own laboratory research.

The first step, the determination of the volume fractions of each phase, is the same as in section 5.1.1 and thus is not repeated.

5.2.1 Validation of proposed expression of P_a

5.2.1.1 Calculation of the aggregate organization factor P_a

The existing expression of P_a proposed by Zhang et al. (2018b) and presented in paragraph 2.5.1 is applied on the test results of this research to study if it is possible to apply this expression on those mixtures. For this, equation 2.22 is used with the fitting parameters presented in Table 2.1. Further, there has been made use of the DSR results of the unaged binder specimens (Appendix C) and the calculated volume fractions (Appendix I). The resulting P_a values are shown in Figure 5.5. Detailed calculations can be found in Appendix I.

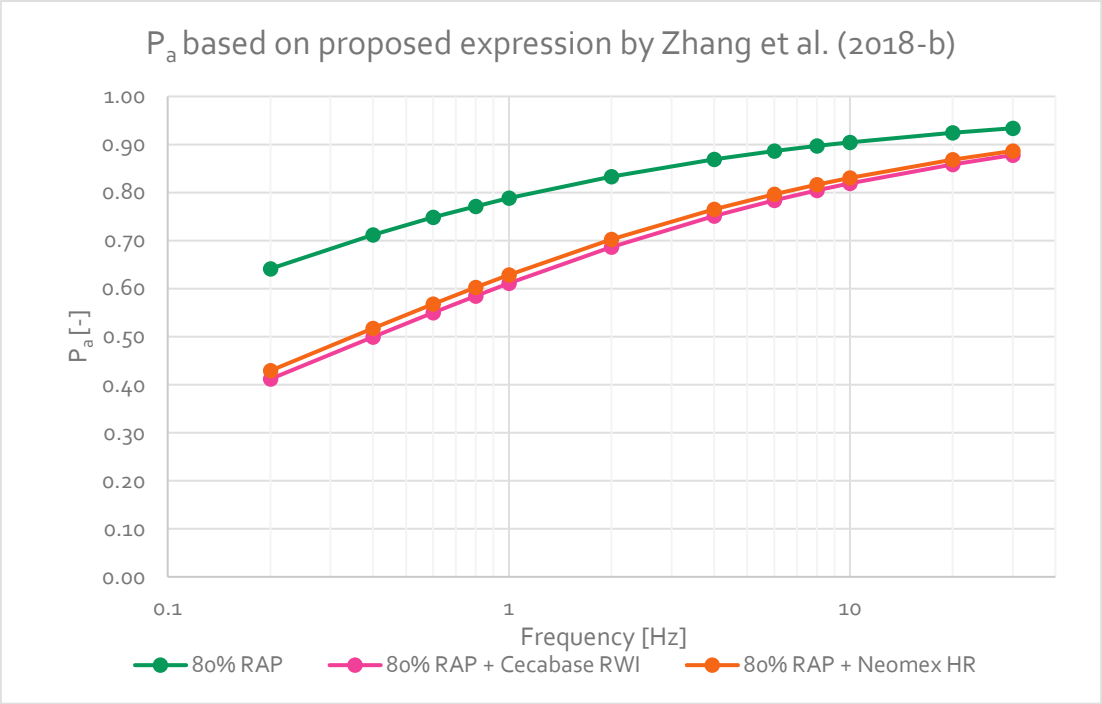

Figure 5.5: P_a values based on proposed expression by Zhang et al. (2018-b)

In Figure 5.5, it can be seen that the 80% RAP mixture shows the highest value for P_a, which suggests that the stiffness value will be the highest for this mixture. Further, it can be seen that the P_a values are almost the same for the two mixtures with rejuvenator. Also, the difference between the mixtures with additive and without additive is smaller when the frequency increases.

5.2.1.2 Calculation of the stiffness values

For the calculation of the stiffness values of the asphalt mixtures, equation 2.21 is used. Besides the calculated P_a values (section 5.2.1.1), the volume fractions (section 5.1.1) and the complex shear modulus (Appendix C), the Poisson's ratio of the binder and the Young's modulus of the aggregates are needed. Those two parameters are estimated. For the Poisson's ratio, a value of 0.35 is assumed and for the Young's modulus of the aggregate, a value of 53000 MPa is assumed.

Detailed calculations are shown in Appendix I.

Likewise with the Hirsch model, the resulting stiffness values are compared with the measured stiffness results from the cyclic ITT. The comparisons for the three mixtures are given in Figure 5.6, Figure 5.7 and Figure 5.8.

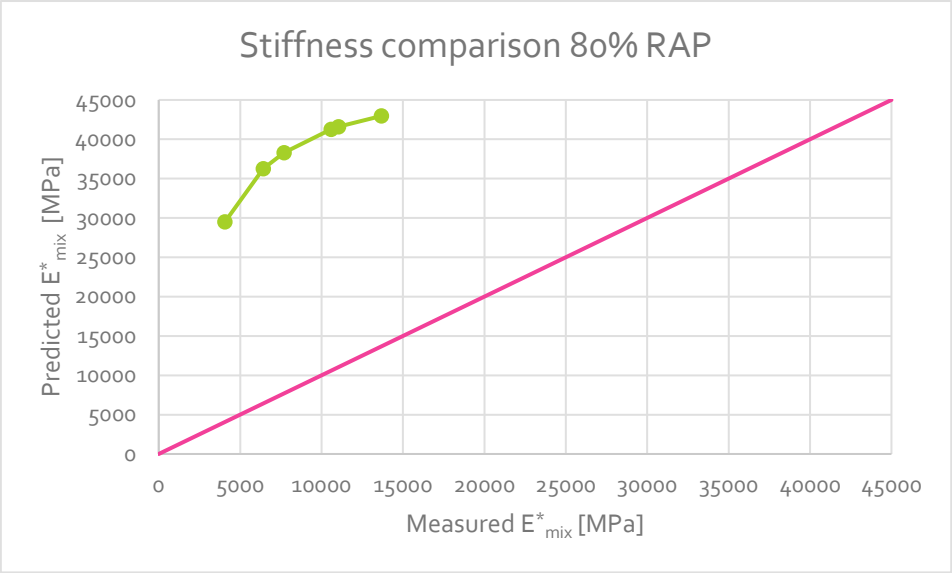

Figure 5.6: Comparison between measured stiffness and predicted stiffness using P_a values of Figure 5.5 – 80% RAP

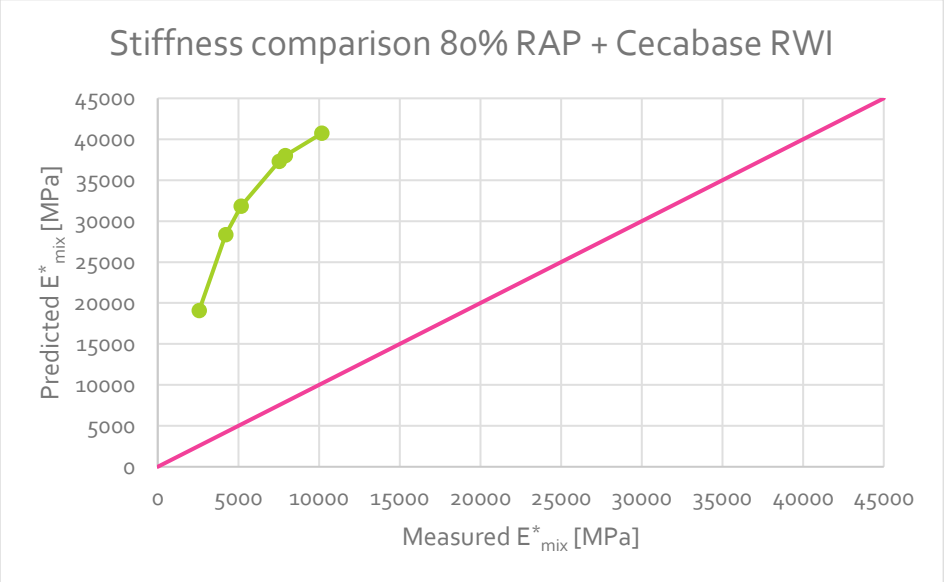

Figure 5.7: Comparison between measured stiffness and predicted stiffness using P_a values of Figure 5.5 – 80% RAP + Cecabase RWI

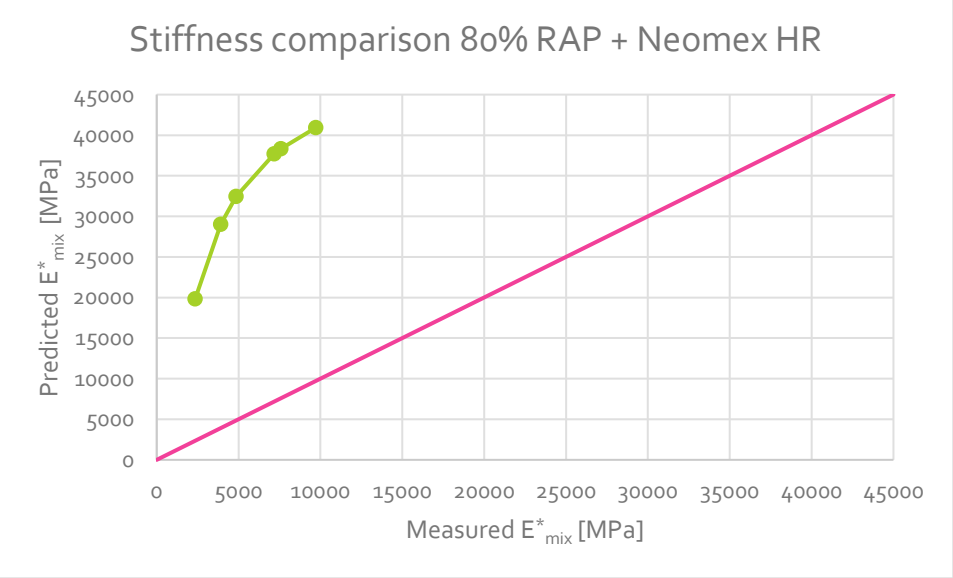

Figure 5.8: Comparison between measured stiffness and predicted stiffness using P_a values of Figure 5.5 – 80% RAP + Neomex HR

From Figure 5.6, Figure 5.7 and Figure 5.8, it becomes clear that the proposed parameters cannot be used to predict the stiffness of this kind of mixtures. The predicted values are much higher in comparison with the measured stiffness values. The resulting P_a values of Figure 5.5 are too high with the result that the stiffness values are also too high. The expression for P_a was calibrated to an open graded mixture without RAP material, so it turns out that the fitting parameters are not applicable to other kind of mixtures such as the asphalt mixtures with high RAP percentages and rejuvenators as considered in this study.

5.2.2 Application of alternative fitting values for P_a

Because the P_a values of the paper of Zhang et al. (2018b) do not lead to reliable stiffness predictions, the fitting parameters a, b, c and d in equation 2.9 are modified and determined with the own laboratory results. The stiffness measurements of the 80% RAP mixture are used to fit equation 2.22 to the measured results. Then, this newly fitted expression is used to predict the stiffness for the two mixtures with rejuvenating additive.

It can be expected that the modification of the fitting parameters leads to better prediction of the stiffness values. This is because the same type of mixture was used to calibrate the parameters as for which it is applied. The main difference is the addition of a rejuvenator. It is expected that this does not lead to inaccurate predictions.

5.2.2.1 Calculation of alternative P_a values

Equation 2.21 is converted so that P_a can be calculated on the based of the measured stiffness of the mixture (equation 5.3).

$$\mathbf{P_a} = \frac{\mathbf{|E^*|_{mix} - f_b * 2 * (1 + \nu) * |G^*|_{binder}}}{\mathbf{f_a * E_a}} \tag{5.3}$$

where:

P_a	=	aggregate organization factor	[-]
$\|E^*\|_{mix}$	=	dynamic complex modulus mixture	[N/mm²]
f_b	=	volume fraction binder	[-]
ν	=	Poisson's ratio binder	[-]
$\|G^*\|_{binder}$	=	complex shear modulus binder	[N/mm²]
f_a	=	volume fraction aggregate	[-]
E_a	=	Young's modulus aggregate	[N/mm²]

Equation 5.3 is used to determine the P_a values of the 80% RAP mixture and those results are fit in equation 2.22, resulting in new values for the parameters a, b, c and d. Those new values are shown in Table 5.2.

Table 5.2: New fitting parameters

Parameters	a	b	c	d
Values	0.0030	-2.46	0.52	0.81

Comparing the new fitting parameters in Table 5.2 with the proposed fitting parameters by Zhang et al. (2018b) in Table 2.1, it turns out that parameters b and d in particular differ greatly. These two parameters also change sign.

With the new fitting parameters, P_a can be calculated for the three mixtures with equation 2.22. The results are shown in Figure 5.9. More detailed results can be found in Appendix I.

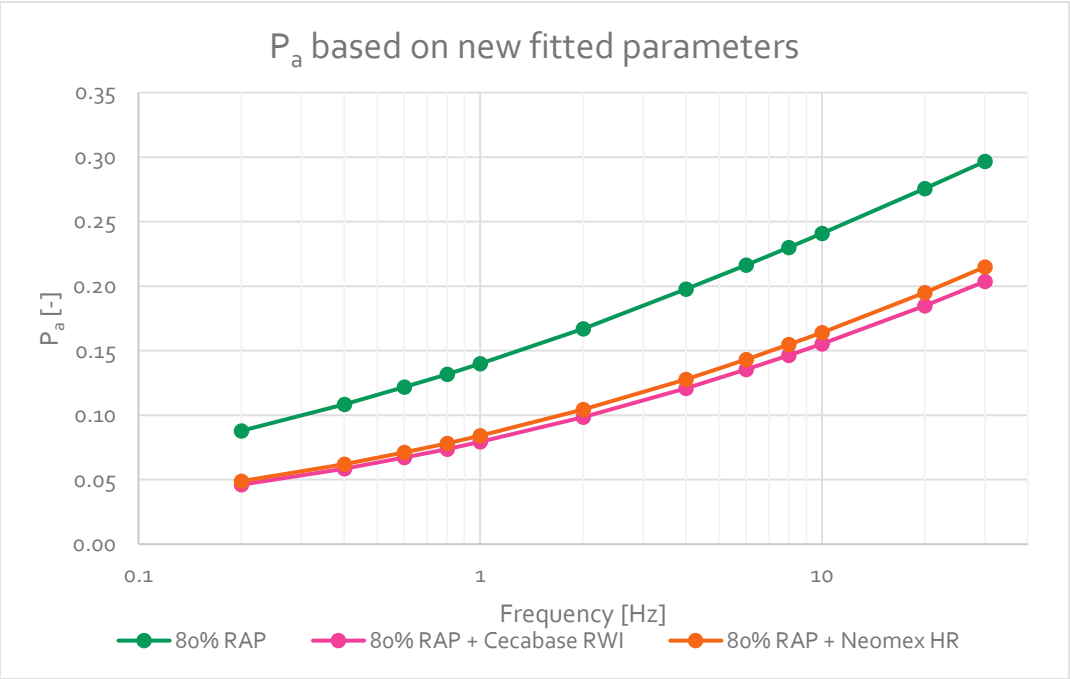

Figure 5.9: P_a values based on new fitted parameters

Comparing the P_a values based on the existing fitting parameters (Figure 5.5) and the P_a values based on the new fitted parameters (Figure 5.9), it turns out that the values based on the new fitted parameters are much lower. Moreover, the progress over the frequency differs greatly. The values based on the existing parameters are decreasingly increasing with increasing frequency while the values based on the new parameters are increasingly increasing.

5.2.2.2 Calculation of the stiffness values

Equation 2.21 is then used to determine the stiffness values, in the same way as it is done in section 5.2.1.2. The results are shown in Figure 5.10, Figure 5.11 and Figure 5.12. Detailed results can be found in Appendix I.

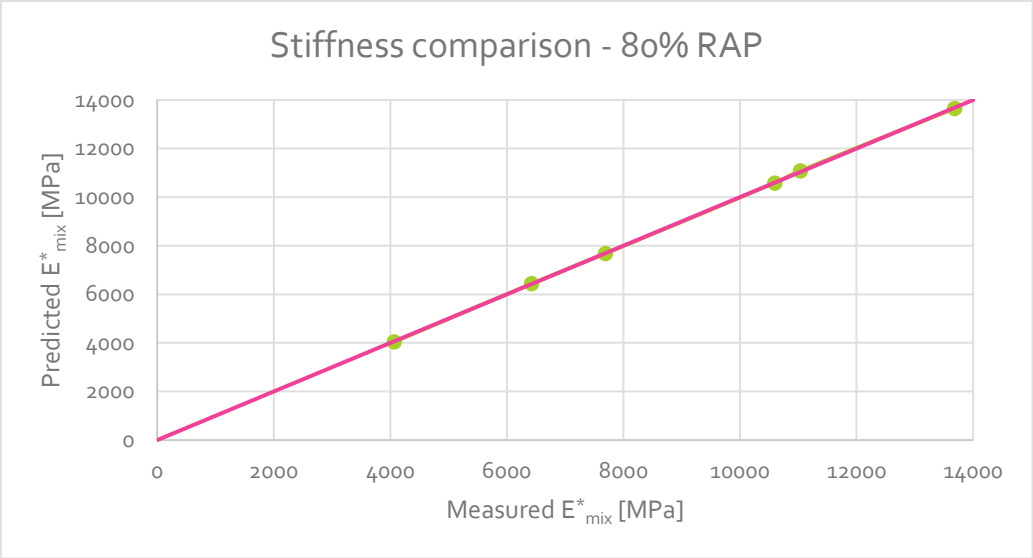

Figure 5.10: Comparison between measured stiffness and predicted stiffness using alternative fitting values for P_a – 80% RAP

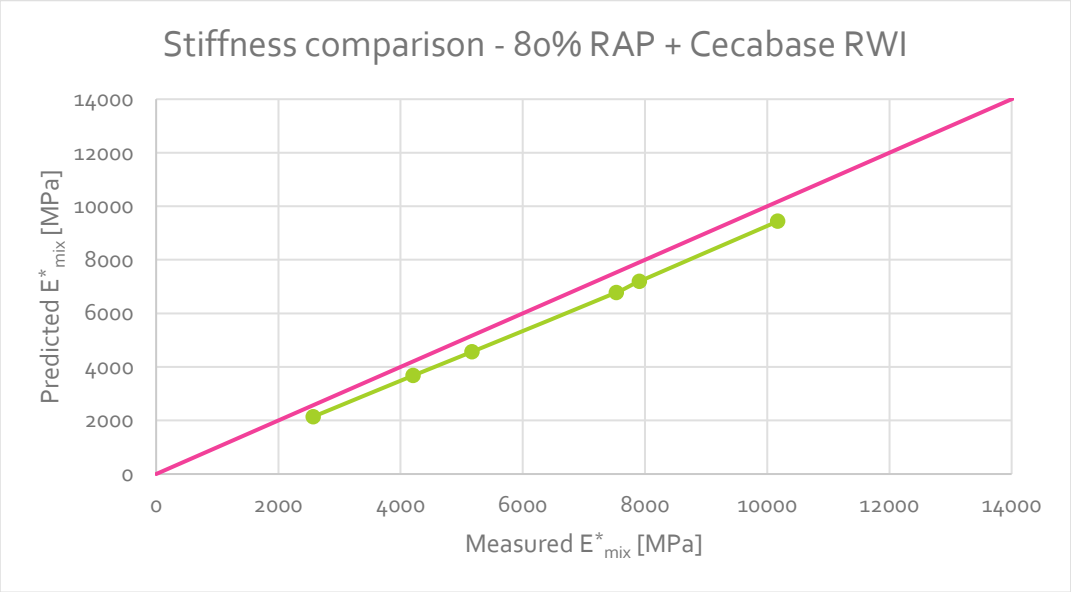

Figure 5.11: Comparison between measured stiffness and predicted stiffness using alternative fitting values for Pa – 80% RAP + Cecabase RWI

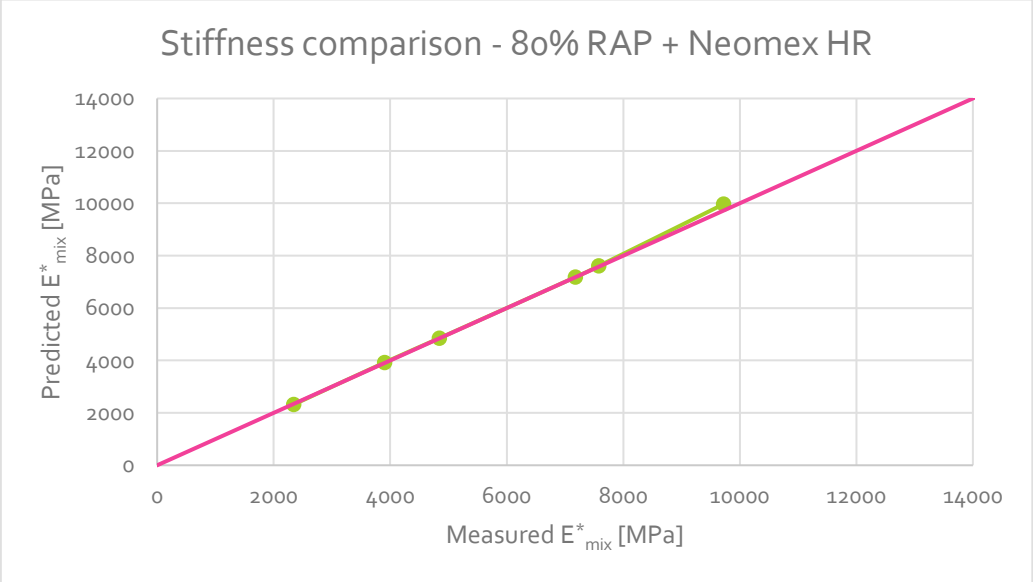

Figure 5.12: Comparison between measured stiffness and predicted stiffness using alternative fitting values for Pa – 80% RAP + Neomex HR

It turns out that the results fit a lot better when the expression for P_a is fit for the kind of used mixture. The results are best predicted for the 80% RAP mixture because the results are fit using this mixture. For the other two mixtures, it is the case that the results can be predicted with a reasonably high accuracy. The predicted stiffness for the mixture with Cecabase is systematically underestimated but the difference is quite small.

So, it becomes clear that the model is applicable on the type of asphalt mixtures for which it is calibrated. For comparable mixtures with rejuvenating additives, the model is still applicable.

The root mean squared error for the three mixtures is given in Table 5.3.

Table 5.3: Root mean squared error for stiffness predictions using alternative fitting values for Pa

Mixture	Root mean squared error [MPa]
80% RAP	23.0
80% RAP + Cecabase RWI	562.9
80% RAP + Neomex HR	101.6

The root mean squared error in Table 5.3 confirms that the prediction for the 80% RAP mixture is the most accurately. This is logical because the model is fit with the laboratory results of this mixture. The root mean squared error for the other two mixture is quite small. It appears that the stiffness of the mixture with Neomex HR is better predicted than the stiffness of the mixture with Cecabase RWI. The addition of rejuvenating additives does not mean that the fitting parameters are no longer applicable.

Furthermore, the error values for the simplified Hirsch model are also lower than the standard deviation of the stiffness tests except for the mixture with Cecabase. From this it can be noted that the model shows accurate results and are comparable with the accuracy of the laboratory results.

The error values in Table 5.3 are also lower than the error values of the original Hirsch model. This suggests that the application of the simplified Hirsch model with inclusion of P_a is more accurate than the original Hirsch model. However, it should be noted that the original Hirsch model was applied with general model coefficients and the simplified model was calibrated for the type of mixture applied.

6 Conclusions and recommendations

In this chapter, conclusions are drawn and the answers are given on the research questions. First, the conclusions for the main research objective are discussed and then the sub-questions are answered. Further, recommendations are made for future research.

6.1 Conclusions

6.1.1 Main research objective

In this research, the main objective was to study the multi-scale material properties of hot mix asphalt mixtures with high RAP percentages, to study if it is possible to increase the RAP content. This was done by a DSR test on binder level and the ITT, the cyclic ITT, the triaxial cyclic compression test and the four point bending test on mixture level.

Based on the material tests and comparing it with the reference (65% RAP mixture), it turns out that there is potential to implement 80% RAP mixtures. Both moisture sensitivity and the rutting resistance are improved when a higher RAP content is applied, while the total fracture toughness has remained the same. The stiffness of the 80% RAP mixture is substantially higher, but it is still applicable. The biggest concern is the fatigue resistance, because the fatigue resistance of the 80% RAP mixture without additive is worse for higher strains relative to the 65% RAP mixture.

The application of the rejuvenating additives leads to the properties of the 80% RAP mixtures being more similar to the 65% RAP mixture and the workability is improved. However, it does appear that the dosage of the additives is on the high side. The stiffness is lower than the reference mixture, especially the mixture with Neomex. Also, the rutting resistance is lower than the reference mixture, especially the mixture with Cecabase.

Thus, increasing the RAP content to 80% partially provides better material properties, but attention must be paid to the fatigue resistance, especially for higher strains. The application of a rejuvenator to the mixture with 80% RAP can approach the material properties of the 65% RAP mixtures and greatly improve the workability. However, the application would require the use of a lower dosage than done in this study to avoid overcompensation. It is difficult to indicate which of the two rejuvenators is best for this purpose. The stiffness of the mixture with Cecabase approaches the reference better but in terms of fracture toughness and rutting resistance the mixture with Neomex matches better.

6.1.2 Sub-questions

1. What characterizes a HMA with RAP?

Section 2.3 characterizes HMA with RAP based on its functional properties. Based on literature studies, the stiffness of the mixture is higher when RAP material is applied. Because the binder is hardened over time, the RAP mixtures will have a higher stiffness. For fatigue behaviour, this relation is less clear. It seems that the RAP material has a positive influence on the fatigue

resistance of the mixture. The resistance to permanent deformation seems to retain good or even improve when RAP material is applied due to the aged binder. Regarding water sensitivity, the results are a little bit variable and ambiguous.

2. Which additives can be used in HMA with high RAP percentages?
Section 2.4 showed that there is a great variety in additives and rejuvenating additives. They can be useful in the application of RAP material in asphalt mixtures. It can counteract the increase in stiffness and viscosity and the decrease in workability.

Three main effects of rejuvenators can be distinguished: softening agent effect, effect of recycling in the chemical composition of the binder and the effect of dispersant. Depending on the aforementioned desired effects, suitable additives can be chosen.

Rejuvenating additives are biologically or chemically based. Further, it may differ whether it is waste material or an originally manufactured agent. Additives of certain origin may have specific effect, which can then be selected for. For this study specifically, availability also played an important role in the choice of rejuvenator.

3. What is the influence of high RAP content on the functional properties of the asphalt binder and asphalt mixture?
At the binder level, it turns out that the application of RAP material leads to a much higher stiffness of the bitumen, which is due to the hardening of the binder. This increase is the case for both before and after ageing. Further, the application of RAP material leads to a higher fatigue resistance. For both before ageing and after ageing, a higher ε_6-value is found for the binder with 80% RAP. The ageing simulation itself shows comparable results. Especially after executing the PAV test on the sample, both the stiffness and the ε_6-value increase. So, the ageing simulation matches the actual results of the RAP binder.

At the mixture level, the increase of RAP content leads to a higher mixture stiffness for all frequencies, as follows from the cyclic ITT. However, it is not too high for the current standards. So, regarding the stiffness of the 80% mixture, the application of a rejuvenating additive is not necessary. The increase in RAP content leads to a lower phase angle, following the results of the cyclic ITT. This indicates that the asphalt mixture with more RAP behaves more elastically and less viscous.

Regarding the fatigue resistance, which was also measured with the cyclic ITT, it turns out that the increase of RAP content leads to a steeper fatigue line. For lower strain levels, this means that the fatigue resistance is improved, but for higher strain levels it is deteriorated. So, the 80% RAP mixture without additive cannot be considered an improvement for fatigue resistance due to this deterioration at high strain levels.

The ITT shows that the moisture sensitivity becomes better when more RAP is applied. The fracture toughness stays almost the same when the RAP content is increased. The mixture does not become more brittle by applying more RAP.

Further, it becomes clear that the increase in RAP content leads to an increase in the resistance to permanent deformation. The mixture becomes harder, leading to less permanent deformation. The rutting resistance is thus improved.

The workability, based on the number of required gyrations, does not change when the RAP content is increased from 65% RAP to 80% RAP.

4. What is the influence of the rejuvenators on the functional properties of the asphalt binder and asphalt mixture?

At the binder level, the application of rejuvenating additives leads to a strong decrease in stiffness, for both before and after ageing. The values are even lower than the binder without RAP. So due to the additives, the stiffness decreases more than it increases due to the application of RAP material. A lower dose of additive might balance this out.

Regarding the unaged samples, the binders with rejuvenator have a slightly worse fatigue resistance in comparison with the 80% RAP binder without additive. However, after the long-term ageing, the fatigue resistance increases strongly, except for the Ravasol. So, it turns out that application of RAP with rejuvenating additive outperforms virgin bitumen in terms of fatigue resistance and leads to a similar stiffness. Of concern might be that the fatigue resistance of all binders with additive decreases after two times PAV while this is not the case for the binders without additive. The ε_6-value is still relatively high, but this might end up in a problem towards full circularity when those mixtures with rejuvenators are also recycled.

The application of rejuvenating additives in the cyclic ITT leads to a strong reduction in stiffness, which is similar for both Neomex and Cecabase. Both also show lower values than the 65% RAP reference mixture. A lower dosage might equalize this.

According to the results of the cyclic ITT, the phase angle becomes higher when rejuvenating additives are applied, indicating a more viscous behaviour. For higher frequencies, the values are also higher than the 65% RAP mixture.

The application of rejuvenators leads to a lower fatigue resistance in comparison with the mixtures without rejuvenator. This yields for both rejuvenators.

Regarding the ITT, the application of rejuvenating additives on moisture sensitivity does not have a uniform effect. The ITSR-value of the mixture with Neomex increases in comparison with the 80% RAP mixture without additive, while the ITSR-value of the mixture with Cecabase decreases.

However, all ITSR-values easily meet the current standards. Measuring the fracture toughness with the ITT at 1 °C, it turns out that the fracture toughness is lower when rejuvenators are applied. This shows the function of a rejuvenator as a softener for the mixture.

The application of rejuvenators undoes the increase of the rutting resistance due to the increased RAP content. The mixture with Neomex shows comparable results to the 65% RAP mixture. The mixture with Cecabase is softened so much that the permanent deformation doubled in comparison with the reference mixture and does not meet the criterium.

Finally, a great added value of rejuvenators is found in the workability of asphalt mixtures. The application of rejuvenating additive leads to a large decrease in the number of required gyrations, indicating a better workability.

5. Can micromechanical models (Hirsch model) be used to predict the functional properties of the asphalt mixtures containing a high percentage of RAP?

Regarding the micromechanical prediction of the stiffness, it turns out that the original Hirsch model provides results with reasonably accuracy. Although this model uses general model coefficients, it may be applied on mixtures with high RAP percentages and a rejuvenator with a decent accuracy. The simplified Hirsch model with inclusion of the factor P_a cannot be simply adopted when it is fit for other types of mixtures. The predicted stiffness for all three mixtures is much higher than it actually is. Therefore, the parameters were changed according to the laboratory results of the 80% RAP mixture without additive. It turns out that this adjustment leads to accurate results making the simplified Hirsch model applicable to the mixtures with 80% RAP and a rejuvenating additive.

So, the semi-empirical Hirsch model may be used for predicting the stiffness but its accuracy is improved when it is used for the type of mixture for which it has been calibrated.

6.2 Recommendations

This section provides some recommendations for follow-up research on this topic.

Firstly, it may be interesting to reduce the dosage of the used rejuvenators. As described in the section above, the dosage of the rejuvenator seems to be on the high side. Testing can be done with mixtures containing a lower amount of additive to actually approximate the properties of the reference mixture. Also, the other rejuvenators that have been tested only at the bitumen level could be included because they also showed interesting results at the binder level.

Furthermore, during this testing plan, the fatigue resistance was not measured with the four point bending test. This test was excluded in this study due to limited time, but it is part of the standard type tests. Therefore, it may be valuable to still perform this test.

In addition, follow-up research is needed to take the next step towards a fully circular process. In this research, there has been focused on the increase of the RAP content from 65% to 80% but eventually no more primary raw materials must be used to achieve full circularity. As a first step,

it is recommended to deepen the research with RAP content of 80% because this study has shown that there is potential for this percentage but there is still a need to search for example the optimal dosage of the additives to reduce the negative effects. Subsequently, a further step could be taken to 100% RAP content, but this will certainly create additional challenges, as there would be no room left to add a new product.

Regarding the application of the modified Hirsh model with inclusion of P_a, it may be interesting to extend the results to a wider frequency range. In this study, the binders and mixture were only tested at one temperature making it impossible to construct a master curve. This meant that P_a could only be fitted for a limited range frequency. Testing the mixtures at multiple temperatures allows the calculation of P_a for a wider range of frequencies and the fit of the function for P_a is based on more data.

Further, future research can focus on testing more mixtures and determining the P_a to gain more insight into the behaviour of P_a for different kind of mixtures. Eventually, the understanding in P_a should be such that a solid prediction of the stiffness of asphalt mixtures using only the properties of the components can be made.

References

AASHTO. (2020). Standard Method of Test for Estimating Fatigue Resistance of Asphalt Binders Using the Linear Amplitude Sweep In *AASHTO: T 391-20*.

Al-Qadi, I. L., Aurangzeb, Q., Carpenter, S. H., Pine, W. J., & Trepanier, J. (2012). *Impact of high RAP contents on structural and performance properties of asphalt mixtures* (0197-9191).

Al-Qadi, I. L., Elseifi, M. A., & Carpenter, S. H. (2007). *Reclaimed Aphalt Pavement - A Literature Review*.

Al-Saffar, Z. H., Yaacob, H., Satar, M. K. I. M., Saleem, M. K., Lai, J. C., & Jaya, R. P. (2021). A review on rejuvenating materials used with reclaimed hot mix asphalt. *Canadian Journal of Civil Engineering*, *48*, 233-249. https://doi.org/10.1139/cjce-2019-0635

Almeida-Costa, A., & Benta, A. (2016). Economic and environmental impact study of warm mix asphalt compared to hot mix asphalt. *Journal of Cleaner Production*, *112*, 2308-2317. https://doi.org/10.1016/j.jclepro.2015.10.077

Arkema. (2021). *Chemistry to Easily Maximize the Use of Recyled Asphalt Pavement (RAP)*. https://w6g8s7w6.stackpathcdn.com/wp-content/uploads/2021/01/TDS-Cecabase-RWI_EN.pdf

Arkema. (2022). *Cecabase® RWI Asphalt Rejuvenator for Reclaimed / Recycled Asphalt Pavement (RAP)*. https://www.arkema.com/global/en/products/product-finder/product/surfactantandadditives/cecabase-rwi-asphalt-rejuvenator-reclaimed-recycled-asphalt-pav/

Behnood, A. (2019). Application of rejuvenators to improve the rheological and mechanical properties of asphalt binders and mixtures: A review. *Journal of Cleaner Production*, *231*, 171-182. https://doi.org/10.1016/j.jclepro.2019.05.209

Blankendaal, T., Schuur, P., & Voordijk, H. (2014). Reducing the environmental impact of concrete and asphalt: a scenario approach. *Journal of Cleaner Production*, *66*, 27-36. https://doi.org/10.1016/j.jclepro.2013.10.012

Bonaquist, R. F. (2011). *Mix design practices for warm mix asphalt* (Vol. 691). Transportation Research Board.

Broere, D. J. C., Porot, L., Wistuba, M. P., & Grönniger, J. (2016). *Evaluatie van het lage termperatuur gedrag van een 70% PR asfaltmengsel* CROW Infradagen

Brownridge, J. (2010). The role of an asphalt rejuvenator in pavement preservation: use and need for asphalt rejuvenation. Compendium of papers from the first international conference on pavement preservation,

Christensen, D. W., & Bonaquist, R. (2015). Improved Hirsch model for estimating the modulus of hot-mix asphalt. *Road Materials and Pavement Design*, *16*(sup2), 254-274. https://doi.org/10.1080/14680629.2015.1077635

Christensen Jr, D., Pellinen, T., & Bonaquist, R. (2003). Hirsch model for estimating the modulus of asphalt concrete. *Journal of the Association of Asphalt Paving Technologists*, *72*.

Cirkel, J., van Dam, C., van den Akker, E., & Nell, J. W. (2015). *Handreiking Dijkbekledingen Deel 3: Asfaltbekledingen*. https://tl.iplo.nl/zoeken/@193413/hergebruik-asfalt-asfalt/?PubVrs=22

CROW. (2010). *Asfalt in weg- en waterbouw*. CROW.

CROW. (2020). *Standaard RAW bepalingen 2020*. Wilco.

Daniel, J. S., & Lachance, A. (2005). Mechanistic and volumetric properties of asphalt mixtures with recycled asphalt pavement. *Journal of the Transportation Research Board*, *1929*(1), 28-36. https://doi.org/10.1177/0361198105192900104

De Bock, L., Pierard, N., Vansteenkiste, S., & Vanelstraete, A. (2020). *Classificatie en analyse van verjongingsmiddelen voor asfaltrecycling* A. De Swaef. https://brrc.be/sites/default/files/2020-03/dossier21_nl.pdf

Devulapali, L., Kothandaraman, S., & Sarang, G. (2019). A review on the mechanisms involved in reclaimed asphalt pavement. *International Journal of Pavement Research and Technology*, *12*, 185-196. https://doi.org/10.1007/s42947-019-0024-1

Dinis-Almeida, M., Castro-Gomes, J., Sangiorgi, C., Zoorob, S. E., & Afonso, M. L. (2016). Performance of warm mix recycled asphalt containing up to 100% RAP. *Construction and Building Materials*, *112*, 1-6. https://doi.org/10.1016/j.conbuildmat.2016.02.108

EAPA. (2014). *The use of Warm Mix Asphalt*. EAPA. https://eapa.org/wp-content/uploads/2018/07/EAPA-paper-Warm-Mix-Asphalt-version-2014.pdf

EAPA. (2021). *Asphalt and Circular Economy*. https://eapa.org/recycling/

European Asphalt Pavement Association. (2020). *The use of secondary materials, by-products and waste in asphalt mixtures. Position Paper*. https://eapa.org/eapa-position-papers/

European Comission. (2019). *The European Green deal*. Brussels

European Environment Agency. (2020). *Cutting greenhouse gas emissions through circular economy in the buildings sector*. https://www.eea.europa.eu/downloads/3cf188c4dab74be7adca0381c303d8e6/1606129107/cutting-greenhouse-gas-emissions-through.pdf

Farooq, M. A., & Mir, M. S. (2017). Use of reclaimed asphalt pavement (RAP) in warm mix asphalt (WMA) pavements: a review. *Innovative Infrastructure Solutions*, *2*(1). https://doi.org/10.1007/s41062-017-0058-7

Farooq, M. A., Mir, M. S., & Sharma, A. (2018). Laboratory study on use of RAP in WMA pavements using rejuvenator. *Construction and Building Materials*, *168*, 61-72. https://doi.org/10.1016/j.conbuildmat.2018.02.079

Hettiarachchi, C., Hou, X., Wang, J., & Xiao, F. (2019). A comprehensive review on the utilization of reclaimed asphalt material with warm mix asphalt technology. *Construction and Building Materials*, *227*. https://doi.org/10.1016/j.conbuildmat.2019.117096

Hofko, B., Eberhardsteiner, L., Füssl, J., Grothe, H., Handle, F., Hospodka, M., Grossegger, D., Nahar, S., Schmets, A., & Scarpas, A. (2015). Impact of maltene and asphaltene fraction on mechanical behavior and microstructure of bitumen. *Materials and Structures*, *49*(3), 829-841. https://doi.org/10.1617/s11527-015-0541-6

Im, S., Karki, P., & Zhou, F. (2016). Development of new mix design method for asphalt mixtures containing RAP and rejuvenators. *Construction and Building Materials*, *115*, 727-734. https://doi.org/10.1016/j.conbuildmat.2016.04.081

International Standard. (2006). ISO14040 Environmental management - Life cycle assess ment - Principles and framework. In.

Kandahl, P. S., & Richards, I. (2001). *Premature failure of asphalt overlays from stripping: Case histories*.

Kennedy, T. W., Tam, W. O., & Solaimanian, M. (1998). Optimizing use of reclaimed asphalt pavement with the SuperPave system. *Journal of the Association of Asphalt Paving Technologists*, *67*, 311-333.

Latexfalt. (2022). *Wegenbouw hergebruik*. https://www.latexfalt.com/nl/wegenbouw/hergebruik.html

Leysssens, D., Verstappen, B., & Huybrechts, D. (2013). *Beste Beschikbare Technieken (BBT) voor asfaltcentrales*. Vlaams Kennis Centrum BBT Vito.

Li, Z., Liu, T., Shi, J., Veranko, U., & Zankavich, V. (2017). Fatigue resistance of asphalt concrete pavements. Peculiarity and assessments of potentials. *The baltic journal of road and bridge engineering*, *12*(4), 270-275. https://doi.org/10.3846/bjrbe.2017.34

Lizárraga, J. M., Ramírez, A., Díaz, P., Marcobal, J. R., & Gallego, J. (2018). Short-term performance appraisal of half-warm mix asphalt mixtures containing high (70%) and total RAP contents (100%): From laboratory mix design to its full-scale implementation. *Construction and Building Materials*, *170*, 433-445. https://doi.org/10.1016/j.conbuildmat.2018.03.051

Lu, X. D., & Saleh, M. (2016). Evaluation of warm mix asphalt performance incorporating high RAP content. *Canadian Journal of Civil Engineering*, *43*(4), 343-350. https://doi.org/10.1139/cjce-2015-04544216

Lundy, J. (1972). Pollution Control for the Asphalt Industry. *Canadian Technical Asphalt Association, Proceeding*, *17*.
Mackiewicz, P., & Szydło, A. (2019). Viscoelastic Parameters of Asphalt Mixtures Identified in Static and Dynamic Tests. *Materials*, *12*(13), 2084. https://doi.org/10.3390/ma12132084
Mantalovas, K., & Di Mino, G. (2020). Integrating circularity in the sustainability assessment of asphalt mixtures. *Sustainability*, *12*(2), 594. https://doi.org/10.3390/su12020594
Mastrad Limited. (n.d.). *Roller compactor*. https://www.mastrad.com/roller.htm
Mazumder, M., Sriraman, V., Kim, H. H., & Soon-Jae Lee. (2016). Quantifying the environmental burdens of the hot mix asphalt (HMA) pavements and the production of warm mix asphalt (WMA). *International Journal of Pavement Research and Technology*, *9*(3), 190-201. https://doi.org/10.1016/j.ijprt.2016.06.001
McManus, M. C., & Taylor, C. M. (2018). Chapter 3 - Greenhouse Gas Balances of Bioenergy Systems: The Role of Life Cycle Assessment. In P. Thornley & P. Adams (Eds.), *Greenhouse Gas Balances of Bioenergy Systems* (pp. 29-41). Academic Press. https://doi.org/10.1016/B978-0-08-101036-5.00003-3
Milad, A., Taib, A. M., Ahmeda, A. G. F., Solla, M., & Yusoff, N. I. M. (2020). A review of the use of reclaimed asphalt pavement for road paving applications. *Jurnal Teknologi (Sciences & Engineering)*, *82*(3), 35-44. https://doi.org/10.1113/jt.v82.14320
Ministerie van Infrastructuur en Waterstaat, & Rijkswaterstaat Water Verkeer en Leefomgeving (RWS WVL). (2020). *Circulaire ontwerpprincipes Rijkswaterstaat [Factsheet]*. Retrieved from https://puc.overheid.nl/rijkswaterstaat/doc/PUC_166723_31/
Mogawer, W. S., Austerman, A. J., Kluttz, R., & Roussel, M. (2012). High-performance thin-lift overlays with high reclaimed asphalt pavement content and warm-mix asphalt technology: Performance and workability characteristics. *Transportation Research Record*, *2293*(1), 18-28. https://doi.org/10.3141/2293-03
Mullapudi, R. S., Noojilla, S. L. A., & Reddy, K. S. (2020). Fatigue and Healing Characteristics of RAP Mixtures. *Journal of Materials in Civil Engineering*, *32*(12). https://doi.org/10.1061/(ASCE)MT.1943-5533.0003484
Nazzal, M. D., Mogawer, W., Austerman, A., Qtaish, L. A., & Kaya, S. (2015). Multi-scale evaluation of the effect of rejuvenators on the performance of high RAP content mixtures. *Construction and Building Materials*, *101*, 50-56. https://doi.org/https://doi.org/10.1016/j.conbuildmat.2015.10.029
Nederlandse Norm (NEN). (2012a). Bitumen and bituminous binders - Accelerated long-term ageing conditioning by a Pressure Ageing Vessel (PAV) In *NEN-EN 14769:2012*.
Nederlandse Norm (NEN). (2012b). Bitumen and bituminous binders - Determination of complex shear modulus and phase angle - Dynamic Shear Rheometer (DSR). In *NEN-EN 14770:2012*.
Nederlandse Norm (NEN). (2014). Bitumen and bituminous binders - Determination of the resistance to hardening under influence of heat and air - Part 1: RTFOT method. In *NEN-EN-12607-1:2014*.
Nederlandse Norm (NEN). (2016a). Bituminous mixtures - Material specifications - Part 1: Asphalt Concrete. In.
Nederlandse Norm (NEN). (2016b). Bituminous mixtures - Test methods - Part 25: Cyclic compression test In *(NEN-EN 12697-25:2016)*.
Nederlandse Norm (NEN). (2017). Bituminous mixtures - Test methods - Part 23: Determination of the indirect tensile strength of bituminous specimens. In *NEN-EN 12697-23:2017*.
Nederlandse Norm (NEN). (2018a). Bituminous mixtures ‑ Test methods ‑ Part 12: Determination of the water sensitivity of bituminous specimens In *NEN-EN 12697-12:2018*.
Nederlandse Norm (NEN). (2018b). Bituminous mixtures ‑ Test methods ‑ Part 24: Resistance to fatigue. In *NEN-EN 12697-24:2018*.
Nederlandse Norm (NEN). (2018c). Bituminous mixtures ‑ Test methods ‑ Part 26: Stiffness. In *NEN-EN 12697-26:2018*.

Ongel, A., & Hugener, M. (2015). Impact of rejuvenators on aging properties of bitumen. *Construction and Building Materials*, *94*, 467-474. https://doi.org/https://doi.org/10.1016/j.conbuildmat.2015.07.030
Partal, P., & Martínez-Boza, F. J. (2011). 3 - Modification of bitumen using polyurethanes. In T. McNally (Ed.), *Polymer Modified Bitumen* (pp. 43 - 71). Woodhead Publishing. https://doi.org/10.1533/9780857093721.1.43
Ravago Chemicals. (2021). *Green rejuvenator*. https://emea.ravagochemicals.com/green-rejuvenator
Reyes-Ortiz, O. J., Alvarez-Lugo, A. E., & Botella-Nieto, R. (2011). Study of a hot mix asphalt mixture response based on energy concepts. *Dyna*, *78*(168), 45-52.
Rijksoverheid. (2016). *Nederland circulair in 2050. Rijksbreed programma Circulaire Economie*. Retrieved from https://www.rijksoverheid.nl/documenten/rapporten/2016/09/14/bijlage-1-nederland-circulair-in-2050
Roberts, F. L., Kandhal, P. S., Ray Brown, E., Lee, D. Y., & Kennedy, T. W. (1996). *Hot mix asphalt materials, mixture design and construction*. National Asphalt Pavement Association Research and Education Foundation.
Shafabakhsh, G., Akbari, M., & Bahrami, H. (2020). Evaluating the fatigue resistance of the innovative modified-reinforced composite asphalt mixture. *Advances in Civil Engineering*, *2020*. https://doi.org/10.1155/2020/8845647
Shirodkar, P., Mehta, Y., Nolan, A., Sonpal, K., Norton, A., Tomlinson, C., Dubois, E., Sullivan, P., & Sauber, R. (2011). A study to determine the degree of partial blending of reclaimed asphalt pavement (RAP) binder for high RAP hot mix asphalt. *Construction and Building Materials*, *25*(1), 150-155. https://doi.org/10.1016/j.conbuildmat.2010.06.045
Song, W., Huang, B., & Shu, X. (2018). Influence of warm-mix asphalt technology and rejuvenator on performance of asphalt mixtures containing 50% reclaimed asphalt pavement. *Journal of Cleaner Production*, *192*, 191-198. https://doi.org/https://doi.org/10.1016/j.jclepro.2018.04.269
Subhy, A. (2017). Advanced analytical techniques in fatigue and rutting related characterisations of modified bitumen: Literature review. *Construction and Building Materials*, *156*, 28-45. https://doi.org/10.1016/j.conbuildmat.2017.08.147
Tarsi, G., Tataranni, P., & Sangiorgi, C. (2020). The challenges of using reclaimed asphalt pavement for new asphalt mixtures: A review. *Materials*, *13*(18), 4052. https://doi.org/10.3390/ma13184052
Thives, L. P., & Ghisi, E. (2017). Asphalt mixtures emission and energy consumption: A review. *Renewable and Sustainable Energy Reviews*, *72*, 473-484. https://doi.org/10.1016/j.rser.2017.01.087
Total Nederland N.V. (2008). Regenis. Bitumen voor hergebruik. In.
Tran, N. H., Taylor, A., & Willis, R. (2012). Effect of rejuvenator on performance properties of HMA mixtures with high RAP and RAS contents. *NCAT report*(1), 12-05.
Van Dam, T. J., Harvey, J., Muench, S. T., Smith, K. D., Snyder, M. B., Al-Qadi, I. L., Ozer, H., Meijer, J., Ram, P., & Roesler, J. R. (2015). *Towards sustainable pavement systems: a reference document*.
van de Wall, A. R. G., Hagos, E., Mooijekind, A., & Naus, R. W. M. (2018). *Beoordeling van verjongers in asfalt* CROW Infradagen,
Van den Bergh, W. (2011). *The Effect of Ageing on the Fatigue and Healing Properties of Bituminous Mortars* Delft University of Technology].
Van den Bergh, W., Couscheir, K., Duerinckx, B., & Tanghe, T. (2021a). *Proefvak 4 - Eindrapportage PV4* (HBC.2018.0021, Issue. REjuveBIT.
Van den Bergh, W., Couscheir, K., Duerinckx, B., & Tanghe, T. (2021b). *Proefvak 5- Eindrapportage PV 5* (HBC.2018.0021, Issue. REjuveBIT.
Van den Bergh, W., Couscheir, K., Duerinckx, B., & Tanghe, T. (2021c). *Proefvak 6 - Eindrapportage PV 6* (HBC.2018.0021, Issue. REjuveBIT.
Van Oosterhout, E. (2017). *Vergelijking 3 verjongers voor bitumen*.

Voskuilen, J. (2017). *Hergebruik van asfalt - Ervaringen Rijkswaterstaat*. https://docplayer.nl/50286743-Hergebruik-van-asfalt.html
Wang, Y., Huang, Y., Rattanachot, W., Lau, K., & Suwansawas, S. (2015). Improvement of pavement design and management for more frequent flooding caused by climate change. *Advances in Structural Engineering*, *18*(4), 487-496. https://doi.org/10.1260/1369-4332.18.4.487
Yousefi, A., Behnood, A., Nowruzi, A., & Haghshenas, H. (2021). Performance evaluation of asphalt mixtures containing warm mix asphalt (WMA) additives and reclaimed asphalt pavement (RAP). *Construction and Building Materials*, *268*, 121200. https://doi.org/10.1016/j.conbuildmat.2020.121200
Yu, S., Shen, S., Zhou, X., & Li, X. (2018). Effect of partial blending on high content reclaimed asphalt pavement (RAP) mix design and mixture properties. *Transportation Research Record*, *2672*(28), 79-87. https://doi.org/10.1177/0361198118780703
Yuan, Q., Liu, Z., Zheng, K., & Ma, C. (2021). 7- Asphalt. In *Civil Engineering Materials: From Theory to Practice*. Elsevier Ltd. https://doi.org/10.1016/C2019-0-05032-7
Zaumanis, M., & Mallick, R. B. (2014). Review of very high-content reclaimed asphalt use in plant-produced pavements: state of the art. *International Journal of Pavement Engineering*, *16*(1), 39-55. https://doi.org/10.1080/10298436.2014.893331
Zaumanis, M., Mallick, R. B., & Frank, R. (2014). 100% recycled hot mix asphalt: A review and analysis. *Resources, Conservation and Recycling*, *92*, 230-245. https://doi.org/10.1016/j.resconrec.2014.07.007
Zhang, C., Shen, S., & Jia, X. (2017). Modification of the Hirsch dynamic modulus prediction model for asphalt mixtures. *Journal of Materials in Civil Engineering*, *29*(12), 04017241. https://doi.org/10.1061/(ASCE)MT.1943-5533.0002099
Zhang, D., Birgisson, B., & Luo, X. (2020b). A new dynamic modulus predictive model for asphalt mixtures based on the law of mixtures. *Construction and Building Materials*, *255*. https://doi.org/10.1016/j.conbuildmat.2020.119348
Zhang, H., Anupam, K., Scarpas, A., & Kasbergen, C. (2018a). Comparison of different micromechanical models for predicting the effective properties of open graded mixes. *Transportation Research Record*, *2672*(28), 404-415. https://doi.org/10.1177/0361198118794713
Zhang, H., Anupam, K., Scarpas, A., Kasbergen, C., & Erkens, S. (2021a). Understanding the Stiffness of Porous Asphalt Mixture through Micromechanics. *Transportation Research Record*, *2675*(8), 528-537. https://doi.org/10.1177/0361198121999060
Zhang, H., Anupam, K., Scarpas, T., Kasbergen, C., & Erkens, S. (2021b). Contact mechanics based solution to predict modulus of asphalt materials with high porosities. *Materials and Design*, *206*, 1-18. https://doi.org/10.1016/j.matdes.2021.109752
Zhang, H., Anupam, K., Scarpas, T., Kasbergen, C., Erkens, S., & Al Khateeb, L. (2020a). Continuum-based micromechanical models for asphalt materials: Current practices & beyond. *Construction and Building Materials*, *260*, 119675. https://doi.org/https://doi.org/10.1016/j.conbuildmat.2020.119675
Zhang, H., Anupam, K., Skarpas, A., & Kasbergen, C. (2018b). Issues in the Prediction of the Mechanical Properties of Open Graded Mixes. *Transportation Research Record*, *2672*(3). https://doi.org/10.1177/0361198118792117
Zhang, H., Anupam, K., Skarpas, A., Kasbergen, C., & Erkens, S. (2020c). Simple Homogenization-Based Approach to Predict Raveling in Porous Asphalt. *Transportation Research Record*, *2674*(12), 263-277. https://doi.org/10.1177/0361198120953159
Zhao, S., Huang, B., Shu, X., & Woods, M. (2015). Quantitative Characterization of Binder Blending: How Much RAP-RAS Binder Is Mobilized During Mixing? *Transportation Research Record*, *2506*, 72-80. https://doi.org/10.3141/2506-08
Zimek, M., & Baumgartner, R. (2017). Corporate sustainability activities and sustainability performance of first and second order. 18th European Roundtable on Sustainable Consumption and Production Conference (ERSCP 2017), Skiathos Island, Greece,

Appendix

Appendix A: Binder composition

In addition to the bitumen 70/100 without RAP, which is considered the reference, five variants are tested at binder level. Their composition is given in this appendix. Because the bitumen percentage of the RAP material is higher than the desired bitumen content, less bitumen is added than the RAP percentage would suggest. Furthermore, the amounts of additive are kept the same as much as possible to make the best possible comparison.

Table A.1: Binder composition 80% RAP

Component	Mass percentage
RAP bitumen	91.2%
Bitumen 160/220	8.8 %

Table A.2: Binder composition 80% RAP +Regenis 50

Component	Mass percentage
RAP bitumen	91.2%
Regenis 50	8.8 %

Table A.3: Binder composition 80% RAP + Neomex HR

Component	Mass percentage
RAP bitumen	91.2 %
Neomex HR	3.7 %
Bitumen 70/100	5.1 %

Table A.4: Binder composition 80% RAP + Cecabase RWI

Component	Mass percentage
RAP bitumen	91.2 %
Cecabase RWI	3.7 %
Bitumen 70/100	5.1 %

Table A.5: Binder composition 80% RAP + Ravasol RAP-5V

Component	Mass percentage
RAP bitumen	91.2 %
Ravasol RAP-5V	3.7 %
Bitumen 70/100	5.1 %

Appendix B: Mix composition

This appendix shows the mix composition of the four tested mixtures. In the mixture with 80% RAP, 70/100 bitumen is applied to make the best comparison with the 80% RAP mixtures with rejuvenator. The dosage of the rejuvenators is an initial estimation and is kept the same to compare the two rejuvenators.

Mixture A: 65% RAP

Material type	Description	Quantity (% m/m)
Fine aggregate	Coarse sand 0/2	17.12
Coarse aggregate	< 2 mm	0.46
	5.6 mm – 2 mm	3.12
	22.4 mm – 16 mm	1.46
	16 mm – 11.2 mm	7.20
	11.2 mm – 8 mm	1.95
	8 mm – 5.6 mm	1.24
Mineral filler	Wigro 50K 0/0.1	0.34
	Own filler 0/0.1	1.00
Reclaimed asphalt pavement	Milled asphalt base layer	-
	> 16 mm	22.49
	8 – 16 mm	20.35
	< 8 mm	22.16
Binder	Penetration bitumen 160/220	1.11

Mixture B: 80% RAP

Material type	Description	Quantity (% m/m)
Fine aggregate	Coarse sand 0/2	12.68
Coarse aggregate	< 2 mm	0.06
	5.6 mm – 2 mm	0.31
	22.4 mm – 16 mm	0.68
	16 mm – 11.2 mm	3.44
	11.2 mm – 8 mm	1.42
	8 mm – 5.6 mm	0.64
Mineral filler	Wigro 50K 0/0.1	0.14
	Own filler 0/0.1	0.25
Reclaimed asphalt pavement	Milled asphalt base layer	-
	> 16 mm	27.68
	8 – 16 mm	25.04
	< 8 mm	27.28
Binder	Penetration bitumen 70/100	0.38

Mixture C: 80% RAP + Cecabase RWI

Material type	Description	Quantity (% m/m)
Fine aggregate	Coarse sand 0/2	12.68
Coarse aggregate	< 2 mm	0.06
	5.6 mm – 2 mm	0.31
	22.4 mm – 16 mm	0.68
	16 mm – 11.2 mm	3.44
	11.2 mm – 8 mm	1.42
	8 mm – 5.6 mm	0.64
Mineral filler	Wigro 50K 0/0.1	0.14
	Own filler 0/0.1	0.25
Reclaimed asphalt pavement	Milled asphalt base layer	-
	> 16 mm	27.68
	8 – 16 mm	25.04
	< 8 mm	27.28
Binder	Penetration bitumen 70/100	0.22
Rejuvenating agent	Cecabase RWI	0.16

Mixture D: 80% RAP + Neomex HR

Material type	Description	Quantity (% m/m)
Fine aggregate	Coarse sand 0/2	12.68
Coarse aggregate	< 2 mm	0.06
	5.6 mm – 2 mm	0.31
	22.4 mm – 16 mm	0.68
	16 mm – 11.2 mm	3.44
	11.2 mm – 8 mm	1.42
	8 mm – 5.6 mm	0.64
Mineral filler	Wigro 50K 0/0.1	0.14
	Own filler 0/0.1	0.25
Reclaimed asphalt pavement	Milled asphalt base layer	-
	> 16 mm	27.68
	8 – 16 mm	25.04
	< 8 mm	27.28
Binder	Penetration bitumen 70/100	0.22
Rejuvenating agent	Neomex HR	0.16

Appendix C: Results LAS

The results of the LAS test method are given in this appendix. Firstly, the overall results are given and then the detailed results of the stiffness are presented.

Table C.1: LAS Results 0% RAP (bitumen 70/100)

0 % RAP (bitumen 70/100)		
Unaged	Stiffness at 8 Hz	6.5 MPa
	ε_6	0.428 %
RTFOT	Stiffness at 8 Hz	10.9 MPa
	ε_6	0.520 %
PAV	Stiffness at 8 Hz	19.9 MPa
	ε_6	0.555 %
2x PAV	Stiffness at 8 Hz	25.6 MPa
	ε_6	0.663 %

Table C.2: LAS Results 80% RAP

80 % RAP		
Unaged	Stiffness at 8 Hz	11.5 MPa
	ε_6	0.596 %
RTFOT	Stiffness at 8 Hz	15.7 MPa
	ε_6	0.552 %
PAV	Stiffness at 8 Hz	26.5 MPa
	ε_6	0.663 %
2x PAV	Stiffness at 8 Hz	31.5 MPa
	ε_6	0.755 %

Table C.3: LAS Results 80% RAP + Cecabase RWI

80% RAP + Cecabase RWI		
Unaged	Stiffness at 8 Hz	3.8 MPa
	ε_6	0.538 %
RTFOT	Stiffness at 8 Hz	6.7 MPa
	ε_6	0.603 %
PAV	Stiffness at 8 Hz	15.0 MPa
	ε_6	1.228 %
2x PAV	Stiffness at 8 Hz	17.9 MPa
	ε_6	1.106 %

Table C.4: LAS Results 80% RAP + Neomex HR

80% RAP + Neomex HR		
Unaged	Stiffness at 8 Hz	4.4 MPa
	ε_6	0.574 %
RTFOT	Stiffness at 8 Hz	5.3 MPa
	ε_6	0.628 %
PAV	Stiffness at 8 Hz	12.5 MPa
	ε_6	0.999 %
2x PAV	Stiffness at 8 Hz	17.8 MPa
	ε_6	0.726 %

Table C.5: LAS Results 80% RAP + Ravasol RAP-5V

80% RAP + Ravasol RAP-5V		
Unaged	Stiffness at 8 Hz	4.4 MPa
	ε_6	0.380 %
RTFOT	Stiffness at 8 Hz	7.6 MPa
	ε_6	0.434 %
PAV	Stiffness at 8 Hz	18.1 MPa
	ε_6	0.510 %
2x PAV	Stiffness at 8 Hz	21.5 MPa
	ε_6	0.405 %

Table C.6: LAS Results 80% RAP + Regenis 50

80% RAP + Regenis 50		
Unaged	Stiffness at 8 Hz	5.6 MPa
	ε_6	0.485 %
RTFOT	Stiffness at 8 Hz	7.3 MPa
	ε_6	0.613 %
PAV	Stiffness at 8 Hz	15.8 MPa
	ε_6	0.979 %
2x PAV	Stiffness at 8 Hz	18.9 MPa
	ε_6	0.907 %

Table C.7: Stiffness Results 80% RAP

80% RAP				
Frequency [Hz]	**Complex shear modulus [MPa] Unaged**	**Complex shear modulus [MPa] RTFOT**	**Complex shear modulus [MPa] 1x PAV**	**Complex shear modulus [MPa] 2x PAV**
0.2	1.27	2.21	5.70	6.71
0.4	2.00	3.31	7.83	8.97
0.6	2.58	4.14	9.36	10.6
0.8	3.08	4.84	10.6	11.8
1	3.53	5.50	11.6	12.9
2	5.30	7.92	15.5	16.8
4	7.90	11.2	20.4	22.9
6	9.86	13.7	23.8	27.5
8	11.5	15.7	26.5	31.5
10	12.9	17.4	28.8	34.2
20	18.4	23.8	37.0	42.4
30	22.5	28.5	42.8	47.7

Table C.8: Stiffness Results 80% RAP + Cecabase RWI

80% RAP + Cecabase RWI				
Frequency [Hz]	**Complex shear modulus [MPa] Unaged**	**Complex shear modulus [MPa] RTFOT**	**Complex shear modulus [MPa] 1x PAV**	**Complex shear modulus [MPa] 2x PAV**
0.2	0.33	0.77	2.49	3.84
0.4	0.53	1.19	3.58	5.25
0.6	0.71	1.53	4.41	6.27
0.8	0.86	1.82	5.09	7.10
1	1.00	2.08	5.69	7.80
2	1.59	3.11	7.95	10.4
4	2.49	4.59	11.0	13.7
6	3.21	5.67	13.2	16.0
8	3.82	6.70	15.0	17.9
10	4.38	7.55	16.5	19.5
20	6.58	10.8	22.2	25.2
30	8.33	13.4	26.3	29.2

Table C.9: Stiffness Results 80% RAP + Neomex HR

80% RAP + Neomex HR				
Frequency [Hz]	**Complex shear modulus [MPa] Unaged**	**Complex shear modulus [MPa] RTFOT**	**Complex shear modulus [MPa] 1x PAV**	**Complex shear modulus [MPa] 2x PAV**
0.2	0.37	0.52	1.92	3.51
0.4	0.61	0.84	2.82	4.91
0.6	0.81	1.09	3.50	5.92
0.8	0.99	1.32	4.06	6.75
1	1.15	1.52	4.56	7.47
2	1.83	2.35	6.47	10.1
4	2.87	3.57	9.04	13.5
6	3.70	4.53	10.9	15.9
8	4.41	5.35	12.5	17.8
10	5.05	6.06	13.8	19.5
20	7.62	8.96	18.8	25.3
30	9.65	11.2	22.4	29.4

Table C.10: Stiffness Results 80% RAP + Regenis 50

80% RAP + Regenis 50				
Frequency [Hz]	**Complex shear modulus [MPa] Unaged**	**Complex shear modulus [MPa] RTFOT**	**Complex shear modulus [MPa] 1x PAV**	**Complex shear modulus [MPa] 2x PAV**
0.2	0.48	0.79	2.53	3.70
0.4	0.79	1.24	3.67	5.16
0.6	1.05	1.60	4.54	6.23
0.8	1.28	1.91	5.26	7.10
1	1.48	2.19	5.89	7.85
2	2.35	3.30	8.28	10.6
4	3.64	4.90	11.5	14.3
6	4.69	6.20	13.9	16.8
8	5.58	7.26	15.8	18.9
10	6.40	8.20	17.5	20.7
20	9.68	11.9	23.6	27.1
30	12.3	14.7	28.1	31.6

Appendix D: Results indirect tensile test

The results of the indirect tensile test are given in this appendix. Firstly, the test at 15 °C is given for water sensitivity. After that, the test at 1 °C is given for fracture toughness.

Water sensitivity

Table D.1: Results ITT- water sensitivity 65% RAP

Specimen	F max [kN]	ITS [MPa]	Split energy [J]	Fracture toughness to F max [J/m²]	Crack energy [J]	Total fracture toughness [J/m²]
Dry						
1	20.00	2.52	21.018	4166	40.574	8042
2	20.02	2.53	21.409	4244	42.614	8447
3	21.84	2.75	21.675	4292	42.995	8514
4	22.27	2.86	20.712	4176	46.384	9352
Average		2.67		4219		8589
Wet						
1	14.89	1.89	17.217	3430	39.165	7802
2	16.57	2.12	18.436	3713	36.269	7305
3	16.38	2.08	24.406	4871	51.946	10368
4	19.20	2.43	21.322	4247	38.747	7719
Average		2.13		4065		8298
		ITSR [%]				
		80				

Table D.2: Results ITT – water sensitivity 80% RAP

Specimen	F max [kN]	ITS [MPa]	Split energy [J]	Fracture toughness to F max [J/m²]	Crack energy [J]	Total fracture toughness [J/m²]
Dry						
1	27.91	3.59	25.005	5057	41.454	8383
2	27.92	3.62	26.156	5322	43.296	8809
3	28.61	3.65	26.368	5289	42.284	8482
4	25.98	3.33	28.663	5773	36.628	7377
Average		3.55		5360		8263
Wet						
1	27.02	3.48	18.371	3708	31.323	6322
2	24.66	3.15	18.111	3619	33.424	6678
3	28.45	3.65	24.466	4948	33.661	6807
4	26.32	3.42	20.152	4125	30.281	6199
Average		3.43		4100		6501
		ITSR [%]				
		97				

Table D.3: Results ITT – water sensitivity 80% RAP + Cecabase RWI

Specimen	F max [kN]	ITS [MPa]	Split energy [J]	Fracture toughness to F max [J/m²]	Crack energy [J]	Total fracture toughness [J/m²]
Dry						
1	16.17	2.08	17.014	3434	35.244	7113
2	16.35	2.12	18.591	3790	39.157	7983
3	17.92	2.30	14.908	3000	28.604	5755
4	15.39	1.95	18.322	3653	38.747	7726
Average		2.11		3469		7144
Wet						
1	12.49	1.59	17.689	3538	33.697	6739
2	13.41	1.67	15.385	3017	32.468	6366
3	15.37	1.94	15.916	3158	35.422	7028
4	13.47	1.70	15.657	3110	34.580	6868
Average		1.73		3206		6750
		ITSR [%]				
		82				

Table D.4: Results ITT – water sensitivity 80% RAP + Neomex HR

Specimen	F max [kN]	ITS [MPa]	Split energy [J]	Fracture toughness to F max [J/m²]	Crack energy [J]	Total fracture toughness [J/m²]
Dry						
1	19.40	2.47	20.954	4182	39.629	7910
2	18.97	2.40	19.909	3962	45.367	9028
3	20.04	2.54	19.321	3841	42.589	8467
4	20.39	2.62	20.419	4117	41.027	8272
Average		2.51		4026		8419
Wet						
1	21.49	2.76	23.550	4743	46.261	9317
2	19.2	2.48	20.458	4146	40.693	8246
3	19.02	2.40	23.604	4688	40.176	7979
4	20.38	2.61	27.325	5498	43.825	8818
Average		2.56		4769		8590
		ITSR [%]				
		102				

Fracture toughness

Table D.5: Results ITT – fracture toughness 65% RAP

Specimen	F max [kN]	ITS [MPa]	Split energy [J]	Fracture toughness to F max [J/m²]	Crack energy [J]	Total fracture toughness [J/m²]
1	34.72	4.40	34.444	6855	56.727	11289
2	36.19	4.61	68.249	13663	68.986	13811
3	35.39	4.49	63.955	12740	66.825	13312
4	36.08	4.58	49.391	9838	57.433	11441
Average		4.52		10774		12463

Table D.6: Results ITT – fracture toughness 80% RAP

Specimen	F max [kN]	ITS [MPa]	Split energy [J]	Fracture toughness to F max [J/m²]	Crack energy [J]	Total fracture toughness [J/m²]
1	34.99	4.47	12.467	2503	75.517	15164
2	33.32	4.26	64.611	12961	64.637	12966
3	40.52	5.25	36.526	7432	43.902	8932
4	34.14	4.35	53.472	10705	70.091	14032
Average		4.58		8400		12774

Table D.7: Results ITT – fracture toughness 80% RAP + Cecabase RWI

Specimen	F max [kN]	ITS [MPa]	Split energy [J]	Fracture toughness to F max [J/m²]	Crack energy [J]	Total fracture toughness [J/m²]
1	31.27	4.01	25.345	5110	34.228	6901
2	32.46	4.17	23.686	4775	35.789	7216
3	30.29	3.86	22.411	4487	32.673	6541
4	33.08	4.20	25.446	5069	62.092	12369
Average		4.06		4860		8257

Table D.8: Results ITT – fracture toughness 80% RAP + Neomex HR

Specimen	F max [kN]	ITS [MPa]	Split energy [J]	Fracture toughness to F max [J/m²]	Crack energy [J]	Total fracture toughness [J/m²]
1	31.95	4.06	23.861	4763	42.732	8529
2	34.16	4.40	59.747	12095	64.585	13074
3	33.02	4.17	59.961	11897	62.861	12472
4	33.29	4.26	32.969	6634	38.156	7677
Average		4.22		8847		10438

Appendix E: Results cyclic indirect tensile test

The results of the cyclic indirect tensile test are given in this appendix. The stiffness and phase angle results for all specimens are given. Thereafter, the fatigue test results are given

Stiffness and phase angle - 65% RAP

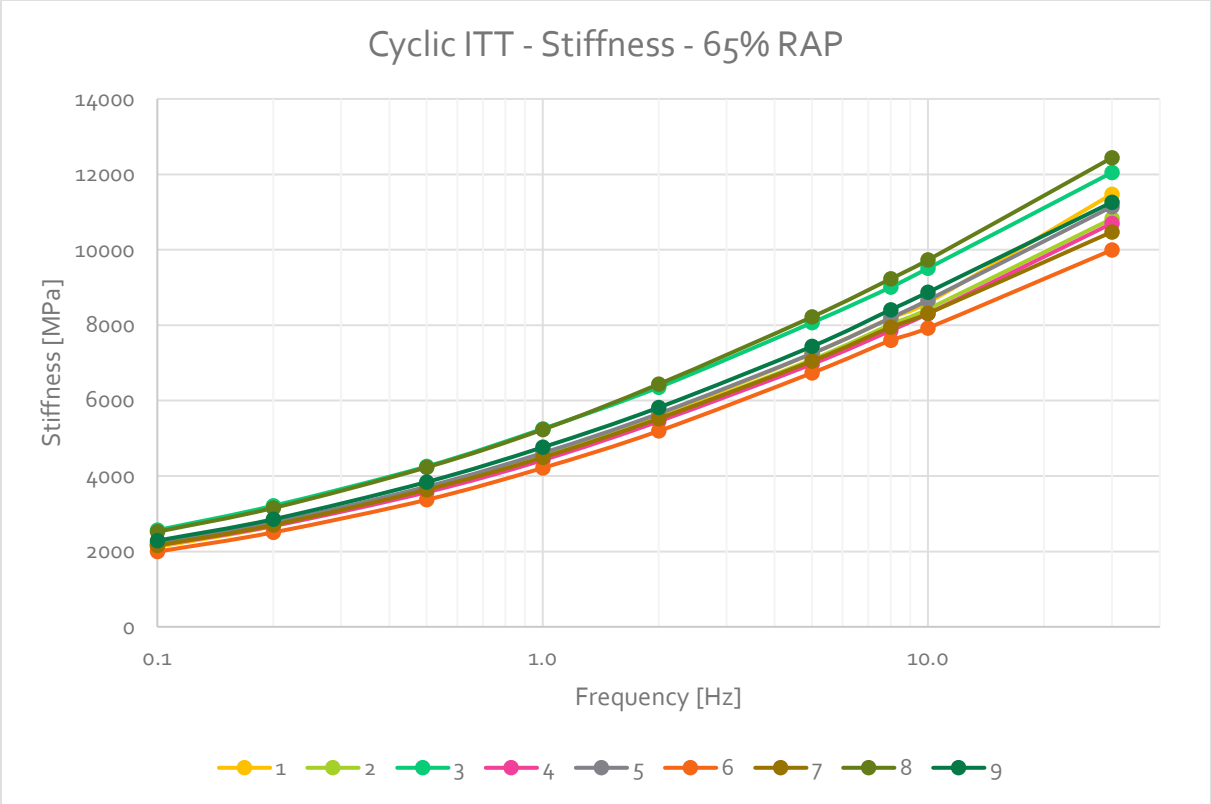

Figure E.1: Results Cyclic ITT - Stiffness 65% RAP

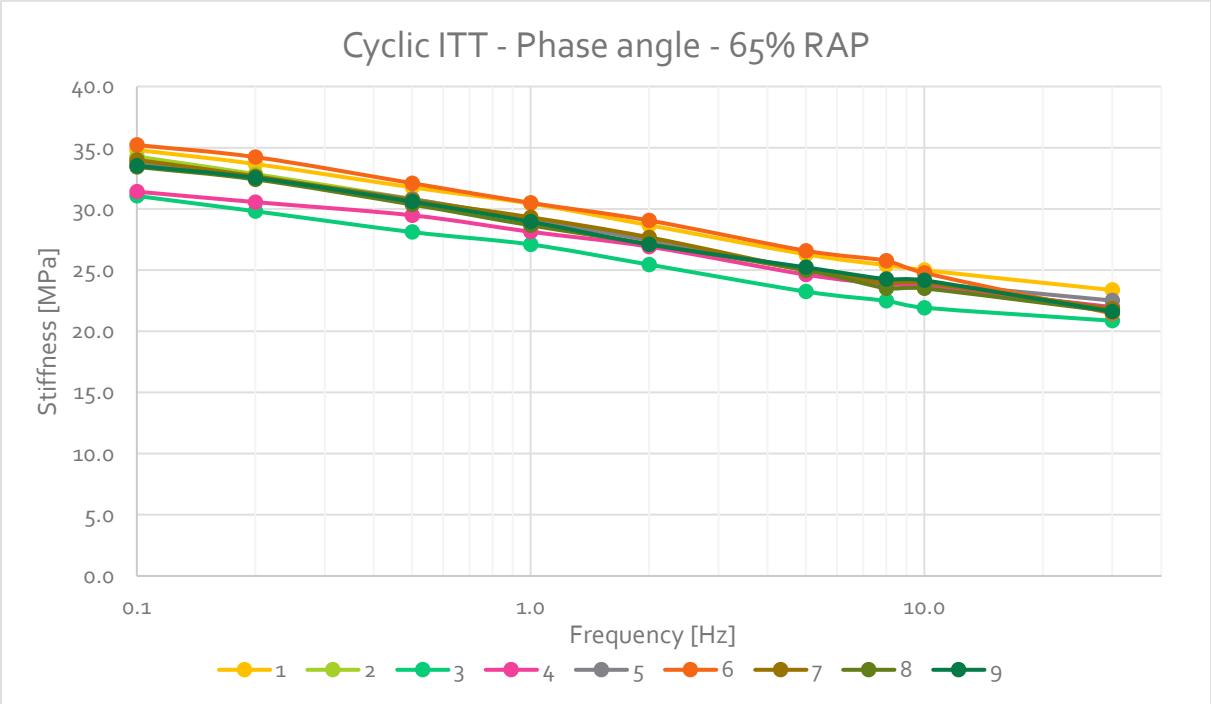

Figure E.2: Results Cyclic ITT – Phase angle 65% RAP

Table E.1: Results Cyclic ITT - Stiffness and phase angle 65% RAP

Mean Results		T [°C]	20.0
Frequency (f)	**Strain (ε)**	**Stiffness (E*)**	**Phase angle**
[Hz]	[μm/m]	[MPa]	[°]
30.0	56.9	11149	21.9
10.0	57.3	8704	23.8
8.0	57.3	8271	24.2
5.0	58.0	7338	25.1
2.0	59.0	5727	27.4
1.0	57.7	4672	29.0
0.5	58.6	3768	30.5
0.2	59.3	2811	32.4
0.1	59.4	2248	33.5
30.0	56.9	11155	21.2

Stiffness and phase angle - 80% RAP

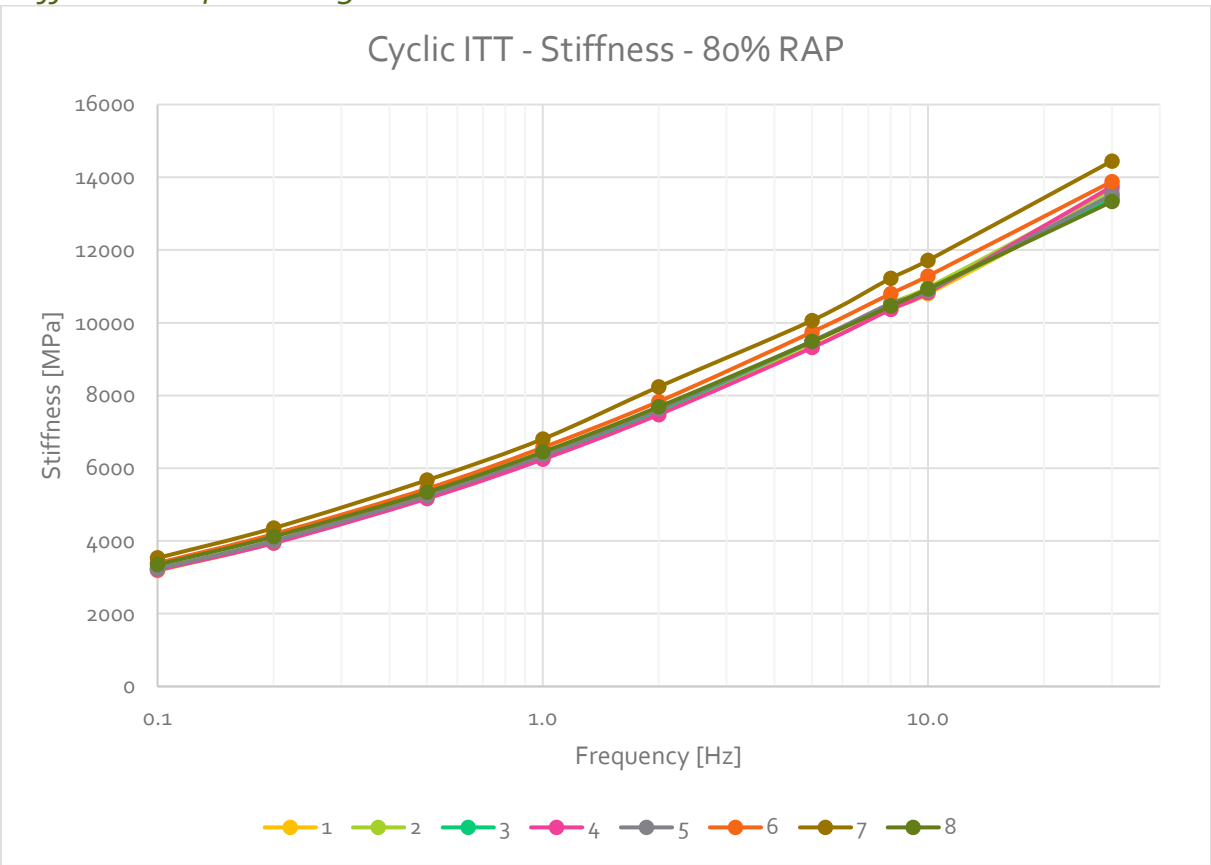

Figure E.3: Results Cyclic ITT - Stiffness 80% RAP

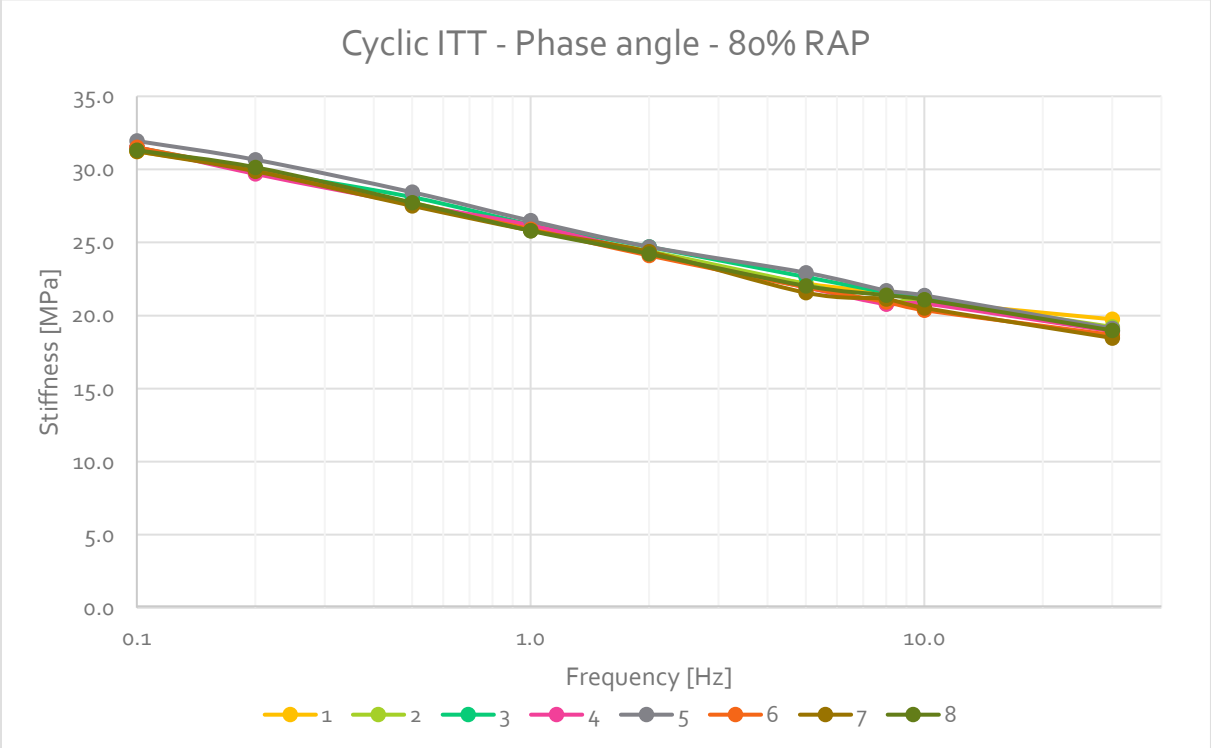

Figure E.4: Results Cyclic ITT – Phase angle 80% RAP

Table E.2: Results Cyclic ITT - Stiffness and phase angle 80% RAP

Mean Results		T [°C]	20.0
Frequency (f)	**Strain (ε)**	**Stiffness (E*)**	**Phase angle**
[Hz]	[μm/m]	[MPa]	[°]
30.0	48.9	13682	19.0
10.0	50.3	11035	20.9
8.0	49.9	10595	21.2
5.0	50.1	9546	22.2
2.0	49.5	7693	24.4
1.0	49.1	6426	26.0
0.5	48.7	5314	27.8
0.2	48.3	4066	30.0
0.1	48.3	3297	31.5
30.0	47.9	13825	18.2

Stiffness and phase angle - 80% RAP + Cecabase RWI

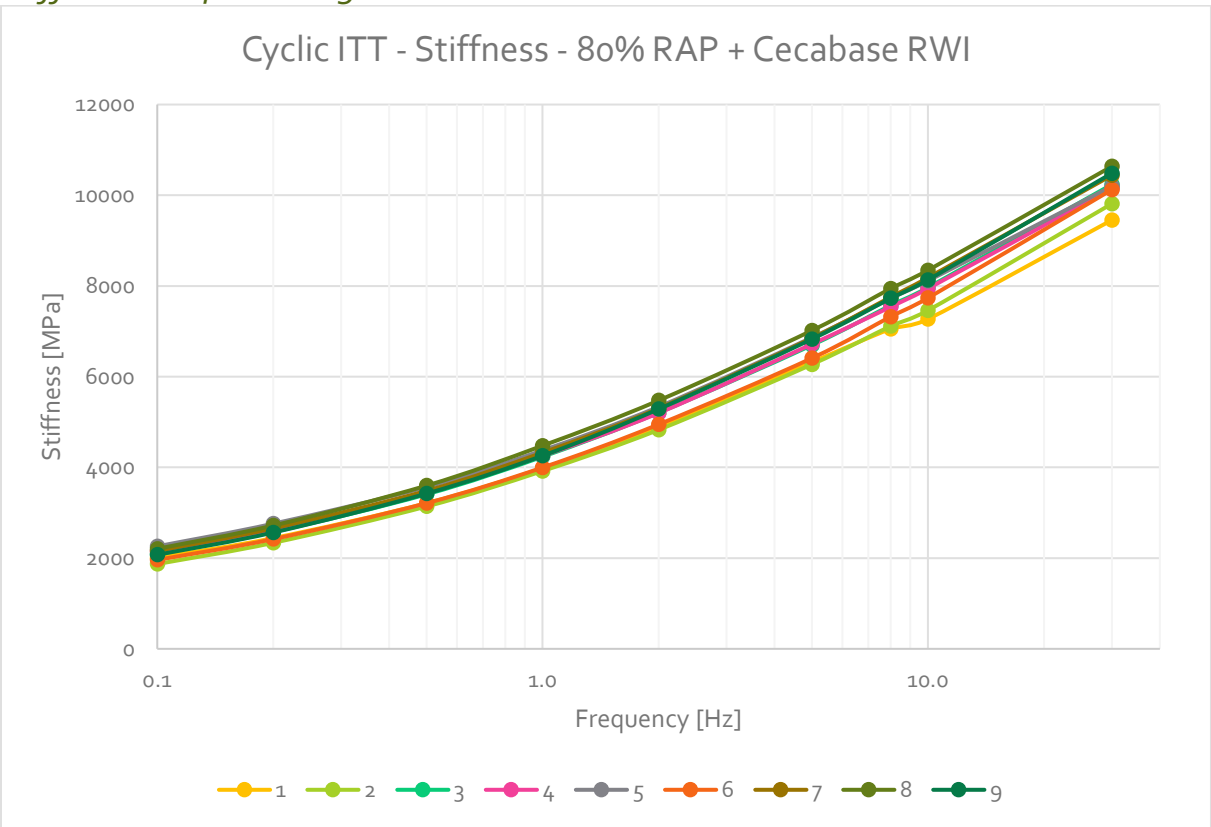

Figure E.5: Results Cyclic ITT - Stiffness 80% RAP + Cecabase RWI

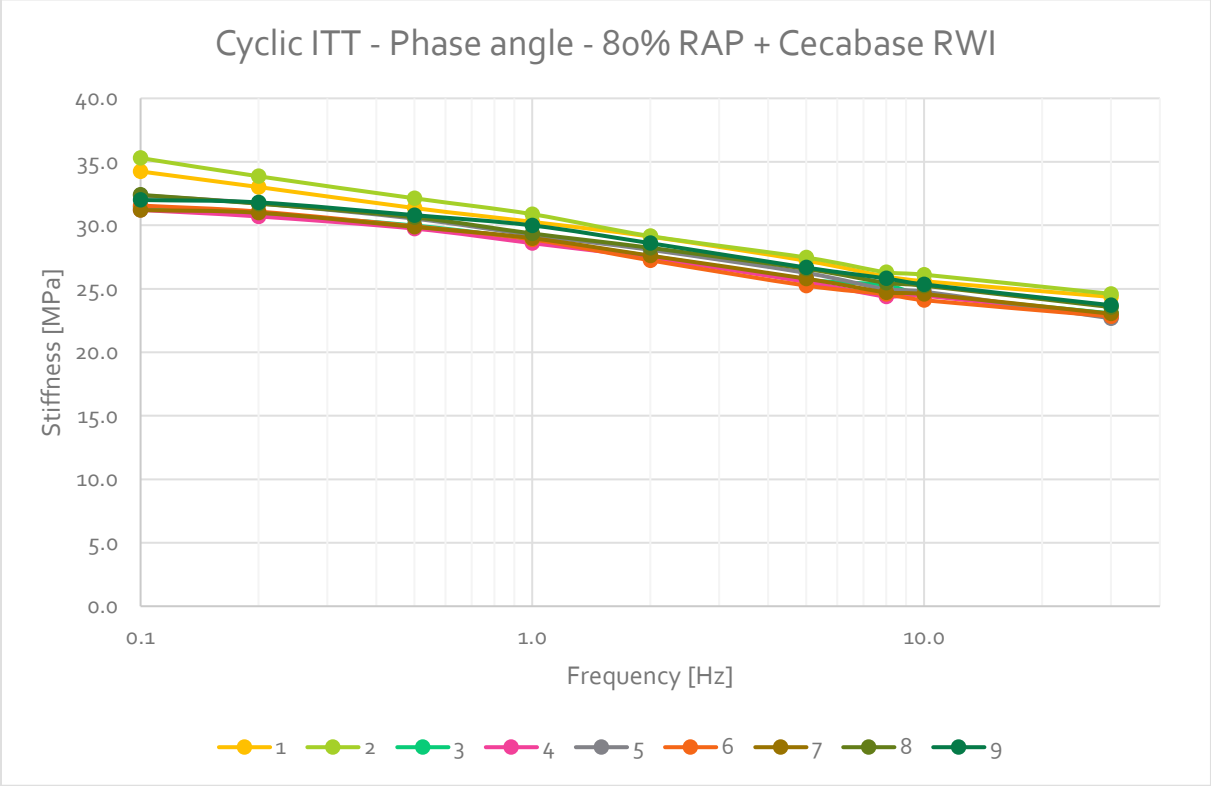

Figure E.6: Results Cyclic ITT – Phase angle 80% RAP + Cecabase RWI

Table E.3: Results Cyclic ITT – Stiffness and phase angle 80% RAP + Cecabase RWI

Mean results		T [°C]	20.0
Frequency (f)	**Strain (ε)**	**Stiffness (E*)**	**Phase angle**
[Hz]	[μm/m]	[MPa]	[°]
30.0	59.5	10170	23.4
10.0	61.0	7905	25.0
8.0	61.0	7528	25.3
5.0	63.1	6664	26.3
2.0	62.4	5165	28.1
1.0	62.5	4203	29.5
0.5	62.5	3389	30.6
0.2	61.8	2567	31.8
0.1	60.5	2085	32.4
30.0	56.8	10249	22.4

Stiffness and phase angle - 80% RAP + Neomex HR

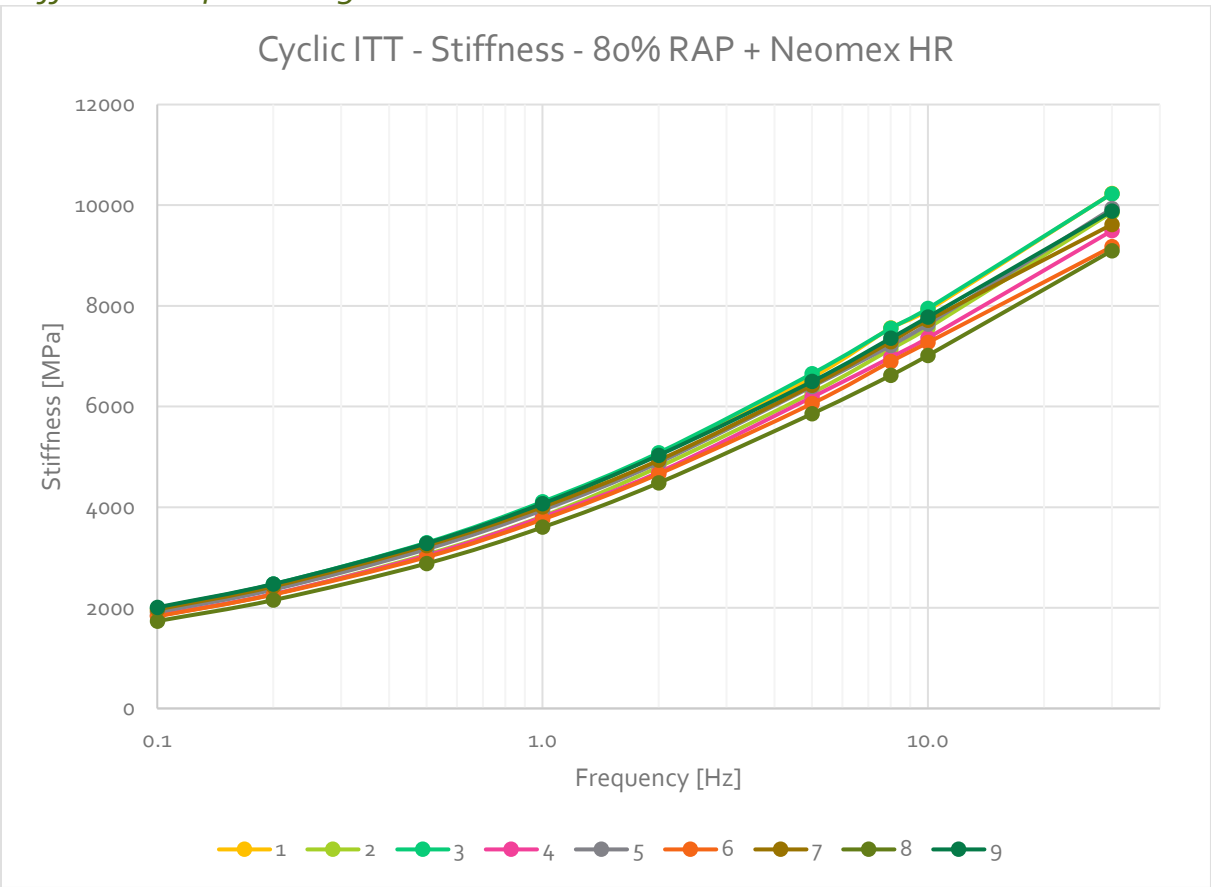

Figure E.7: Results Cyclic ITT - Stiffness 80% RAP + Neomex HR

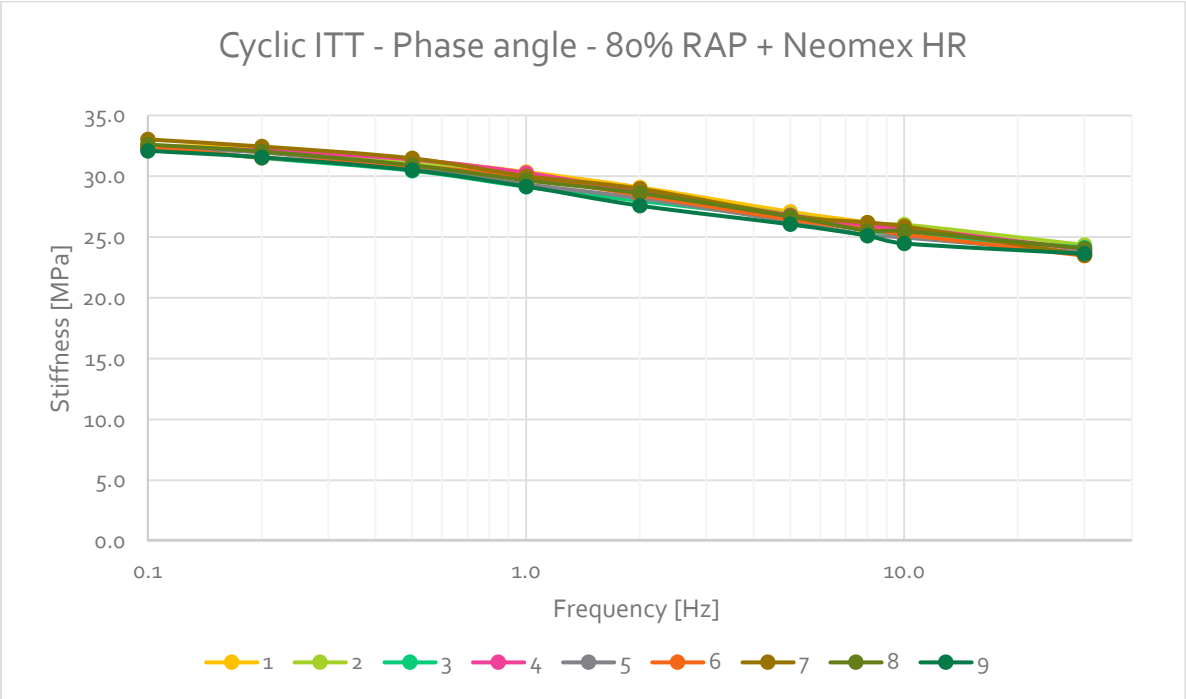

Figure E.8: Results Cyclic ITT – Phase angle 80% RAP + Neomex HR

Table E.4: Results Cyclic ITT - Stiffness and phase angle 80% RAP + Neomex HR

Mean results		T [°C]	20.0
Frequency (f)	**Strain (ε)**	**Stiffness (E*)**	**Phase angle**
[Hz]	[μm/m]	[MPa]	[°]
30.0	58.1	9722	23.9
10.0	54.7	7577	25.4
8.0	54.4	7176	25.7
5.0	54.4	6322	26.6
2.0	54.5	4845	28.5
1.0	54.1	3905	29.8
0.5	53.8	3134	31.0
0.2	53.6	2343	31.9
0.1	52.9	1896	32.5
30.0	57.2	9807	22.9

Fatigue resistance – 65% RAP

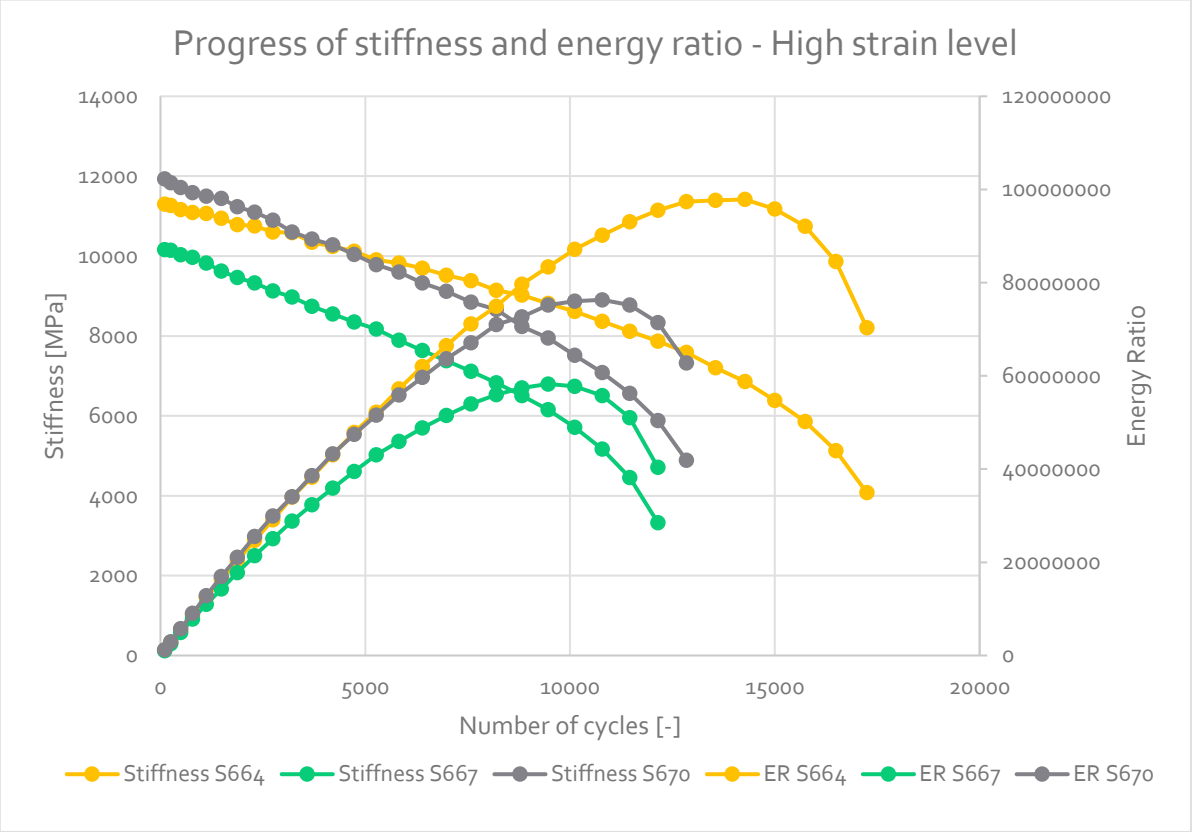

Figure E.9: Results Cyclic ITT – Fatigue resistance 65% RAP – High strain level

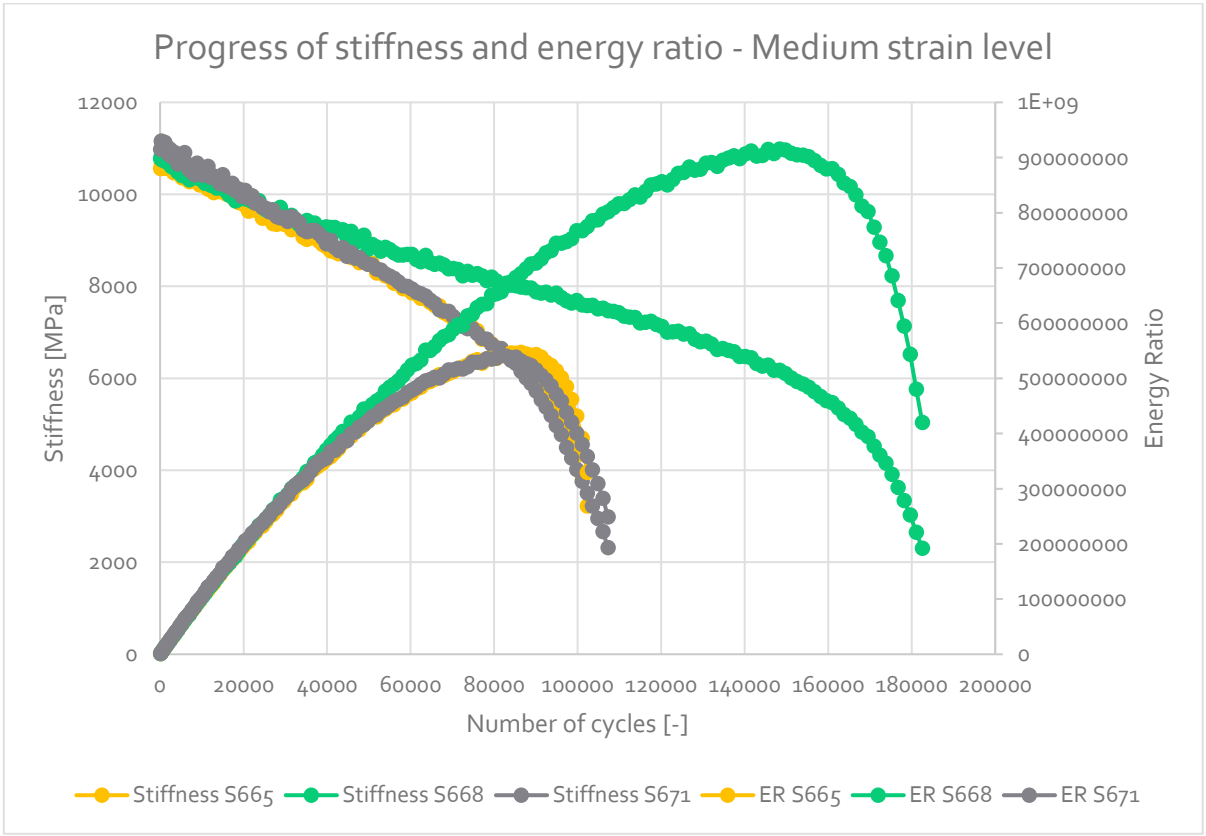

Figure E.10: Results Cyclic ITT – Fatigue resistance 65% RAP – Medium strain level

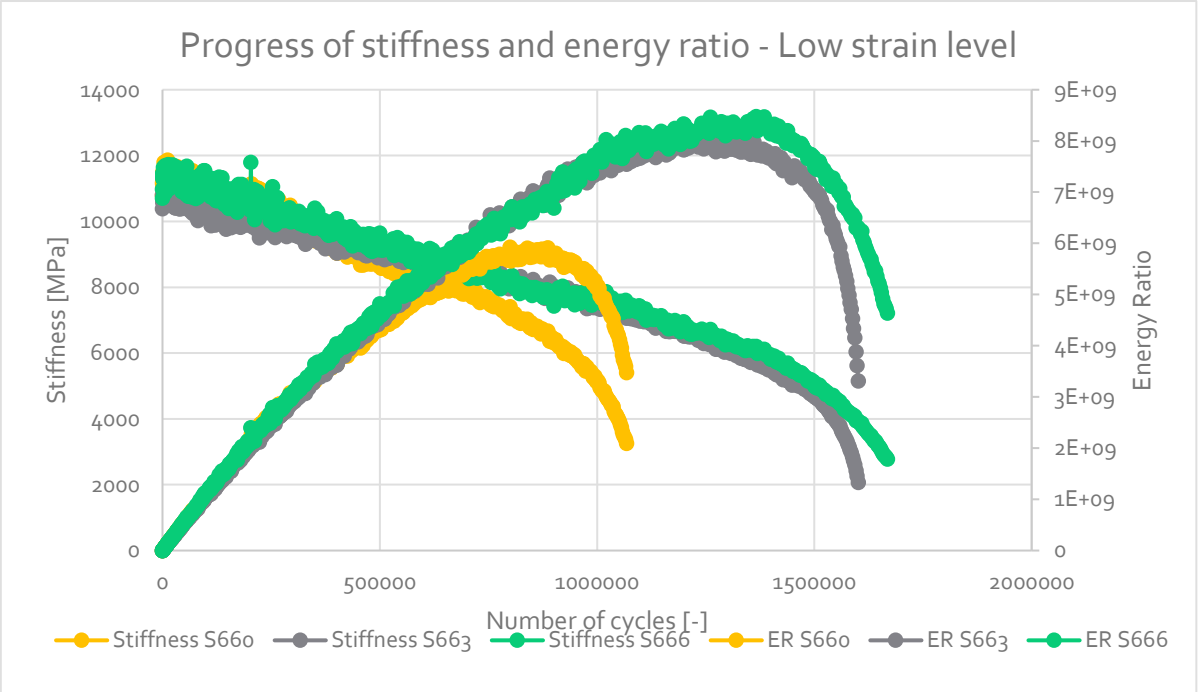

Figure E.11: Results Cyclic ITT – Fatigue resistance 65% RAP – Low strain level

Table E.5: Results Cyclic ITT – Fatigue resistance 65% RAP

Specimen	σ_m [MPa]	σ_a [MPa]	$\varepsilon_{el,ini}$ [‰]	N_f [-]	$\ln(\varepsilon_{el,ini})$	$\ln(N_f)$
S660	0.035	0.180	0.0253	799821	-3.675	13.592
S663	0.035	0.165	0.0228	1253109	-3.781	14.041
S664	0.035	0.660	0.1048	13980	-2.256	9.545
S665	0.035	0.360	0.0583	86276	-2.842	11.365
S666	0.035	0.165	0.0229	1366288	-3.775	14.128
S667	0.035	0.660	0.1162	9556	-2.153	9.165
S668	0.035	0.360	0.0571	148829	-2.862	11.911
S670	0.035	0.660	0.0992	10577	-2.311	9.266
S671	0.035	0.360	0.0561	81908	-2.880	11.313

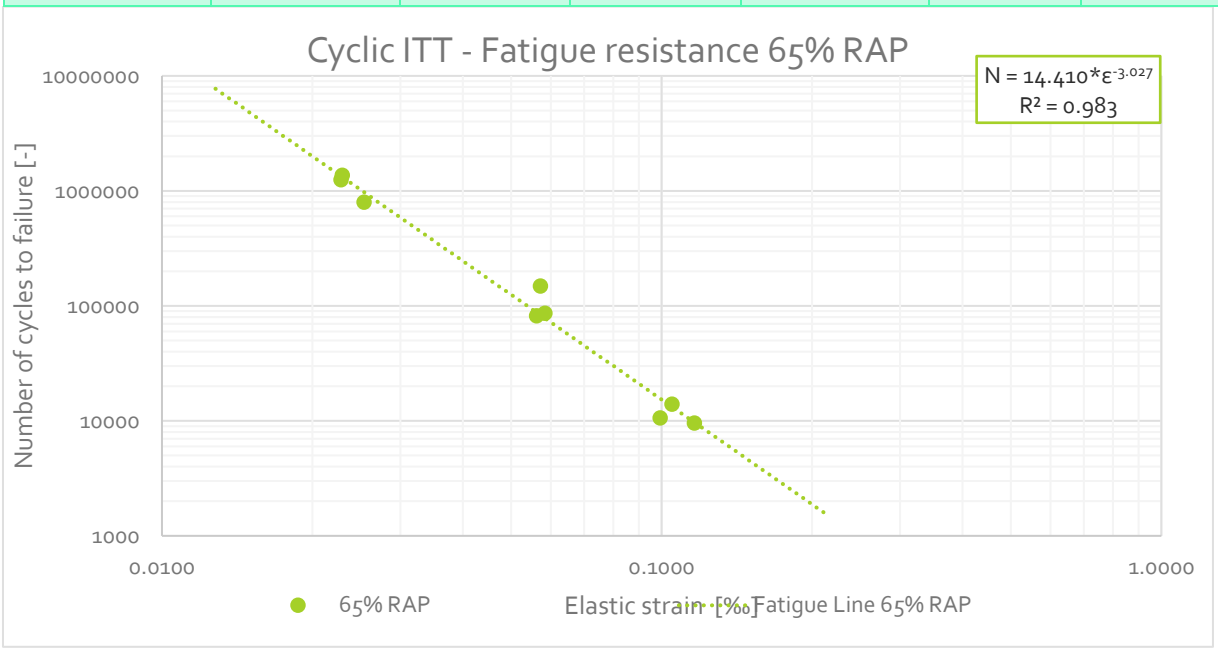

Figure E.12: Results Cyclic ITT – Fatigue resistance 65% RAP

Fatigue resistance – 80% RAP

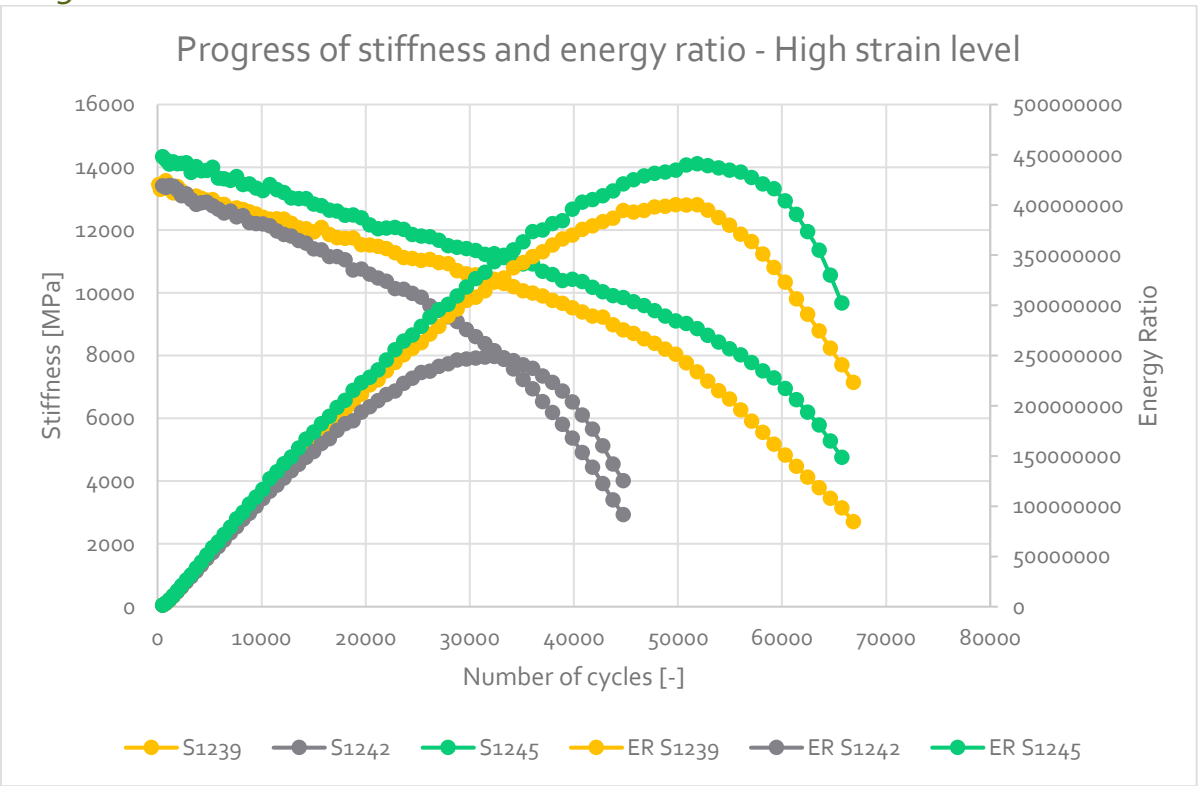

Figure E.13: Results Cyclic ITT – Fatigue resistance 80% RAP – High strain level

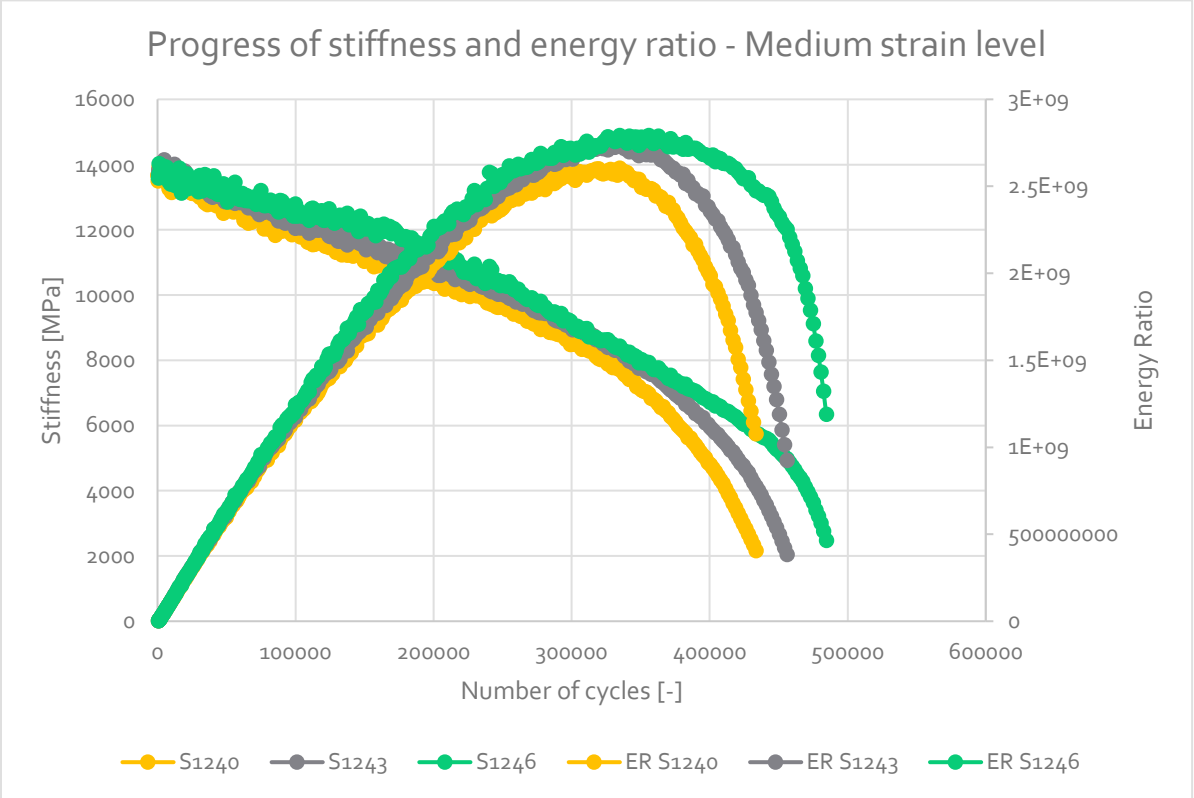

Figure E.14: Results Cyclic ITT – Fatigue resistance 80% RAP – Medium strain level

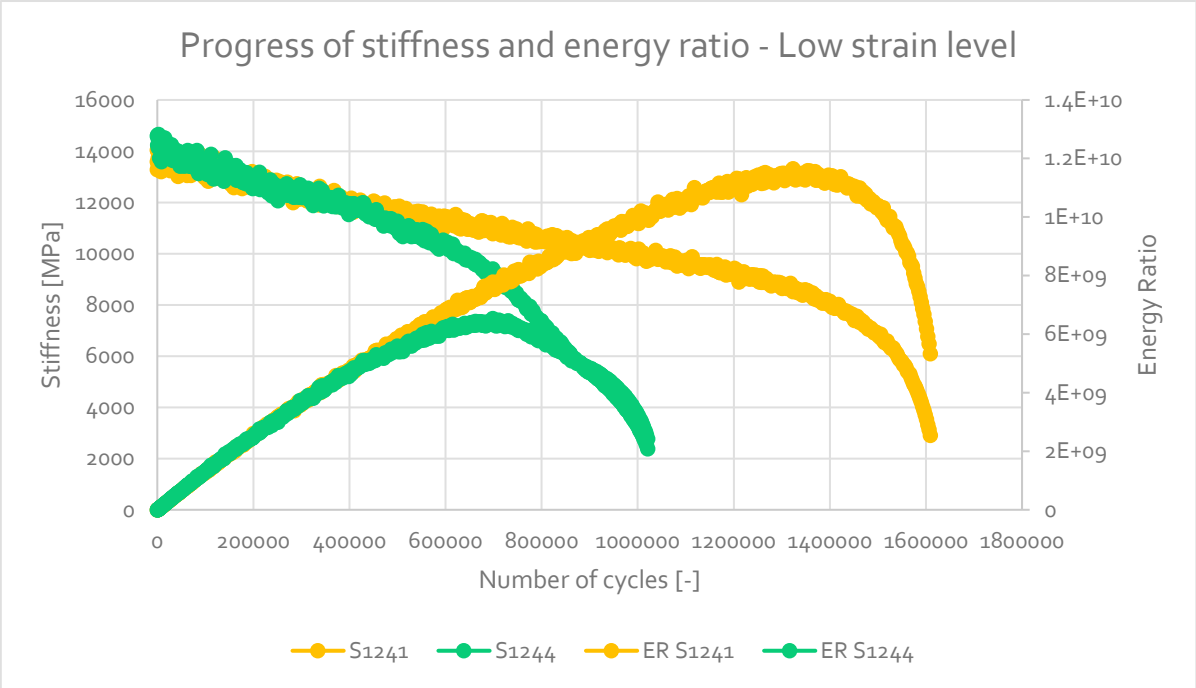

Figure E.15: Results Cyclic ITT – Fatigue resistance 80% RAP – Low strain level

Table E.6: Results Cyclic ITT – Fatigue resistance 80% RAP

Specimen	σ_m [MPa]	σ_a [MPa]	$\varepsilon_{el,ini}$ [‰]	N_f [-]	$\ln(\varepsilon_{el,ini})$	$\ln(N_f)$
S1239	0.035	0.540	0.0711	48038	-2.643	10.780
S1240	0.035	0.350	0.0437	331563	-3.131	12.712
S1241	0.035	0.250	0.0302	1317980	-3.501	14.092
S1242	0.035	0.540	0.0713	30412	-2.641	10.323
S1243	0.035	0.350	0.0435	331282	-3.136	12.711
S1244	0.035	0.250	0.0279	694045	-3.578	13.450
S1245	0.035	0.540	0.0668	49664	-2.706	10.813
S1246	0.035	0.350	0.0439	331491	-3.127	12.711

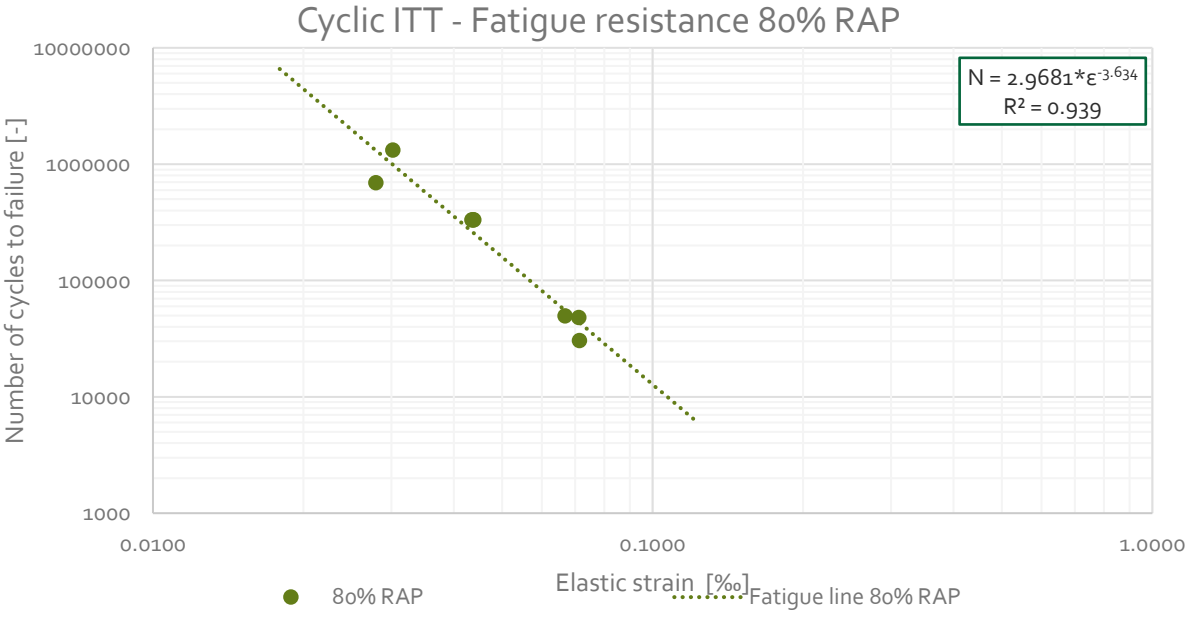

Figure E.16: Results Cyclic ITT – Fatigue resistance 80% RAP

Fatigue resistance - 80% RAP + Cecabase RWI

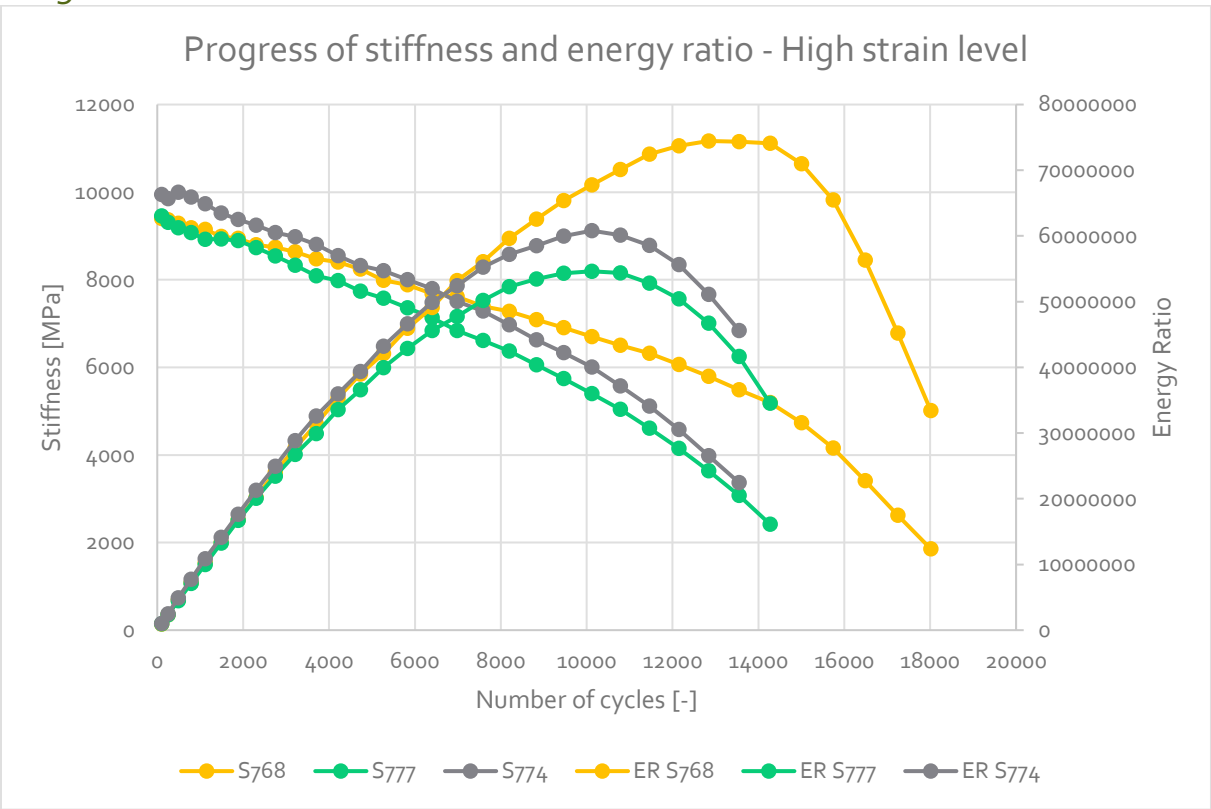

Figure E.17: Results Cyclic ITT - Fatigue resistance 80% RAP + Cecabase RWI– High strain level

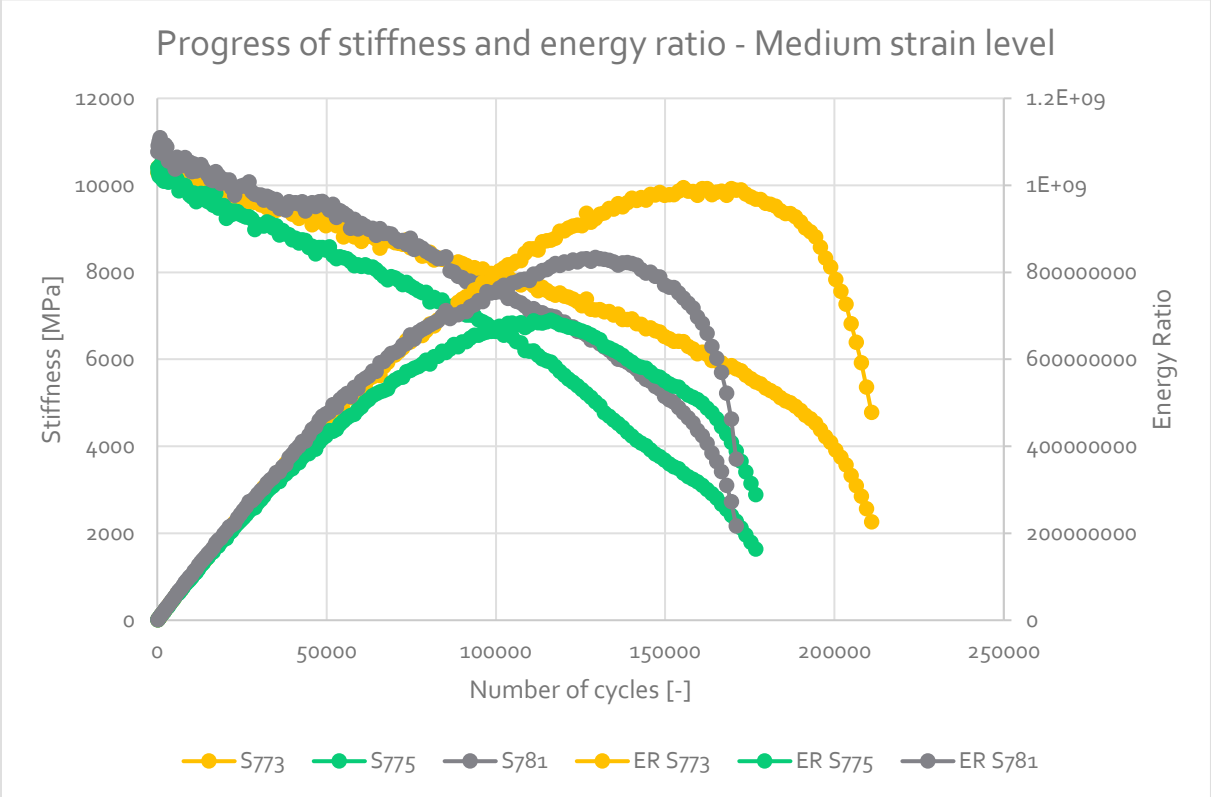

Figure E.18: Results Cyclic ITT - Fatigue resistance 80% RAP + Cecabase RWI – Medium strain level

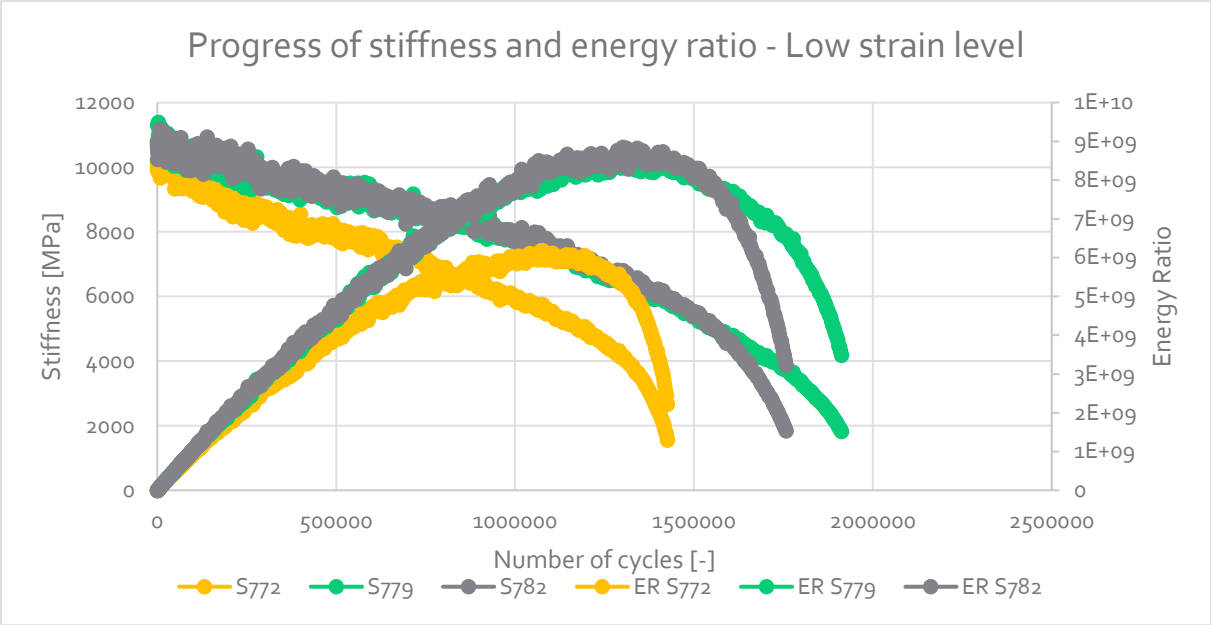

Figure E.19: Results Cyclic ITT - Fatigue resistance 80% RAP + Cecabase RWI – Low strain level

Table E.7: Results Cyclic ITT - Fatigue resistance 80% RAP + Cecabase RWI

Specimen	σ_m [MPa]	σ_a [MPa]	$\varepsilon_{el,ini}$ [‰]	N_f [-]	$\ln(\varepsilon_{el,ini})$	$\ln(N_f)$
S768	0.035	0.480	0.0895	13097	-2.413	9.480
S772	0.035	0.140	0.0198	1077400	-3.922	13.890
S773	0.035	0.290	0.0470	155319	-3.057	11.953
S774	0.035	0.540	0.0961	10151	-2.343	9.225
S775	0.035	0.290	0.0464	116203	-3.071	11.663
S777	0.035	0.540	0.1012	10149	-2.291	9.225
S779	0.035	0.145	0.0192	1213745	-3.952	14.009
S781	0.035	0.290	0.0448	129697	-3.106	11.773
S782	0.035	0.145	0.0193	1300860	-3.947	14.079

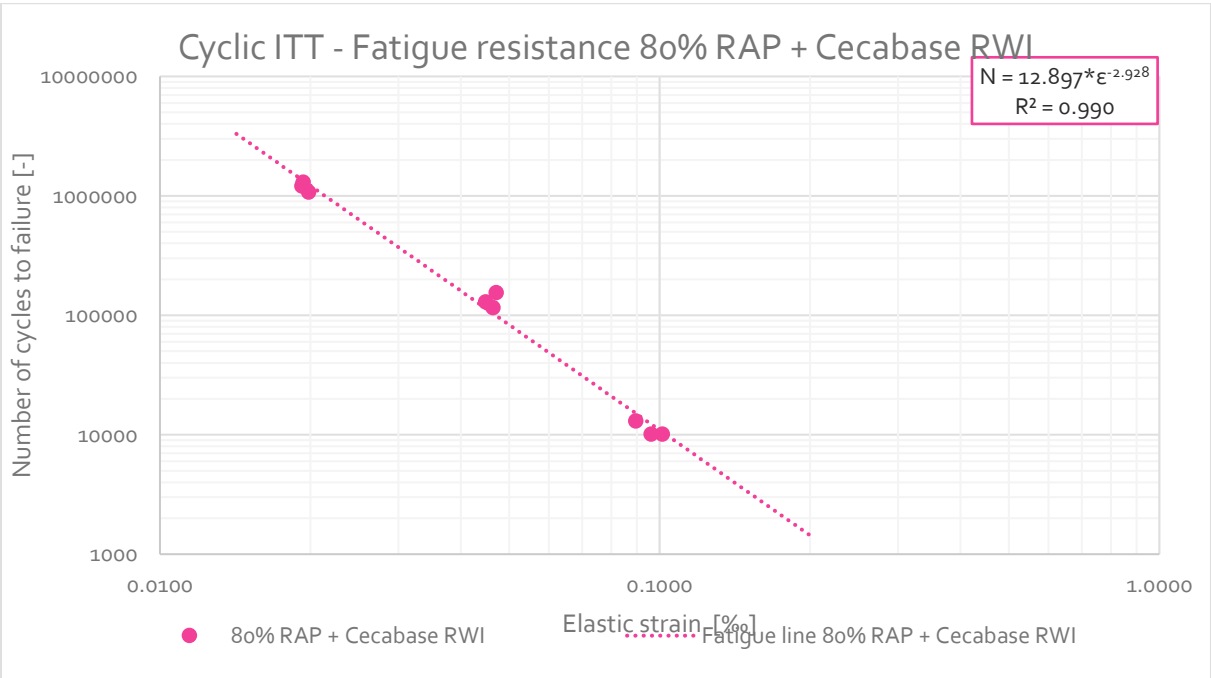

Figure E.20: Results Cyclic ITT – Fatigue resistance 80% RAP + Cecabase RWI

Fatigue resistance – 80% RAP + Neomex HR

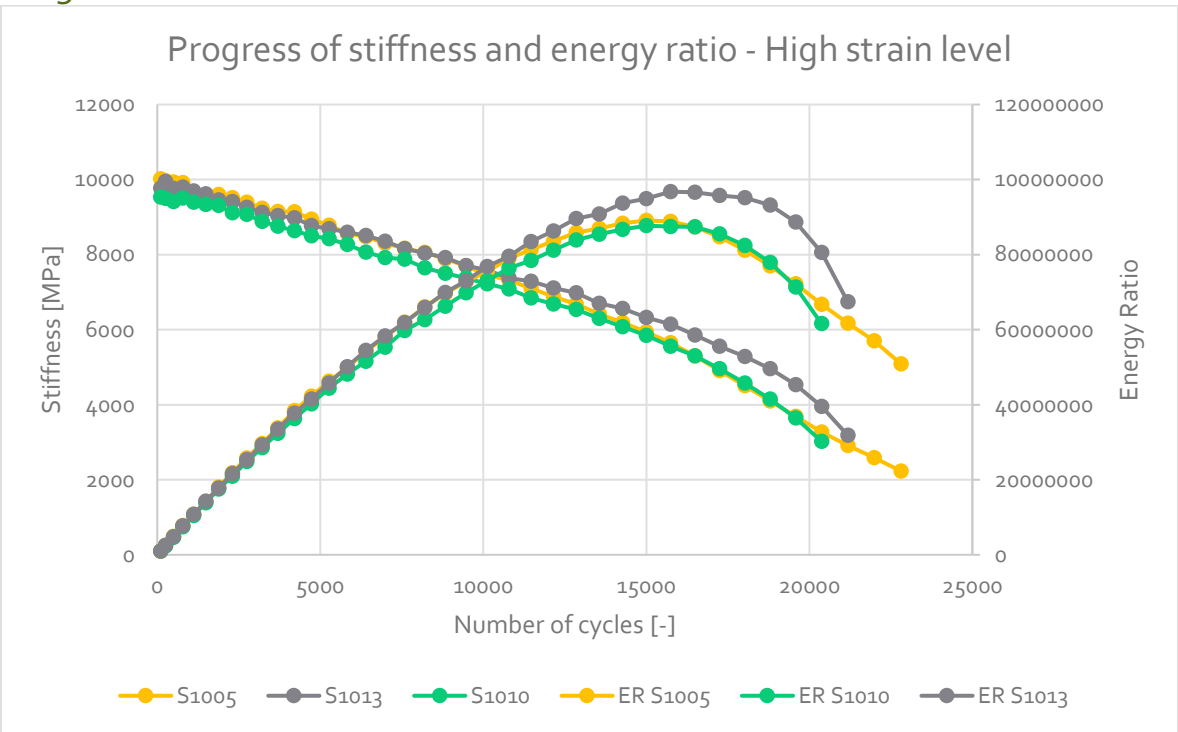

Figure E.21: Results Cyclic ITT - Fatigue resistance 80% RAP + Neomex HR– High strain level

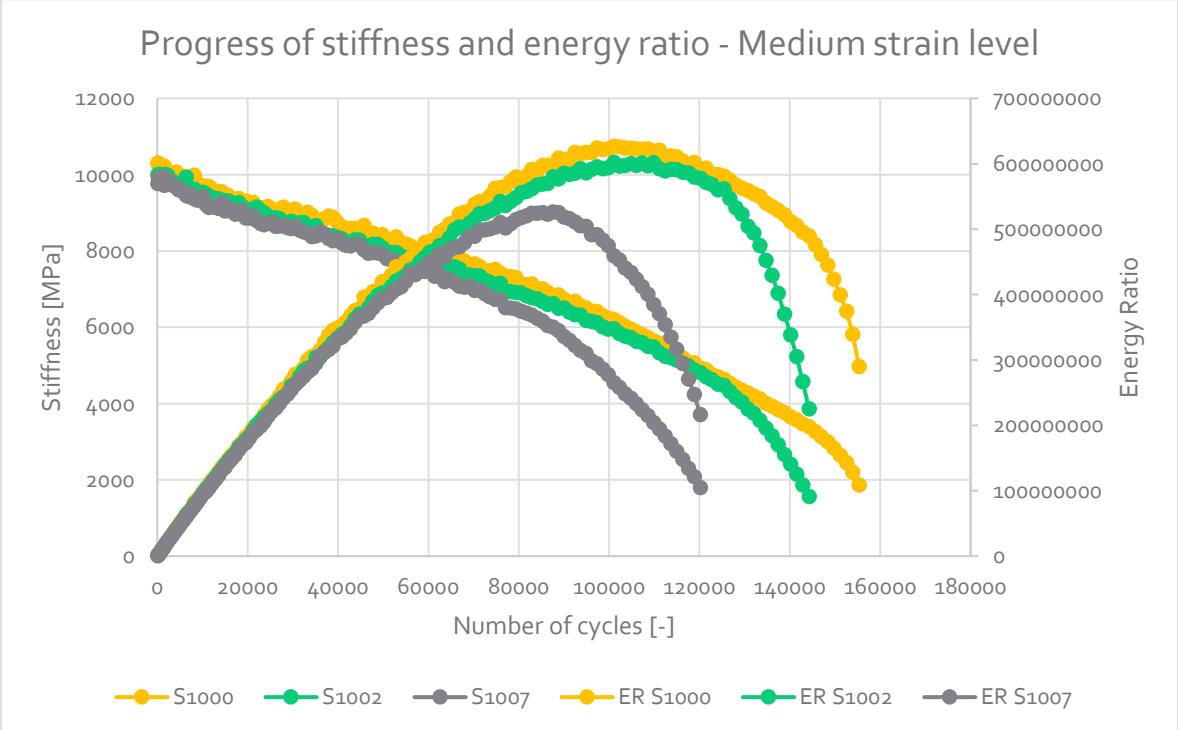

Figure E.22: Results Cyclic ITT - Fatigue resistance 80% RAP + Neomex HR – Medium strain level

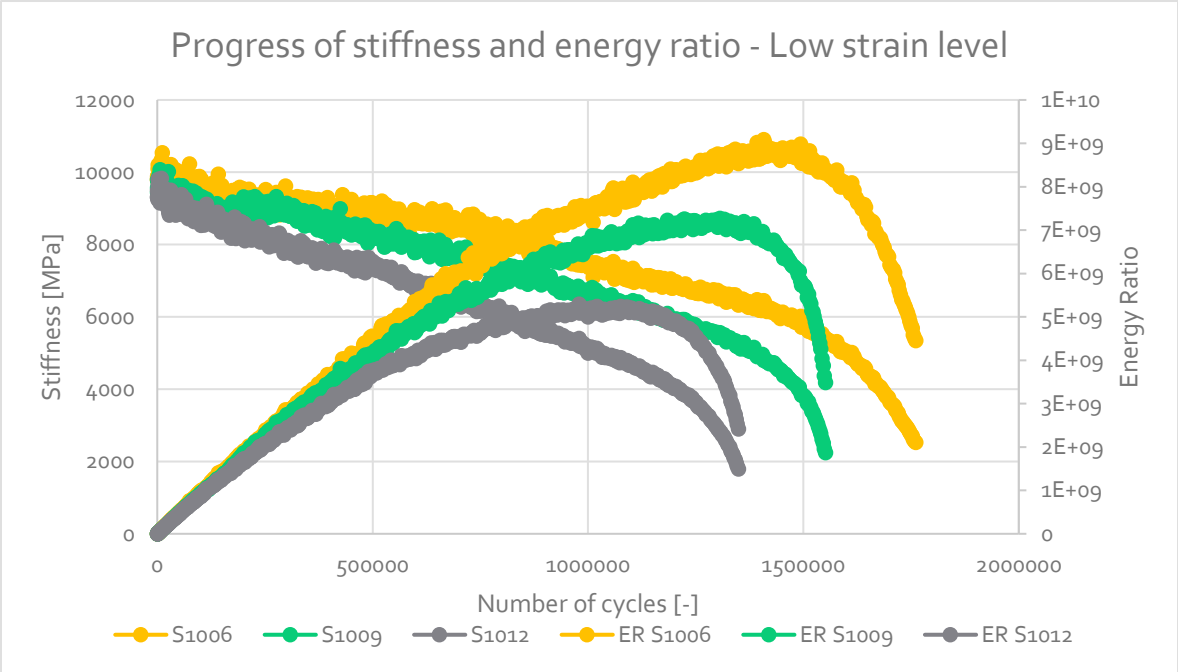

Figure E.23: Results Cyclic ITT – Fatigue resistance 80% RAP + Neomex HR – Low strain level

Table E.8: Results Cyclic ITT – Fatigue resistance 80% RAP + Neomex HR

Specimen	σ_m [MPa]	σ_a [MPa]	$\varepsilon_{el,ini}$ [‰]	N_f [-]	$\ln(\varepsilon_{el,ini})$	$\ln(N_f)$
S1000	0.035	0.290	0.0468	101450	-3.061	11.527
S1002	0.035	0.290	0.0484	101152	-3.028	11.524
S1005	0.035	0.480	0.0840	15197	-2.476	9.629
S1006	0.035	0.145	0.0212	1408388	-3.854	14.158
S1007	0.035	0.290	0.0493	87936	-3.009	11.384
S1009	0.035	0.145	0.0221	1306071	-3.810	14.083
S1010	0.035	0.480	0.0885	15228	-2.425	9.631
S1012	0.035	0.145	0.0220	978587	-3.819	13.794
S1013	0.035	0.480	0.0861	16059	-2.452	9.684

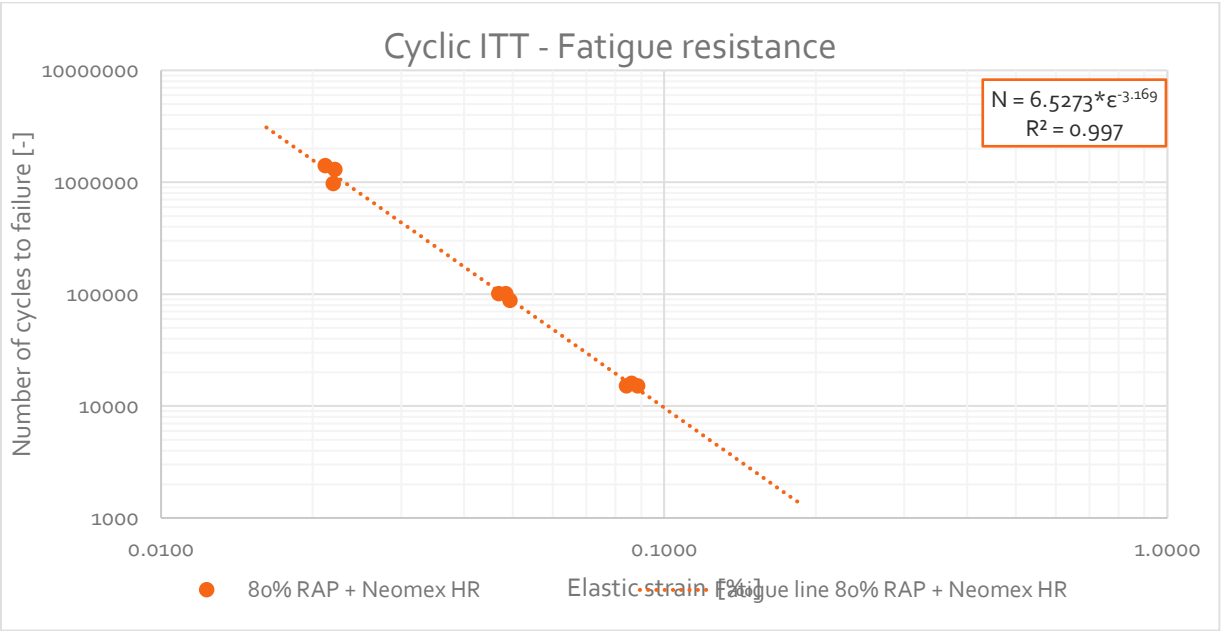

Figure E.24: Results Cyclic ITT – Fatigue resistance 80% RAP + Neomex HR

Appendix F: Results triaxial cyclic compression test

In this appendix, the results of the triaxial cyclic compression test are given. The permanent deformation as a function of number of cycles is shown and the linear fit between the 4000th and 10000th cycle is given together with the creep rate.

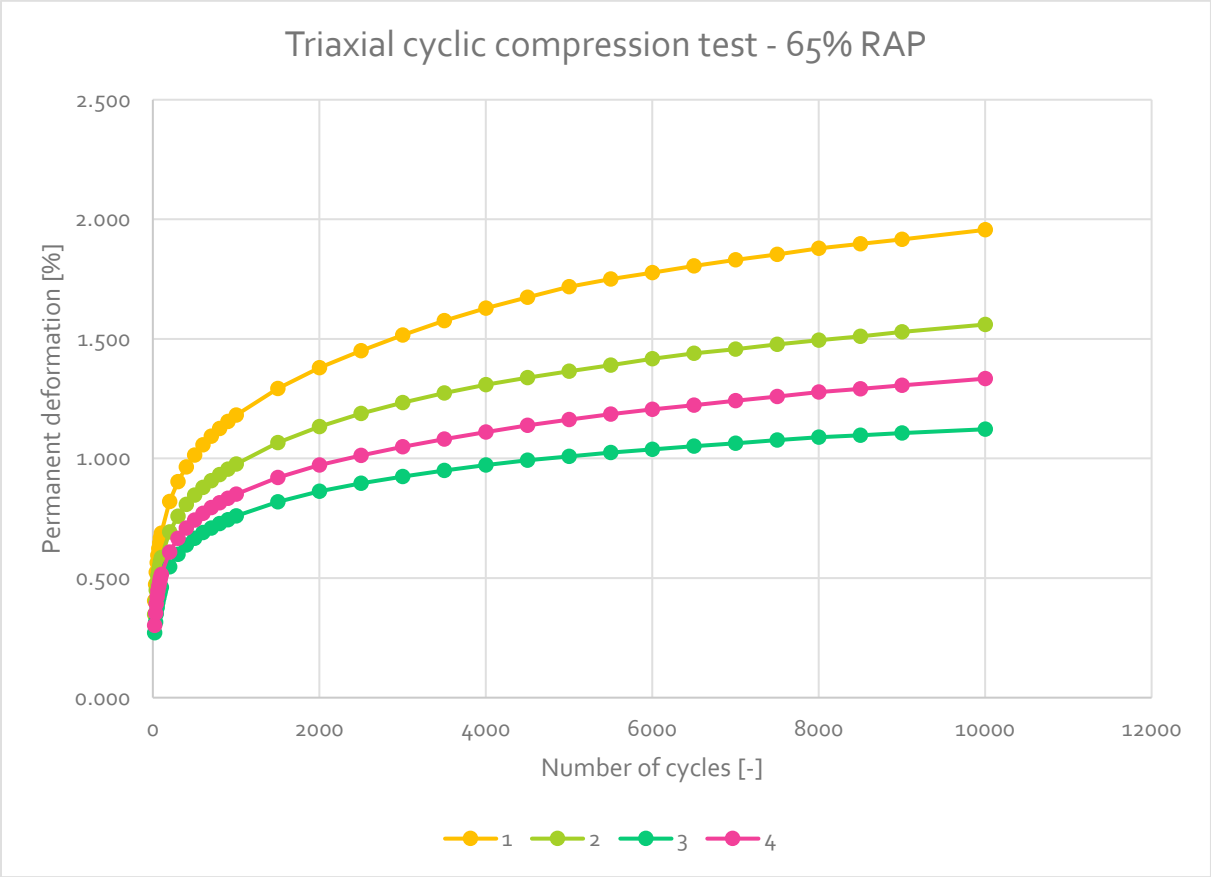

Figure F.1: Results triaxial cyclic compression test – 65% RAP

Table F.1: Results triaxial cyclic compression test – 65% RAP

Specimen	A_1 [%]	B_1 [%]	f_c [µm/m/cycle]
1	1.446	$5.32 * 10^{-5}$	0.53
2	1.156	$4.18 * 10^{-5}$	0.42
3	0.883	$2.50 * 10^{-5}$	0.25
4	0.977	$3.70 * 10^{-5}$	0.37
Mean values	1.115	$3.93 * 10^{-5}$	0.39

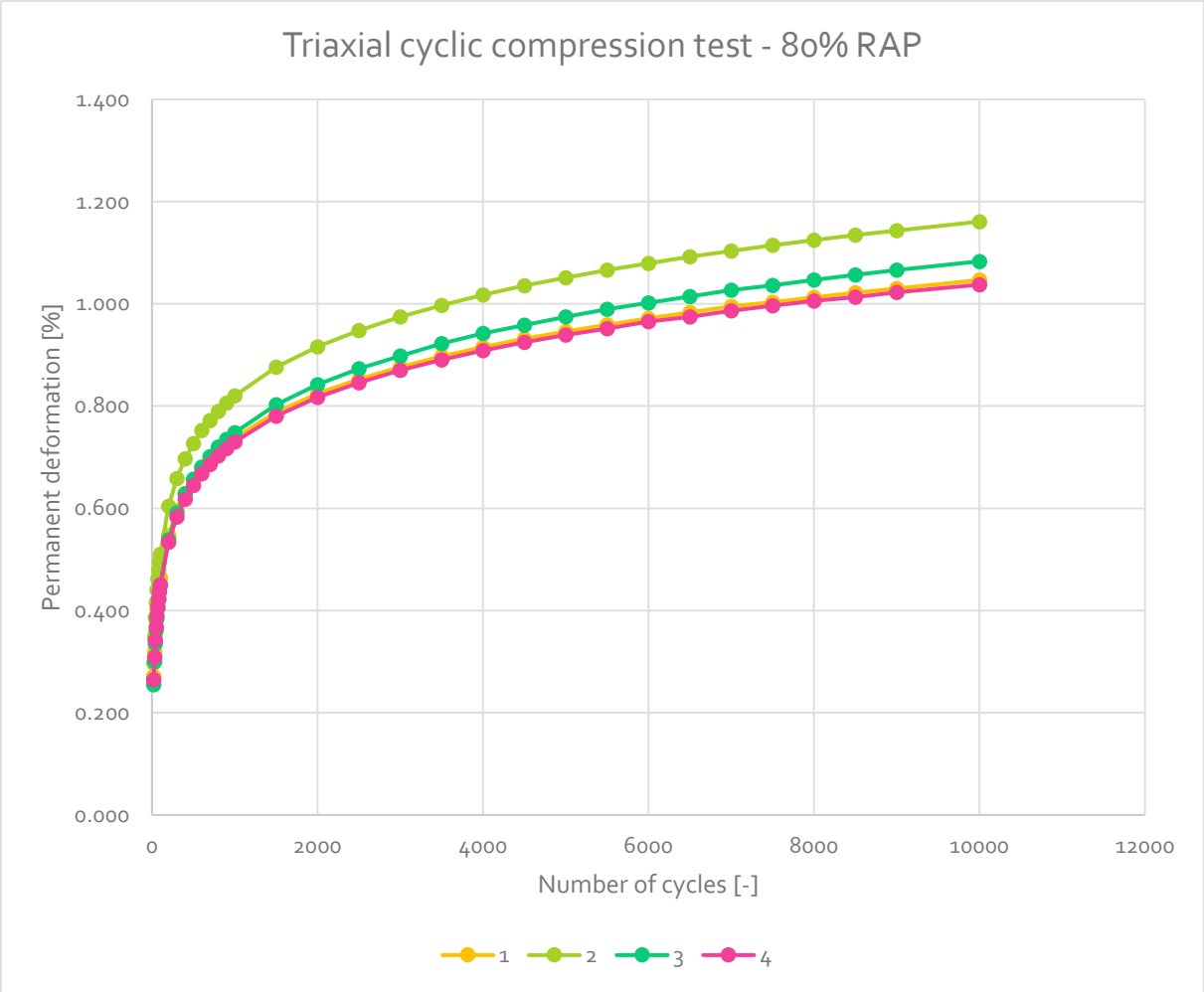

Figure F.2: Results triaxial cyclic compression test – 80% RAP

Table F.2: Results triaxial cyclic compression test – 80% RAP

Specimen	A_1 [%]	B_1 [%]	f_c [µm/m/cycle]
1	0.837	$2.17 * 10^{-5}$	0.22
2	0.932	$2.37 * 10^{-5}$	0.24
3	0.857	$2.34 * 10^{-5}$	0.23
4	0.832	$2.14 * 10^{-5}$	0.21
Mean values	0.865	$2.26 * 10^{-5}$	0.23

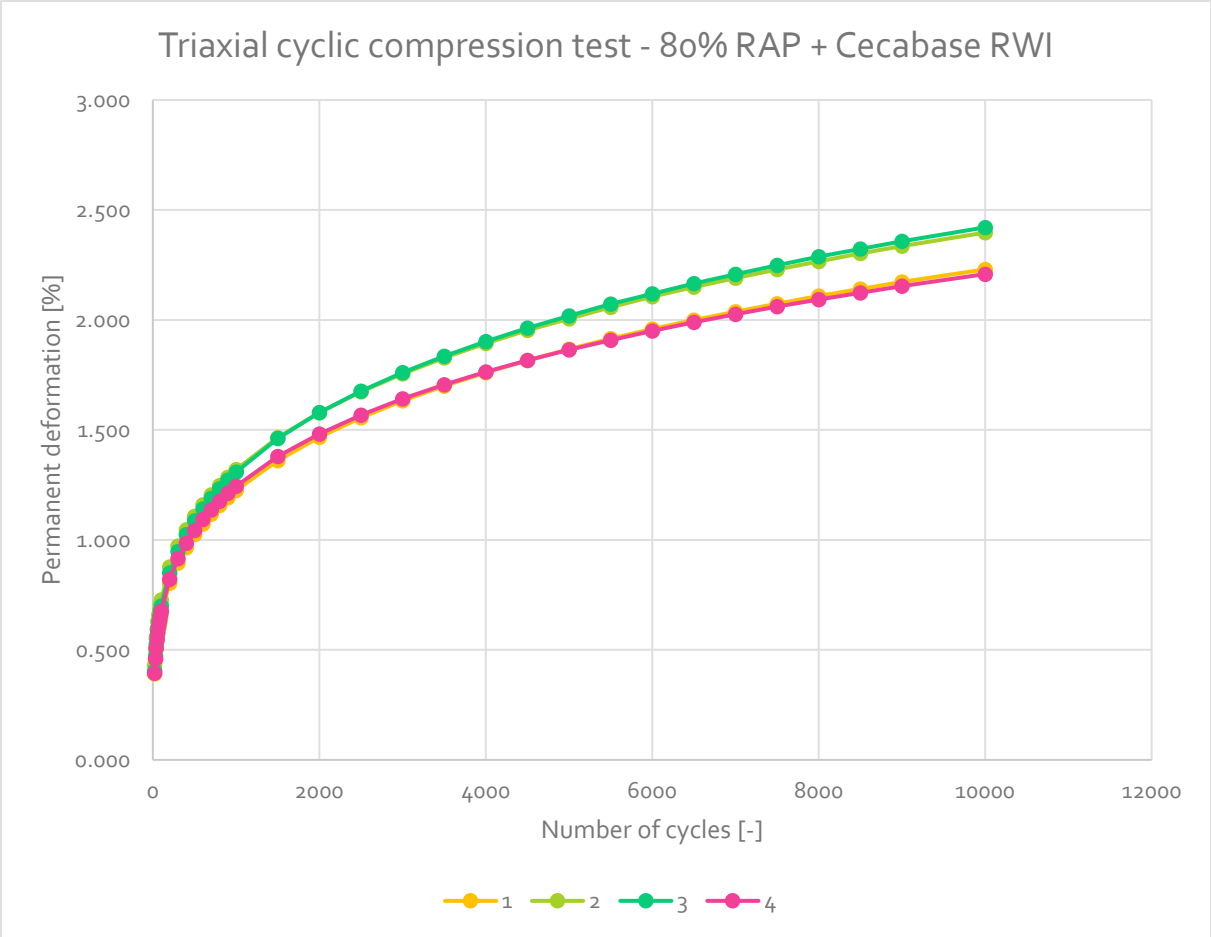

Figure F.3: Results triaxial cyclic compression test – 80% RAP + Cecabase RWI

Table F.3: Results triaxial cyclic compression test – 80% RAP + Cecabase RWI

Specimen	A_1 [%]	B_1 [%]	f_c [µm/m/cycle]
1	1.477	$7.80 * 10^{-5}$	0.78
2	1.587	$8.40 * 10^{-5}$	0.84
3	1.588	$8.63 * 10^{-5}$	0.86
4	1.493	$7.40 * 10^{-5}$	0.74
Mean values	1.536	$8.06 * 10^{-5}$	0.81

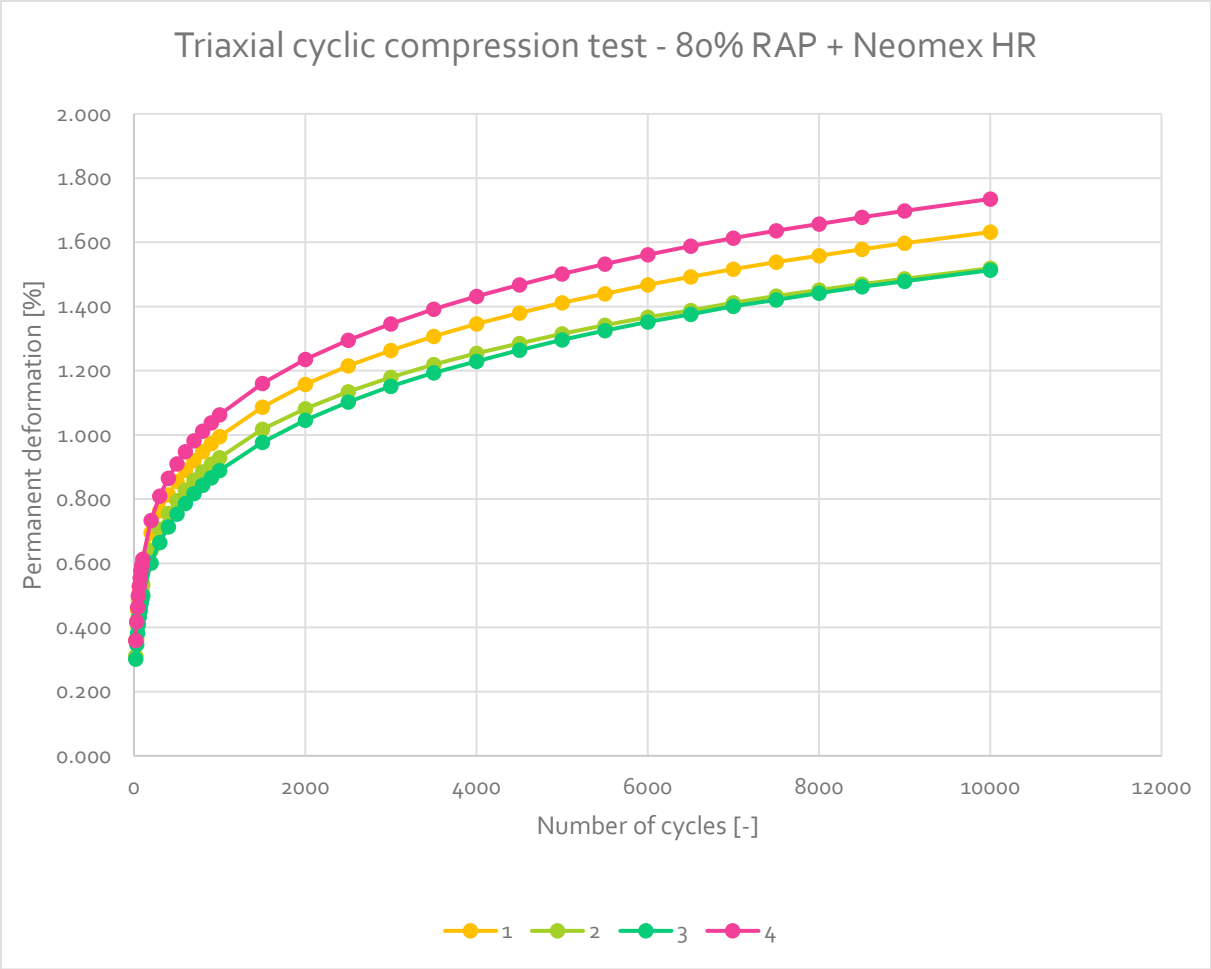

Figure F.4: Results triaxial cyclic compression test – 80% RAP + Neomex HR

Table F.4: Results triaxial cyclic compression test – 80% RAP + Neomex HR

Specimen	A_1 [%]	B_1 [%]	f_c [µm/m/cycle]
1	1.173	$4.76 * 10^{-5}$	0.48
2	1.093	$4.42 * 10^{-5}$	0.44
3	1.060	$4.71 * 10^{-5}$	0.47
4	1.249	$5.04 * 10^{-5}$	0.50
Mean values	1.144	$4.73 * 10^{-5}$	0.47

Appendix G: Results four point bending test

The four point bending test results are given in this appendix. The stiffness and phase angle results for the three tested mixtures are shown.

65% RAP

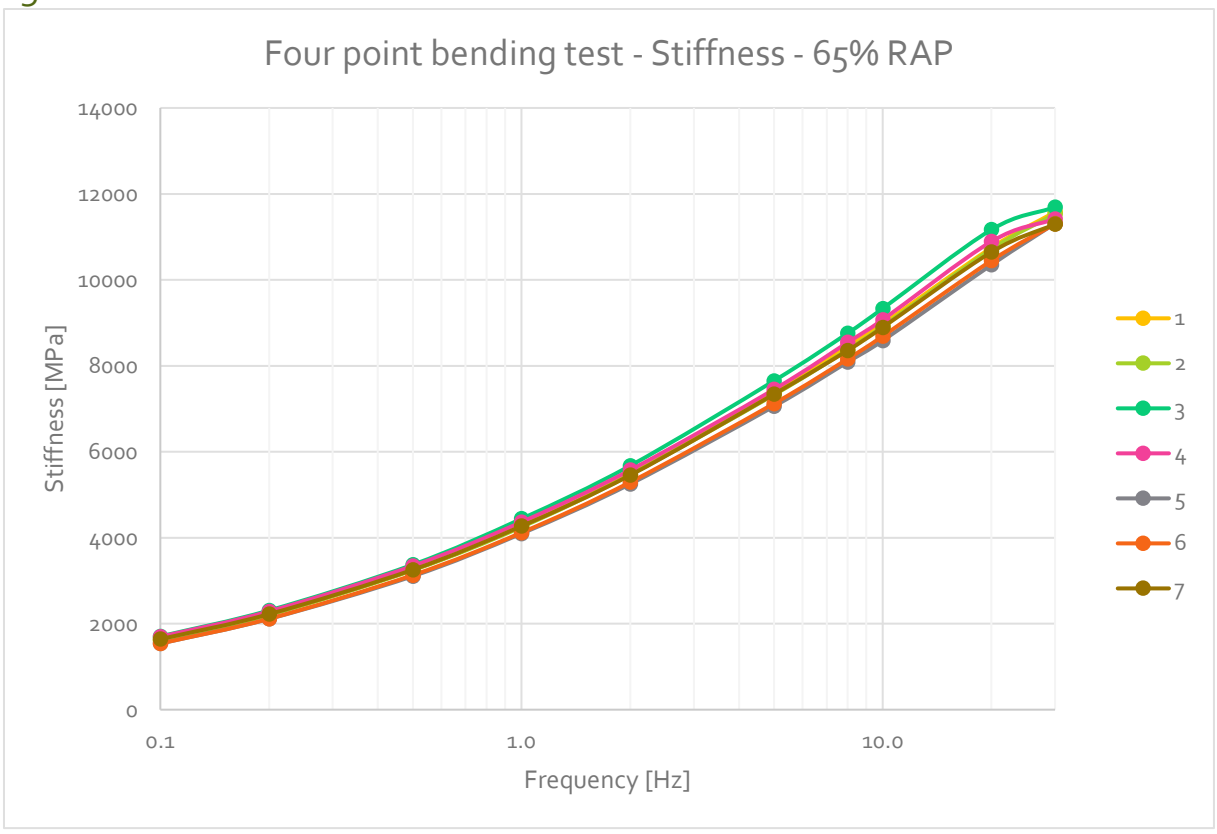

Figure G.1: Results four point bending test - Stiffness 65% RAP

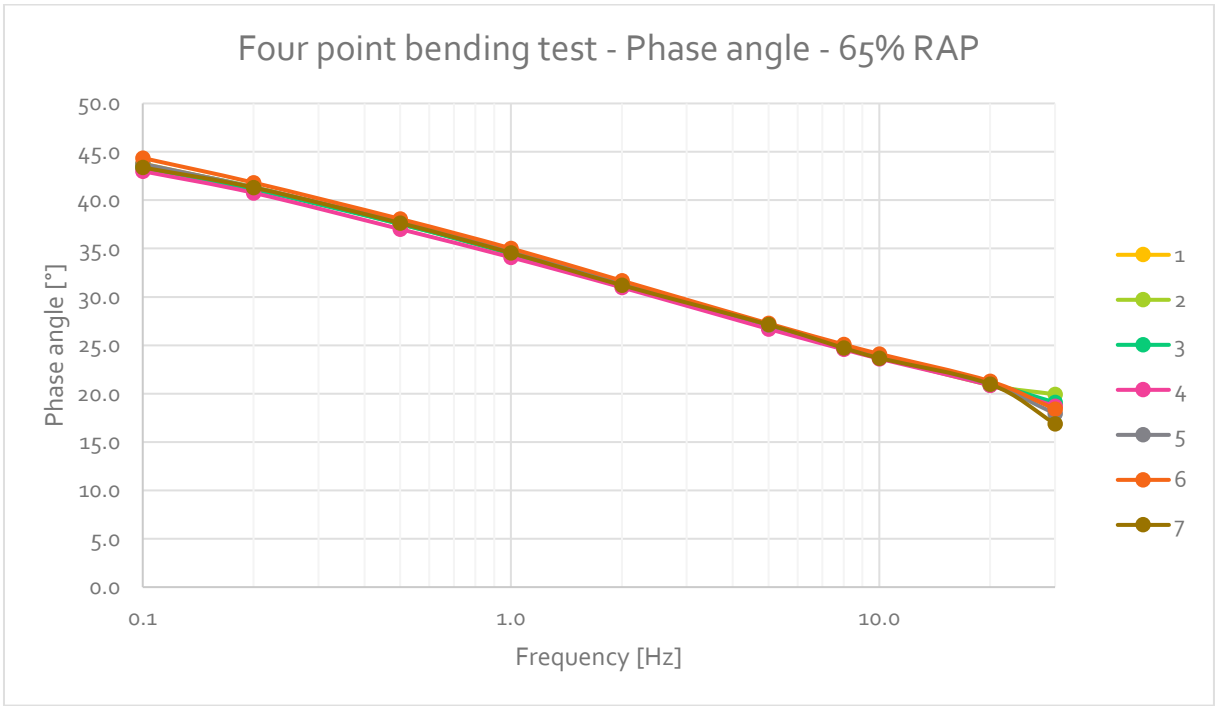

Figure G.2: Results four point bending test – Phase angle 65% RAP

Table G.1: Results four point bending test - Stiffness 65% RAP

Mean Results		T [°C]	20.0
Frequency (f)	Strain (ε)	Stiffness (E*)	Phase angle
Hz	[μm/m]	[MPa]	[°]
0.1	51.3	1622	43.6
0.2	51.3	2210	41.3
0.5	51.4	3244	37.6
1.0	51.2	4259	34.6
2.0	51.3	5457	31.3
5.0	51.3	7331	27.0
8.0	51.3	8391	24.8
10.0	51.3	8924	23.8
20.0	51.4	10709	21.0
30.0	51.4	11448	18.5
0.1	51.2	1584	43.5

80% RAP + Cecabase RWI

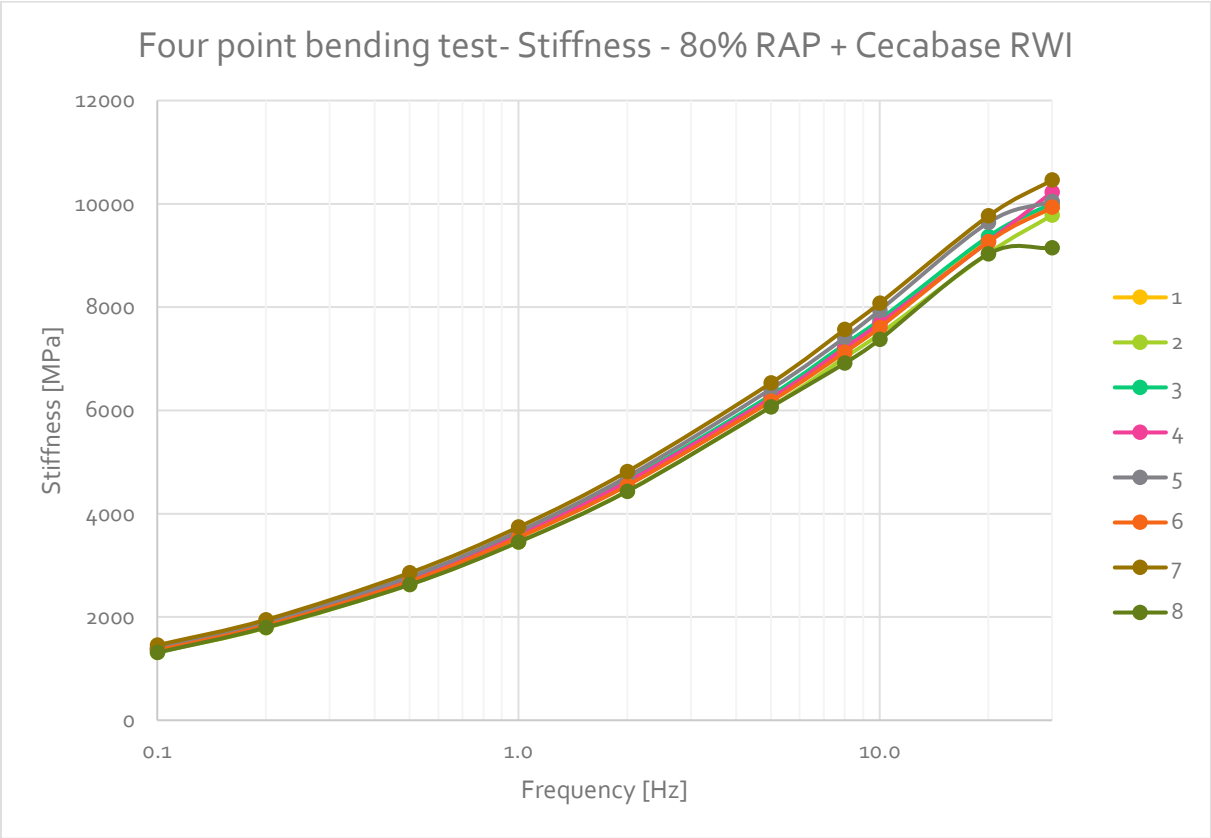

Figure G.3: Results four point bending test - Stiffness 80% RAP + Cecabase RWI

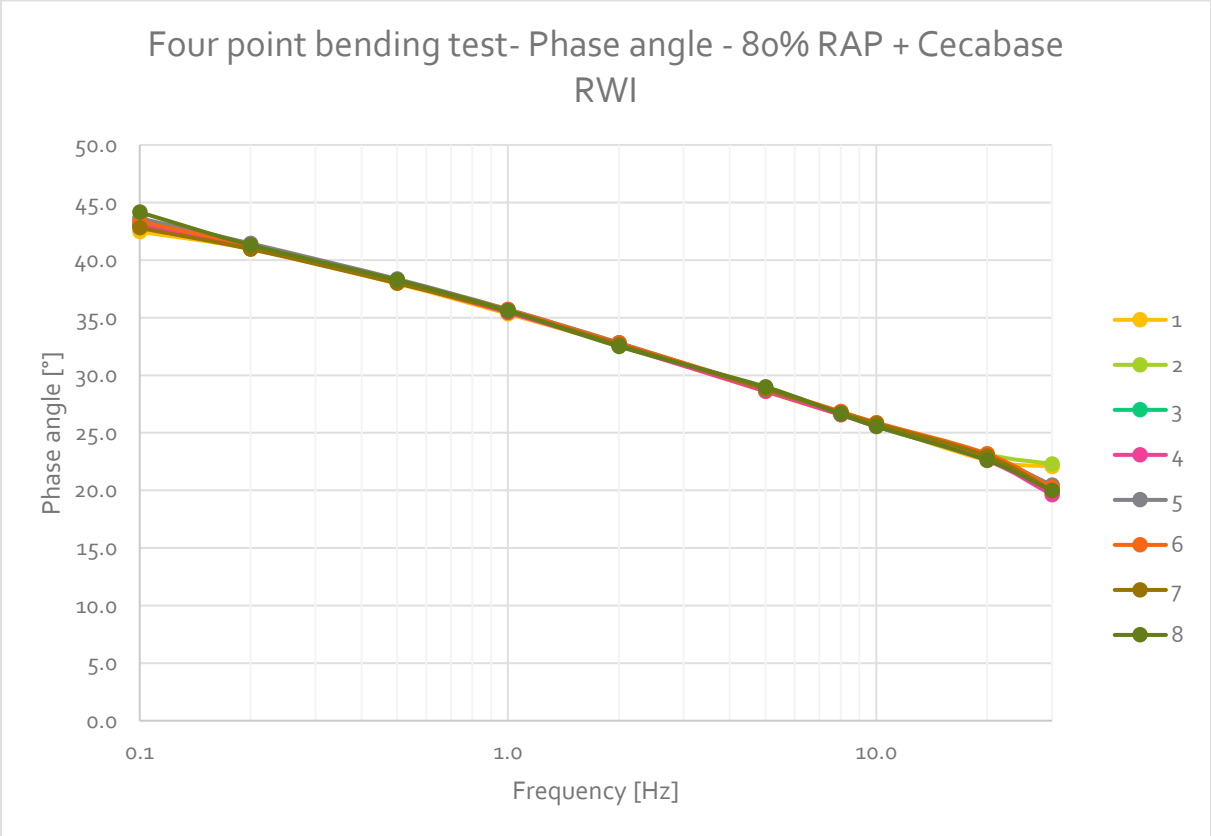

Figure G.4: Results four point bending test – Phase angle 80% RAP + Cecabase RWI

Table G.2: Results four point bending test - Stiffness 80% RAP + Cecabase RWI

Mean Results		T [°C]	20.0
Frequency (f)	Strain (ε)	Stiffness (E*)	Phase angle
Hz	[mm/m]	[MPa]	[°]
0.1	50.8	1371	43.2
0.2	50.8	1856	41.1
0.5	50.7	2715	38.1
1.0	50.8	3571	35.6
2.0	50.7	4599	32.7
5.0	50.8	6254	28.8
8.0	50.8	7215	26.7
10.0	50.8	7700	25.7
20.0	50.8	9335	22.9
30.0	50.8	9940	20.6
0.1	50.8	1335	42.9

80% RAP + Neomex HR

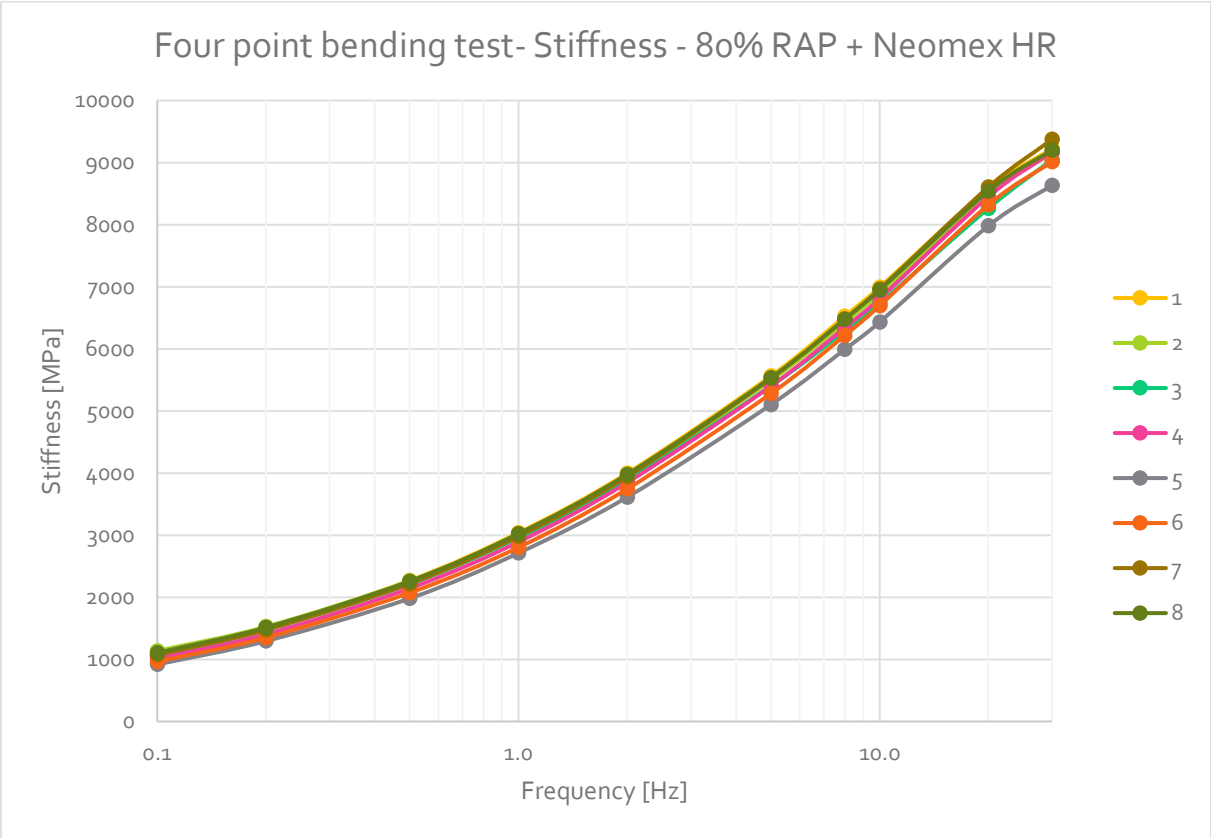

Figure G.5: Results four point bending test - Stiffness 80% RAP + Neomex HR

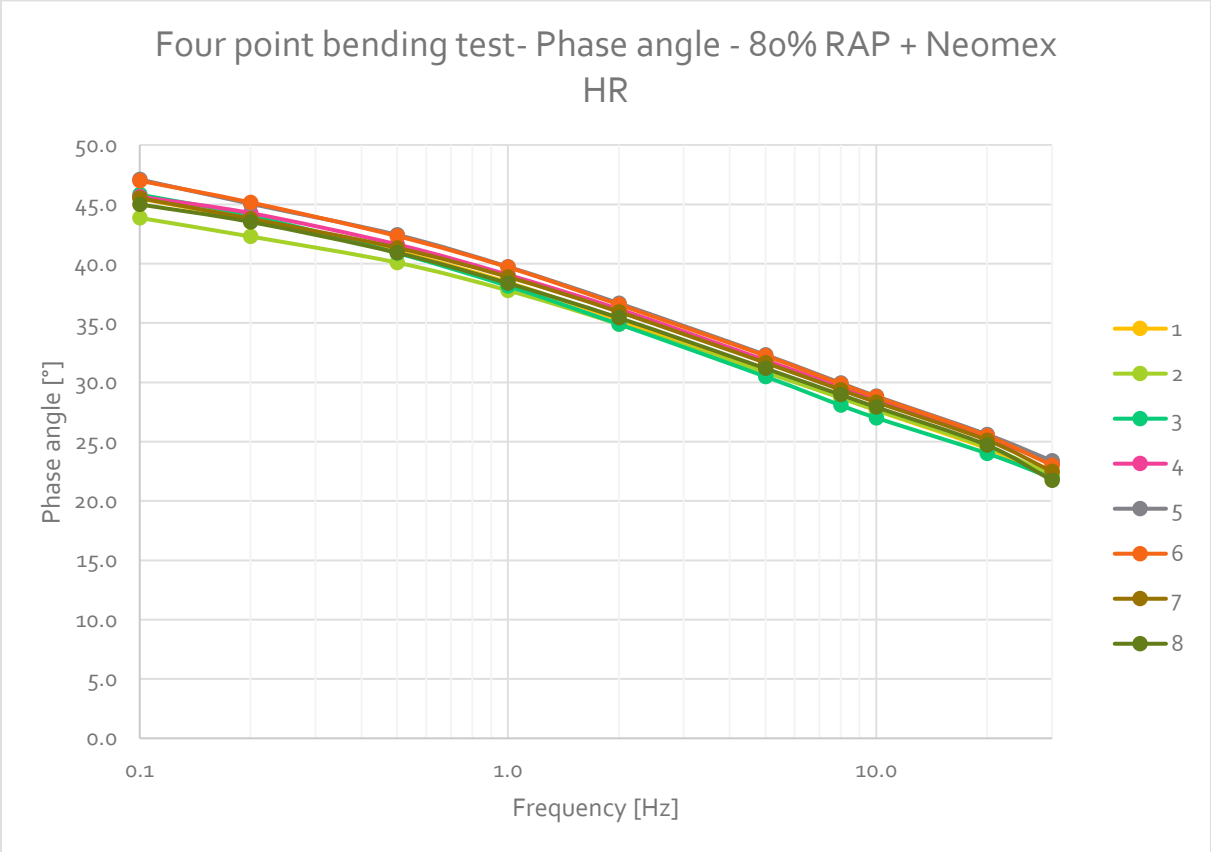

Figure G.6: Results four point bending test – Phase angle 80% RAP + Neomex HR

Table G.3: Results four point bending test - Stiffness 80% RAP + Neomex HR

Mean Results		T [°C]	20.0
Frequency (f)	Strain (ε)	Stiffness (E*)	Phase angle
Hz	[mm/m]	[MPa]	[°]
0.1	51.4	1045	45.7
0.2	51.4	1443	44.0
0.5	51.4	2178	41.3
1.0	51.4	2928	38.7
2.0	51.4	3868	35.7
5.0	51.4	5413	31.4
8.0	51.3	6343	29.1
10.0	51.3	6809	28.1
20.0	51.3	8401	24.9
30.0	51.4	9104	22.5
0.1	51.4	1024	45.3

Appendix H: Workability

Table H.1: Number of gyrations and average per mixture (last row)

65% RAP	80% RAP	80% RAP + Cecabase RWI	80% RAP + Neomex HR
16	23	5	20
20	15	6	10
22	19	6	9
20	21	7	9
20	18	7	11
18	17	7	9
20	25	6	11
15	21	7	13
25	20	7	8
24	21	7	10
19	22	8	13
16	21	8	12
23	22	9	12
18	18	8	10
18	18	6	11
24	22	7	11
18	21	10	13
24	20	9	12
20	**20.22**	**7.22**	**11.33**

Appendix I: Calculations regarding the micromechanical prediction

Determination of the volume fractions

$$f_v = \frac{\rho_{max} - \rho_{mix}}{\rho_{max}} \quad (I.1)$$

where: f_v = volume fraction air voids [-]
ρ_{max} = maximum density [kg/m³]
ρ_{mix} = mixture density [kg/m³]

Table I.1: Determination volume fraction air voids using equation I.1

	80% RAP	80% RAP + Cecabase RWI	80% RAP + Neomex HR
Maximum density [kg/m³]	2479	2479	2479
Measured density mixture [kg/m³]	2401	2420	2410
Volume fraction air voids [-]	0.031	0.024	0.028

$$f_b = \frac{m_{\%,binder}}{100} * \frac{\rho_{mix}}{\rho_b} \quad (I.2)$$

where: f_b = volume fraction binder [-]
$m_{\%,binder}$ = mass percentage binder [%]
ρ_{mix} = mixture density [kg/m³]
ρ_b = binder density [kg/m³]

Table I.2: Determination volume fraction binder using equation I.2

	80% RAP	80% RAP + Cecabase RWI	80% RAP + Neomex HR
Estimated mass percentage binder [%]	4.3	4.3	4.3
Measured density mixture [kg/m³]	2401	2420	2410
Estimated density binder [kg/m³]	1025	1025	1025
Volume fraction binder [-]	0.101	0.102	0.101

Table I.3: Determination volume fraction aggregate

	80% RAP	80% RAP + Cecabase RWI	80% RAP + Neomex HR
Volume fraction air voids [-]	0.031	0.024	0.028
Volume fraction binder [-]	0.101	0.102	0.101
Volume fraction aggregate [-]	0.868	0.874	0.871

$$VMA = 100 - \frac{\rho_{mb} * P_s}{\rho_{sb}} \quad (I.3)$$

where: VMA = voids in mineral aggregate [%]
ρ_{mb} = bulk density mixture [kg/m³]
P_s = mass percentage aggregate [%]
ρ_{sb} = bulk density aggregate [kg/m³]

Table I.4: Determination VMA using equation I.3

	80% RAP	80% RAP + Cecabase RWI	80% RAP + Neomex HR
Measured density mixture [kg/m³]	2401	2420	2410
Mass percentage aggregate [%]	95.7	95.7	95.7
Bulk density aggregate [kg/m³]	2648	2648	2648
VMA [%]	13.2	12.5	12.9

$$VFA = 100 * \frac{VMA - V_a}{VMA} \quad (I.4)$$

where: VFA = voids filled with bitumen [%]
VMA = voids in mineral aggregate [%]
V_a = volume percentage air voids [%]

Table I.5: Determination VFA using equation I.4

	80% RAP	80% RAP + Cecabase RWI	80% RAP + Neomex HR
VMA [%]	13.2	12.5	12.9
Volume percentage air voids [%]	3.1	2.4	2.8
VFA [%]	76.5	80.8	78.3

Calculation of the contact factor P_c and stiffness applying original Hirsch model

To calculate the contact factor and the stiffness according to the original Hirsch model, equations 2.15 and 2.16 are used. Further, the results from Table I.4 and I.5 are used.

Table I.6: Application of original Hirsch model for stiffness prediction – 80% RAP

80% RAP				
Frequency [Hz]	**Complex shear modulus [MPa] Unaged**	**P_c [-]**	**Predicted E^*_{mix} [MPa]**	**Measured $E^*_{mix,\ cyclic\ ITT}$ [MPa]**
0.2	1.27	0.143	3677	4066
0.4	2.00	0.178	4580	-
0.6	2.58	0.201	5168	-
0.8	3.08	0.218	5603	-
1	3.53	0.232	5959	6426
2	5.30	0.276	7113	7693
4	7.90	0.325	8379	-
6	9.86	0.353	9132	-
8	11.5	0.374	9673	10595
10	12.9	0.390	10095	11035
20	18.4	0.440	11403	-
30	22.5	0.469	12166	13682

Table I.7: Application of original Hirsch model for stiffness prediction – 80% RAP + Cecabase RWI

80% RAP + Cecabase RWI				
Frequency [Hz]	**Complex shear modulus [MPa] Unaged**	**P_c [-]**	**Predicted E^*_{mix} [MPa]**	**Measured $E^*_{mix,\ cyclic\ ITT}$ [MPa]**
0.2	0.33	0.075	1948	2567
0.4	0.53	0.098	2518	-
0.6	0.71	0.113	2911	-
0.8	0.86	0.125	3218	-
1	1.00	0.134	3475	4203
2	1.59	0.169	4361	5165
4	2.49	0.208	5385	-
6	3.21	0.233	6043	-
8	3.82	0.252	6532	7528
10	4.38	0.267	6925	7905
20	6.58	0.315	8202	-
30	8.33	0.346	8995	10170

Table I.8: Application of original Hirsch model for stiffness prediction – 80% RAP + Neomex HR

80% RAP + Neomex HR				
Frequency [Hz]	**Complex shear modulus [MPa] Unaged**	**P_c [-]**	**Predicted E^*_{mix} [MPa]**	**Measured $E^*_{mix,\ cyclic\ ITT}$ [MPa]**
0.2	0.37	0.078	2010	2343
0.4	0.61	0.101	2601	-
0.6	0.81	0.117	3009	-
0.8	0.99	0.129	3326	-
1	1.15	0.140	3590	3905
2	1.83	0.175	4504	4845
4	2.87	0.215	5554	-
6	3.70	0.241	6227	-
8	4.41	0.260	6730	7176
10	5.05	0.276	7127	7577
20	7.62	0.326	8437	-
30	9.65	0.357	9244	9722

Calculations regarding validation P_a expression proposed by Zhang et al. (2018-b)

To calculate the P_a value and the predicted stiffness, the expression of Zhang et al. (2018-b) is used with the fitting parameters as indicated in paragraph 2.5.1.

The equation containing the fitting parameters, is shown in equation I.5.

$$P_a = 0.0017 + 0.9983 * \frac{e^{0.62+0.72*ln\left(\frac{f_b}{f_b+f_v}*|G^*|_b\right)-0.17*(f_b+f_v)}}{1+e^{0.62+0.72*ln\left(\frac{f_b}{f_b+f_v}*|G^*|_b\right)-0.17*(f_b+f_v)}} \quad (I.5)$$

where: P_a = aggregate organization factor [-]

f_b = volume fraction binder [-]

f_v = volume fraction air voids [-]

$|G^*|_b$ = complex shear modulus binder [N/mm²]

With the resulting P_a values, the stiffness is calculated with equation I.6 following the simplified Hirsch model. The assumed values for the Young's modulus of the aggregate and the Poisson's ratio are already filled in the equation. The applied volume fractions can be found in Table I.1 – I.3.

$$|E^*|_{mix} = P_a * f_a * 53000 + f_b * 2 * (1 + 0.35) * |G^*|_{binder} \quad (I.6)$$

where: $|E^*|_{mix}$ = predicted dynamic complex modulus mixture [N/mm²]
P_a = aggregate organization factor [-]
f_a = volume fraction aggregate [-]
f_b = volume fraction binder [-]
$|G^*|_{binder}$ = complex shear modulus binder [N/mm²]

Table I.9: Application of proposed P_a expression and simplified Hirsch model for stiffness prediction – 80% RAP

80% RAP				
Frequency [Hz]	**Complex shear modulus [MPa] Unaged**	**P_a [-]**	**Predicted E^*_{mix} [MPa]**	**Measured $E^*_{mix,\ cyclic\ ITT}$ [MPa]**
0.2	1.27	0.641	29505	4066
0.4	2.00	0.712	32761	-
0.6	2.58	0.748	34431	-
0.8	3.08	0.771	35492	-
1	3.53	0.788	36267	6426
2	5.30	0.833	38324	7693
4	7.90	0.869	39994	-
6	9.86	0.886	40782	-
8	11.5	0.897	41273	10595
10	12.9	0.905	41621	11035
20	18.4	0.924	42532	-
30	22.5	0.934	42969	13682

Table I.10: Application of proposed P_a expression and simplified Hirsch model for stiffness prediction – 80% RAP + Cecabase RWI

80% RAP + Cecabase RWI				
Frequency [Hz]	**Complex shear modulus [MPa] Unaged**	**P_a [-]**	**Predicted E^*_{mix} [MPa]**	**Measured $E^*_{mix,\ cyclic\ ITT}$ [MPa]**
0.2	0.33	0.412	19097	2567
0.4	0.53	0.499	23154	-
0.6	0.71	0.550	25496	-
0.8	0.86	0.584	27106	-
1	1.00	0.611	28334	4203
2	1.59	0.686	31832	5165
4	2.49	0.751	34837	-
6	3.21	0.784	36348	-
8	3.82	0.804	37306	7528
10	4.38	0.819	37996	7905
20	6.58	0.859	39828	-
30	8.33	0.878	40723	10170

Table I.11: Application of proposed P_a expression and simplified Hirsch model for stiffness prediction– 80% RAP + Neomex HR

80% RAP + Neomex HR				
Frequency [Hz]	**Complex shear modulus [MPa] Unaged**	**P_a [-]**	**Predicted E^*_{mix} [MPa]**	**Measured $E^*_{mix,\ cyclic\ ITT}$ [MPa]**
0.2	0.37	0.429	19807	2343
0.4	0.61	0.517	23888	-
0.6	0.81	0.568	26227	-
0.8	0.99	0.603	27822	-
1	1.15	0.629	29022	3905
2	1.83	0.703	32439	4845
4	2.87	0.765	35331	-
6	3.70	0.797	36774	-
8	4.41	0.817	37695	7176
10	5.05	0.831	38342	7577
20	7.62	0.868	40086	-
30	9.65	0.887	40929	9722

Calculations regarding determination alternative fitting parameters for P_a expression

Because the proposed P_a expression does not lead to reliable predictions, alternative fitting parameters are determined using the laboratory tests of the 80% RAP mixture without additive. Firstly, the P_a values based on the stiffness of the mixture are determined using equation I.7. The assumed values for the Young's modulus of the aggregate and the Poisson's ratio are already filled in the equation.

$$\boldsymbol{P_a = \frac{|E^*|_{mix} - f_b * 2 * (1 + 0.35) * |G^*|_{binder}}{f_a * 53000}} \quad (I.7)$$

where: P_a = aggregate organization factor [-]
$|E^*|_{mix}$ = dynamic complex modulus mixture [N/mm²]
f_b = volume fraction binder [-]
$|G^*|_{binder}$ = complex shear modulus binder [N/mm²]
f_a = volume fraction aggregate [-]

The results are given in Table I.12.

Table I.12: Determination of P_a values 80% RAP mixture based on laboratory tests

80% RAP			
Frequency [Hz]	**Measured $E^*_{mix,\ cyclic\ ITT}$ [MPa]**	**Complex shear modulus [MPa] Unaged**	**P_a [-]**
0.2	4066	1.27	0.088
1	6426	2.00	0.140
2	7693	2.58	0.167
8	10595	3.08	0.230
10	11035	3.53	0.240
30	13682	5.30	0.297

Those results are fit in the expression of P_a proposed by Zhang et al. (2018-b) (equation I.8).

$$P_a = a + (1-a) * \frac{e^{b+c*ln\left(\frac{f_b}{f_b+f_v}*|G^*|_b\right)+d*(f_b+f_v)}}{1+e^{b+c*ln\left(\frac{f_b}{f_b+f_v}*|G^*|_b\right)+d*(f_b+f_v)}} \quad (I.8)$$

where: P_a = aggregate organization factor [-]
f_b = volume fraction binder [-]
f_v = volume fraction air voids [-]
$|G^*|_b$ = complex shear modulus binder [N/mm²]
a, b, c, d = fitting parameters [-]

Then, the Solver function of Microsoft Excel is used to determine the fitting parameters when the deviation between the P_a values based on the laboratory tests and the P_a values based on equation I.8 is minimized.
The resulting values are shown in Table I.13.

Table I.13: New fitting parameters

Parameters	**a**	**b**	**c**	**d**
Values	0.0030	-2.46	0.52	0.81

The values in Table I.13 are implemented in equation I.8 to calculate the P_a values for the three mixtures. Then, the stiffness of the mixtures can be determined using equation I.6. The results are shown in Table I.14, Table I.15 and Table I.16.

Table I.14: Application of new fitting parameters for P_a expression for stiffness prediction – 80% RAP

80% RAP				
Frequency [Hz]	**Complex shear modulus [MPa] Unaged**	**P_a [-]**	**Predicted E^*_{mix} [MPa]**	**Measured $E^*_{mix,\ cyclic\ ITT}$ [MPa]**
0.2	1.27	0.088	4060	4066
0.4	2.00	0.108	4990	-
0.6	2.58	0.122	5601	-
0.8	3.08	0.132	6058	-
1	3.53	0.140	6435	6426
2	5.30	0.167	7676	7693
4	7.90	0.197	9083	-
6	9.86	0.216	9946	-
8	11.5	0.230	10580	10595
10	12.9	0.241	11082	11035
20	18.4	0.276	12688	-
30	22.5	0.297	13663	13682

Table I.15: Application of new fitting parameters for P_a expression for stiffness prediction – 80% RAP + Cecabase RWI

80% RAP + Cecabase RWI				
Frequency [Hz]	**Complex shear modulus [MPa] Unaged**	**P_a [-]**	**Predicted E^*_{mix} [MPa]**	**Measured $E^*_{mix,\ cyclic\ ITT}$ [MPa]**
0.2	0.33	0.048	2216	2567
0.4	0.53	0.060	2789	-
0.6	0.71	0.069	3181	-
0.8	0.86	0.075	3486	-
1	1.00	0.081	3743	4203
2	1.59	0.100	4628	5165
4	2.49	0.122	5665	-
6	3.21	0.137	6342	-
8	3.82	0.148	6851	7528
10	4.38	0.157	7267	7905
20	6.58	0.187	8645	-
30	8.33	0.206	9528	10170

Table I.16: Application of new fitting parameters for P_a expression for stiffness prediction – 80% RAP + Neomex HR

80% RAP + Neomex HR				
Frequency [Hz]	**Complex shear modulus [MPa] Unaged**	**P_a [-]**	**Predicted E^*_{mix} [MPa]**	**Measured $E^*_{mix,\ cyclic\ ITT}$ [MPa]**
0.2	0.37	0.050	2319	2343
0.4	0.61	0.063	2922	-
0.6	0.81	0.072	3335	-
0.8	0.99	0.079	3656	-
1	1.15	0.085	3924	3905
2	1.83	0.105	4853	4845
4	2.87	0.129	5937	-
6	3.70	0.144	6643	-
8	4.41	0.155	7178	7176
10	5.05	0.165	7605	7577
20	7.62	0.196	9048	-
30	9.65	0.216	9967	9722